Spring 2016

From soilscapes to landscapes: a landscape-oriented approach to simulate soil organic carbon dynamics in intensely managed landscapes (IMLS)

Kenneth Michael Wacha
University of Iowa

FROM SOILSCAPES TO LANDSCAPES:

A LANDSCAPE-ORIENTED APPROACH TO SIMULATE SOIL ORGANIC CARBON DYNAMICS IN INTENSELY MANAGED LANDSCAPES (IMLS)

by

Kenneth Michael Wacha

A thesis submitted in partial fulfillment
of the requirements for the Doctor of Philosophy
degree in Civil and Environmental Engineering in the
Graduate College of
The University of Iowa

May 2016

Thesis Supervisors: Professor Athanasios N. Papanicolaou
Professor William E. Eichinger

Graduate College
The University of Iowa
Iowa City, Iowa

CERTIFICATE OF APPROVAL

_____

PH.D. THESIS

_____

This is to certify that the Ph.D. thesis of

Kenneth Michael Wacha

has been approved by the Examining Committee for
the thesis requirement for the Doctor of Philosophy degree
in Civil and Environmental Engineering at the May 2016 graduation.

Thesis Committee: _____
Athanasios N. Papanicolaou, Thesis Supervisor

_____
William E. Eichinger, Thesis Supervisor

_____
David Bennett

_____
Allen Bradley

_____
Art Bettis

_____
Heather Sander

To my beautiful wife, Michelle, who provided me with endless supplies of love and support.

Harmony with land is like harmony with a friend; you cannot cherish his right hand and chop off his left.

Aldo Leopold

ACKNOWLEDGEMENTS

This dissertation has been the culmination of several years of research work performed in the Department of Civil and Environmental Engineering, University of Iowa, U.S.A., under the supervision of Professor Thanos Papanicolaou. Thanos has been a constant supply of guidance and support to me. He has engrained into me the art of critical thinking and how to approach and solve a problem. His unending drive and leadership inspired me to pursue graduate level research to uncover new things and to understand processes. He has built upon my strengths and helped me minimize my weaknesses.

I would like to acknowledge my committee members, specifically Bill, Art, Allen, Heather and Dave for their support over the years. This includes time spent in many of their classrooms, as well as involvement with various research projects. A special thank you to Bill Eichinger for serving as co-chair of my committee and providing excellent discussions along the way.

I would to mention some important induvial I have encountered along the way. First, to my core undergraduate support systems and friends, especially Chad Reittinger, Mehmed (Bill) Diken and Sam Boland. Chad for our tireless work through years of mathematics and physics, Bill for our numerical methods, coding and technical writing, and Sam for eco-hydraulics, GIS and scripts. You are all considered family to me. Next, for the many years spent with my research teammates, especially Dimitrios Dermisis, Achilleas Tsakiris, Chris Wilson, and Benjamin Abban. Dimitri for our late nights working on laser scanning and rainfall simulations, Achilleas for his presentation skills and level of organization that I have adapted; Chris for our work with the critical zone observatory; and Ben for being a sounding board for my new ideas, exhausting field work

campaigns and projects. All of you are associated with some of the most enjoyable times I had during my studies and all are dear friends to me.

I have been lucky to have many inspirational people in my life during the time of my studies. To Barb and Tom Nicknish, for their support and treating me as family. Their relationship inspired me to work towards a similar life for my wife, one that correctly balances family, career, and God. To the many local farmers over the years who let my on their land to conduct research, especially the Maas family, who personifies the traditional Iowa farmer values of hard work, honesty and family. To Larry Gullett, Brad Friedhoff and all of the excellent staff at Kent Park, for their passion for conservation and love of nature.

I would like to acknowledge my Mom and Dad. They raised me with a strong work ethic and stewardship of the land. My father, Merle passed away in 2000, which pushed me to go back to school and pursue my dreams. My mother, Elaine has been like a rock of support for me and my family throughout and provided many endless hours of discussion about farming. In addition I would like to acknowledge my brothers and sisters and their families for love and support.

Lastly I would like to thank God for all of my blessings, starting with my amazing wife Michelle and my beautiful children, Nicholas, Jackson, Olivia and Leonidas. I feel that Michelle has earned this doctoral degree along with me, through listening to me discuss problems and research approaches, practicing my presentations, being there for my ups and downs, and all the while remaining supportive and encouraging. God has indeed blessed me with placing the right people in my path to make sure I crossed the finish line and completed the race.

ABSTRACT

The primary objective of this research was to develop a landscape-oriented, process-based approach that can enhance understanding and prediction of SOC fluxes in IMLs by incorporating the key mechanisms impacting soil carbon dynamics when moving from the soilscape to the landscape. The mechanisms that are considered to be the focus of this study are redistribution of SOC due to erosion and deposition without neglecting the importance of litter incorporation into the soil column, decomposition due to microbial activity, and physical and chemical stabilization of carbon. To accomplish this objective, field experiments were performed to examine how selective entrainment of different soil size fractions, quantified through the enrichment ratio (ER), varies with management and hillslope position. Differential modes in soil mobilization between rill and interrill areas were either elevated or dampened depending on the prevalent management practice, the gradient of the site and landscape position. Sites where sediment and runoff fluxes were highest were found to have lower ER values (around unity) due to the mobilization of all size classes making static and dynamic samples almost identical.

The size fractions analyzed in these experiments were found to have varying levels of carbon associated with them, especially the larger aggregates, which encapsulate organic material. Neglecting them in transport estimates could lead to large errors in predicted fluxes of SOC. For this reason, a careful attention was placed on identifying how aggregate stability varies with respect to management and hillslope position, through controlled experiments looking size distributions to reflect tillage disturbance and aggregate stability to assess resistance to rainsplash.

Lastly, a landscape-oriented modeling framework was developed that captures not only the SOC spatial heterogeneity in IMLs but also determines the impacts that redistribution has on this heterogeneity and ultimately on SOC dynamics. The integrative modeling framework considers the collective effects of both rainsplash/rainfall- and tillage-induced erosion on SOC redistribution in IMLs through an ER-module developed and woven within this framework to connect an upland erosion model with a soil biogeochemical model. It provides not only size fraction updates to the active layer and ER values, but also explicitly considers the effects of splash-driven interrill erosion on those ER estimates.

The model was applied to twentieth-century changes in SOC across a representative agricultural hillslope in the study watershed and compared to recent SOC data. The chronosequence in SOC storage within the erosional zone revealed that soils were continually depleted of the rich organic matter long after the 1930's "Dust bowl" due to enhanced erosion that accompanied agricultural practices. However, conservation tillage and enhanced crop production that began in the late 1980's reversed the downward trend in SOC losses, causing nearly 26% of the lost SOC to be regained. Results from this study can be used to aid policy and decision makers in developing a food-system that accounts for the co-evolution of human and natural activity, to develop sustainable agro-ecosystems through the use of data supported recommended best management practices.

PUBLIC ABSTRACT

Most available biogeochemical models focus within a soil column and cannot simulate the redistribution of soil organic carbon (SOC) across the landscape, thereby causing unintended errors in carbon budgets. These soil-column models originated primarily within grasslands and forests, which focus primarily on processes in the vertical (i.e., production and decay), but neglect downslope contributions of material, which can have huge implications on soil-water-carbon interactions, especially within intensely managed landscapes (IMLs). Therefore, to accurately simulate SOC dynamics in IMLs it is necessary to account for a series of mechanistic processes related to the collective erosion effects from rainsplash/runoff and tillage-induced erosion on biogeochemical cycling, which have not been studied in detail before.

The goal of this research is to provide spatiotemporal predictions of SOC stocks at the hillslope scale, within a representative study watershed in Iowa, that account for erosion and deposition of material. An ER module was merged with a watershed erosion model and organic matter cycling model to build new functionality, allowing the simulation of the transport of light organic matter across the topographic gradient, while considering changes in runoff, residue, tillage, and roughness on SOC redistribution and storage. The model was applied to twentieth-century changes in SOC across a representative agricultural hillslope in the study watershed and compared to recent SOC data. The chronosequence in SOC storage revealed that conservation practices and enhanced crop production that began in the late 1980's reversed the downward trend in SOC losses.

TABLE OF CONTENTS

LIST OF TABLES

TABLE

LIST OF FIGURES

FIGURE

CHAPTER 1. INTRODUCTION

Developing a more complete understanding of the mechanisms impacting soil organic carbon (SOC) dynamics within intensively managed landscapes (IMLs) remains a key scientific challenge to providing accurate estimates of carbon storage potential in the soil column using a budget approach. Much of the pioneering ground work on SOC dynamics has been conducted in well-established and stable systems, such as forests or grasslands. These systems are often treated as soilscapes, defined here as homogenous soil units that were formed under same environmental factors and experience the same management [Lagacherie et al., 2001]. In fact, many current biogeochemical models have been developed based on studies in these stable (almost static) ecosystems [Parton et al., 1987; Smith et al., 1997]. However, IMLs when compared to these pseudo-equilibrated systems are highly dynamic due in part to (1) anthropogenic perturbations, such as tillage that breaks apart the aggregated soil structure; and (2) seasonal vegetative cover, which in conjunction with the tillage leaves the soil exposed at times thereby making it vulnerable to the effects of rainsplash and runoff [Van Oost et al., 2000; Papanicolaou et al., 2015]. As a result, water, soil, organic matter and biomass are mobilized and then transported downslope. These constituents are deposited along flow pathways leading to high heterogeneity of biogeochemical properties across the landscape, both in space and time.

Due to this heterogeneity, the soilscape-based models used for simulating SOC fluxes, which were developed in well-established grassland or forested systems, most likely lack the mechanistic capabilities to simulate the dynamic processes occurring within IMLs. This negligence can potentially propagate to significant errors in carbon

budgets that may even cover up the benefits of certain conservation practices. *Therefore, the primary goal of this dissertation study is to develop a landscape-oriented, process-based approach that can simulate SOC fluxes in IMLs by incorporating the key mechanisms impacting soil carbon dynamics that become apparent when moving from the soilscape to the landscape*. The mechanisms most pertinent to this study are erosion and deposition.

1.1 Research Approach and Structure of the Dissertation

The study site selected to help accomplish the above goal is the Clear Creek watershed, located in southeastern Iowa. This area, like much of the U.S. Midwest, has been converted from intrinsic prairie conditions to a leading corn and soybean producer. Moreover, this watershed is representative of the U.S. Midwest in terms of soils, management, making this an ideal study location [Papanicolaou et al., 2015].

Clear Creek is part of the Intensively Managed Landscapes - Critical Zone Observatory, which is funded by the National Science Foundation (http://criticalzone.org/iml). The site, through its involvement in the Critical Zone network, offers extensive geospatial, chemical, and eco-hydrological databases, as well as a detailed history of local land uses and management practices [e.g., Abaci and Papanicolaou, 2009; Papanicolaou et al., 2015], which were utilized in this study.

Through this study and using the Clear Creek site as an example, a landscape-oriented, process-based approach is developed for assessing SOC dynamics in IMLs. This dissertation, which discusses the approach, is designed in the following manner. Chapter 2 provides a detailed summary of the key mechanisms impacting SOC in IMLs, focusing primarily on the redistribution mechanisms of erosion and deposition which

have been neglected or (at best) over-simplified in many numerical studies. This chapter also presents the topics of selective size fraction mobilization, aggregate stability, and the enrichment ratio, which are central to discussing SOC mobilization and transport in IMLs.

Chapters 3 and 4 provide a summary of the field and experimental data collected throughout this study in Clear Creek. Chapter 3 focuses on the methodological development and results of rainfall plot simulations to understand and quantify better enrichment ratios under a variety of management practices and hillslope locations. Chapter 4 presents the development and conduction of systematic tests to assess soil aggregate dynamics by examining the effects that raindrop impact has on stability and the role that management and hillslope position have on aggregate size distributions.

Chapter 5 provides details on the numerical modeling framework developed to simulate SOC redistribution (mobilization, transport, and deposition) in IMLs. This chapter first discusses the selection of models and the development and formulation of an enrichment ratio (ER) module to simulate selective size fraction mobilization and corresponding enrichment. Next, the implementation of the framework using a representative hillslope in Clear Creek is considered as a case study to assess changes in SOC stocks due to redistribution processes impacted through a detailed time series of historic local management and climatic conditions.

Chapter 6 is the conclusion. It offers a synthesis of the key findings uncovered during the field experiments and integrative modeling. The last part of this chapter discusses some of the limitations encountered with proposed methods and recommendations for future research in this area.

To help along the journey through this dissertation, a summary "road map" highlighting the key waypoints of this study, as well as the specific research goals, is provided in Figure 1.1.

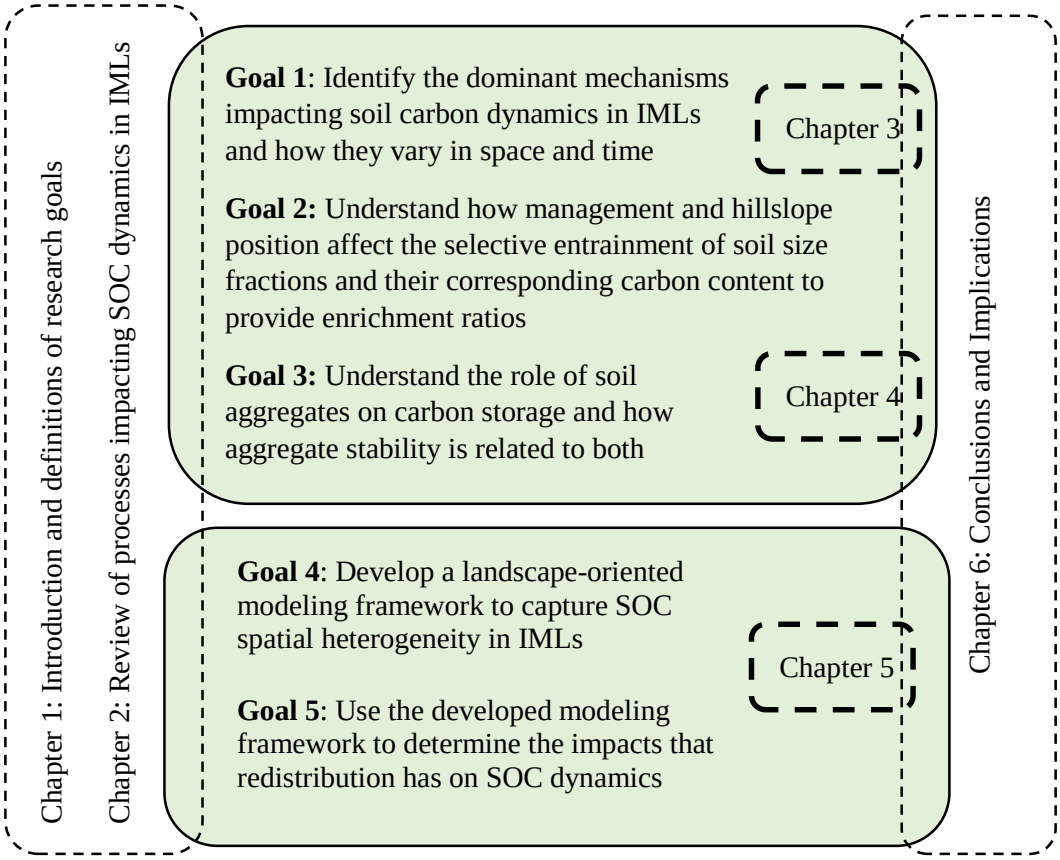

Figure 1.1 Goals and dissertation chapters

CHAPTER 2. SOIL ORGANIC CARBON MECHANISMS IN IMLs

2.1 Limitations of the "Soilscape Approach" to Simulate SOC Dynamics

Soil organic carbon (SOC) is an important constituent of the Earth's fabric derived from the breakdown of above-ground plant residue, rhizomes, and root exudates [Lal, 2011]. Enhancing SOC storage potential in intensively managed landscapes (IMLs) is vital for sustaining soil health and crop productivity [Andrews et al., 2002; Sperow et al., 2003; Cambardella et al., 2004; Lal, 2011], as well as for mitigating rising carbon dioxide (CO_2) levels in the atmosphere [Houghton, 2008; Kuhn et al., 2009; Ogle et al., 2010; Hatfield and Parkin, 2012]. IMLs, like Clear Creek, IA in the U.S. Midwest, are said to have some of the highest potential to store carbon, if the appropriate (i.e., conservation) land management practices are implemented [e.g., Sperow et al., 2003].

Due to this importance of IMLs for storing carbon, much research has been devoted over the past decades to understanding the key biogeochemical processes impacting SOC dynamics and storage [e.g., Paustian et al., 1992; Gregorich et al., 1998; Richter et al., 1999; Metting et al., 1999; Lal, 2004; Jacinthe et al., 2009; Kuhn et al., 2009; Li et al., 2012; Navas et al., 2012; Zhang et al., 2013]. But despite considerable advances in knowledge regarding SOC process, the majority of these studies have been conducted in well-established, pseudo-equilibrated systems, such as forests or grasslands, rather than in continuously disturbed IMLs [e.g., Li et al., 1997; Yoo et al., 2005; Parton et al., 2007]. Furthermore, these studies have been, for the most part, geospatially limited to the soilscape, which is a homogenous soil parcel formed under similar topographic, management or climatic factors [McBratney et al., 2003; Mangan et al., 2004; Jan van Groenigen et al., 2011].

Many of the biogeochemical models that adopt a soilscape approach do a reasonable job of simulating processes in a soil column that act mostly in the vertical direction, like the decomposition and stabilization of organic material [Kelly at al., 1997; Paustian et al., 2002; Leite et al., 2004; Bricklemyer et al., 2007; Wilson et al., 2009; Bortolon et al., 2011; Ogle et al., 2012; Smith et al., 2012; Alvaro-Fuentes et al., 2012; Vaccari et al., 2012]. However, the soilscape approach, due to its spatially-limited and homogenous, control volume, inherently lacks the mechanistic capacity to simulate landscape processes, specifically the redistribution (i.e., mobilization, transport and deposition) of SOC [Papanicolaou et al., 2015].

The limitations of the soilscape approach become apparent when looking at the differences between well-established grassland systems and IMLs in the context of SOC. First off, IMLs lack permanent surface cover. Periodically, the soil surface is left exposed and vulnerable to rainsplash, and freeze-thaw cycles, which weaken the soil structure [Morgan and Rickson, 1995; Gyssels and Poesen, 2002]. Additionally, tillage in IMLs fracture the soil structure, breaking apart soil aggregates, and thereby facilitating the entrainment of the finer grain soil and lighter SOC by runoff [Tisdall and Oades, 1982; Kuhn et al., 2009; Van Oost et al., 2009; Papanicolaou et al., 2009]. Here the absence of cover allows runoff velocities to increase, which in turn increases its entrainment potential [e.g., Yalin, 1963]. These natural and human-induced mechanisms, make it easier for soil, residue, and the associated SOC to move about the landscape, augmenting the heterogeneity in SOC stocks both within a field and across different fields.

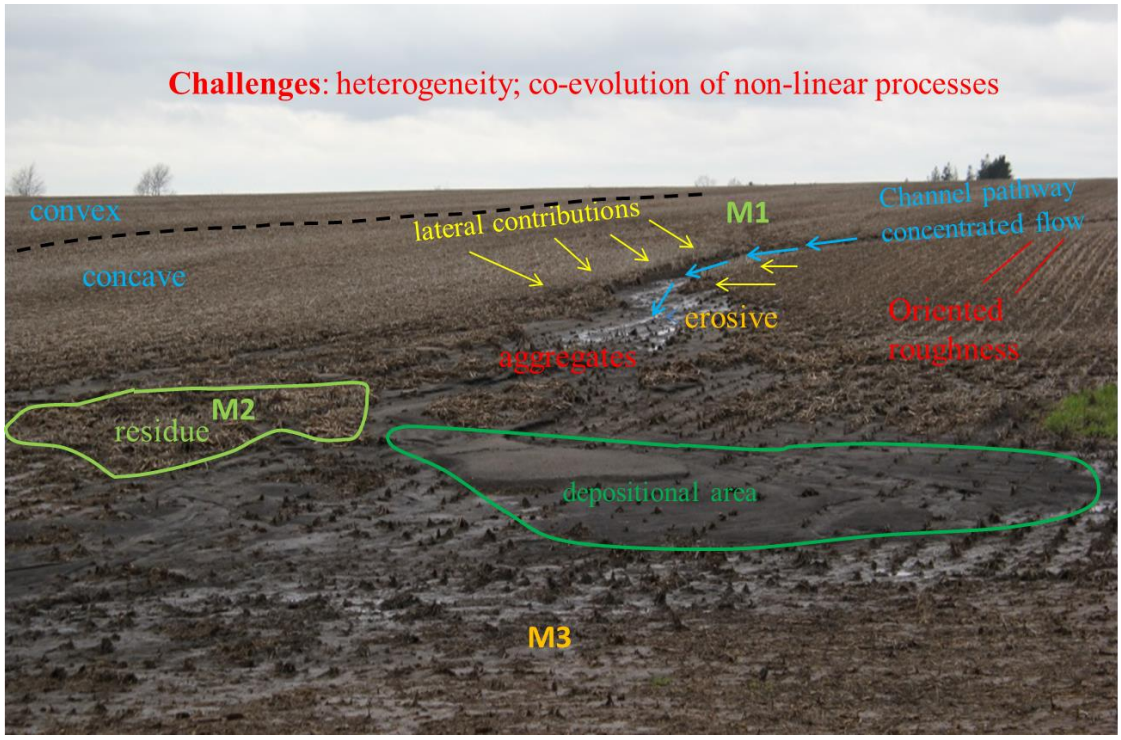

Figure 2.1 Heterogeneity of an IML [Papanicolaou et al., 2015]

The mosaic of landscape processes and features found within an IML that facilitate redistribution of SOC across the landscape and enhance its heterogeneity of SOC is shown in Figure 2.1. The figure highlights the processes which shape the heterogeneity found across the landscape.

Topography, downslope curvature (concave vs. convex), and roughness are major influences on the redistribution of SOC [Moore and Burch, 1986; Van Oost et al., 2000; Rieke-Zapp and Nearing, 2005], as they shape the different flow pathways, in which the SOC travels across the landscape. These pathways include the formation of rill/gully networks at the hillslope or watershed scale [e.g., Davidson and Ackerman, 1993; Hollinger et al., 2005; Dobermann et al., 2006; Blanco-Canqui and Lal, 2008].

The flow pathways control the energy of the entraining runoff. On one hand, the flow concentrates and accelerates; however, these pathways can also have localized

storage areas causing large resting times and diminishing the likelihood of mobilization [Stallard, 1998; Campbell et al., 1998; Kuhn et al., 2009]. These topographical and roughness features that shape the flow pathways in a field, as well as the processes occurring in them have not been systematically examined in IMLs at the landscape level [Papanicolaou et al., 2016]; however, it is known the these flow pathways play a significant role in shaping the degree of spatial heterogeneity and temporal variability of soil properties, biomass, and SOC stocks in a landscape [Dermisis et al., 2010; Papanicolaou et al., 2010].

Therefore, without considering downslope and lateral flow pathways and the associated mechanisms that transport and redistribute soil, biomass, and SOC, predictions of the SOC storage potential can be either over or underestimated on the seasonal or crop rotational scale [Gregorich et al., 1998; Harden et al., 1999; Li et al., 2001]. In fact, using a soilscape approach to determine carbon budgets for a given ecosystem, especially IMLs, may lead to large error propagations or even conceal the benefits that certain conservation practices may have on highly erosive landscapes [Canadell et al., 2011].

To help circumvent the limitations of the soilscape, an IML can be discretized into a sequence of individual soilscapes (Figure 2.2) that are connected through the preferential pathways for flow and other constituents in the downslope. For example, the i^{th} soilscape (shaded red square) receives material from the upslope soilscape (i-1), and supplies material to the downslope soilscape (i+1). This "landscape-oriented" approach is needed to set the boundary conditions for the vertical soilscape processes, as the lateral/ downslope landscape processes directly affect the stocks of carbon at a location [e.g. Billings et al., 2010; Papanicolaou et al., 2015]. Therefore to develop carbon budget

for hillslopes, watersheds or drainage networks within IMLs, an interconnected approach is needed of both vertical process and the lateral processes, which is the goal of this dissertation.

Below is a summary of the vertical and lateral processes that were considered in developing this coupled approach. Yet the centerpiece of this dissertation is the redistribution mechanisms, namely erosion and deposition.

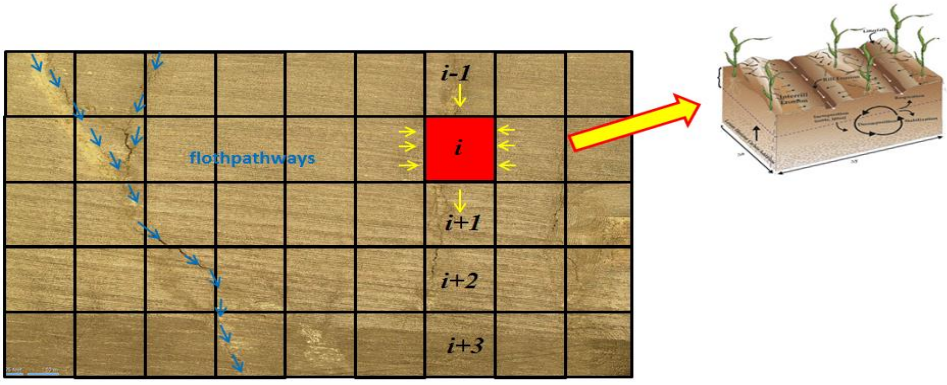

Figure 2.2 Connectivity of soilscapes

2.2 Soil Organic Carbon Mechanisms within IMLs

Within the top 20 cm of soil, or soil active layer of IMLs, SOC stocks are driven by four key mechanisms [Schlesinger, 1990; Chapman, 2010], which are shown in Figure 2.1. Changes in SOC stocks over time can be estimated using a mass balance relation consisting of these mechanisms:

$$\frac{\Delta SOC}{\Delta t} = \left\{\begin{matrix} replacement\ of \\ SOC\ at \\ erosion\ site \end{matrix}\right\} + \left\{\begin{matrix} burial\ of \\ non- \\ complexed\ OC \end{matrix}\right\} + \left\{\begin{matrix} respiration\ of \\ non- \\ complexed\ OC \end{matrix}\right\} + \left\{\begin{matrix} formation\ of \\ OC-mineral \\ complex \end{matrix}\right\} \quad \text{[Eq.1.1]}$$

Mechanism: ***M1*** ***M2*** ***M3*** ***M4***

where, mechanism M1 represents the amount of SOC lost or gained from the active layer due to redistribution (i.e., erosion and deposition); M2 is the amount of litterfall

incorporated into the soil active layer through tillage events; M3 is the amount of carbon lost from the soil column via microbial decomposition and heterotrophic respiration; and M4 is the amount of carbon stabilized into more recalcitrant forms of SOC, which includes both chemical stabilization and physical stabilization in aggregates.

Mechanisms M1 (SOC redistribution) and M2 (litter incorporation) are high amplitude, low-frequency processes. Essentially they are episodic, resulting from higher intensity storm events and scheduled tillage events. M3 (respiration) is a continuous (i.e., high frequency) process, though, that experiences high amplitude episodic fluctuations due to discrete tillage and fertilizer events. It is heavily influenced through microclimatic conditions. Mechanism M4 (stabilization) is a high-frequency but low amplitude process, resulting from biogeochemical cycling in the soil and is a function of the carbon residence times.

The seasonal scale best captures the changes in all mechanisms, M1-M4, as it incorporates plant growth cycles, management schedules (planting, cultivation, harvesting), and the variability of soil microclimates, but the approach herein is not necessarily limited to the seasonal time scale. Below is a description of the four mechanisms. The redistribution mechanism though will be discussed last as it is the most pertinent to this study.

2.2.1 Litter Incorporation (M2)

Litter or crop residue is a collection of the dead plant material (e.g., stems, leaves) left after harvest. The total available amounts of litter and its surface coverage across the landscape is dependent on the productivity of the field, crop choice, and associated litterfall rates, as well as the harvest index [Raich and Tufekcioglu, 1999; Larson et al.,

1999]. In corn or soybean fields, harvesting removes the grain portions from the field leaving a relatively uniform distribution of litter across the soil surface [Allmaras et al., 2006]. But based on the timing and tillage intensity performed afterwards, in conjunction with the seasonal patterns of rainfall, the amount and distribution of residue will change as patches develop [Thompson and Katul, 2009]. This patchiness directly affects the amounts of litter stock that are transferred (incorporated) vertically within the soil column [Tonneijck and Jongmans, 2008], as well as redistribution of surface SOC through erosion and deposition [Abaci and Papanicolaou, 2009].

2.2.2 Soil Respiration (M3)

The decomposition of organic material is mediated through microbial activity [Parkin et al., 2005; Ryan and Law, 2009]. During this process, a limited portion of organic material is stabilized into more recalcitrant forms, while the majority of carbon is expelled from the soil as carbon dioxide through heterotrophic respiration [Richardson et al. 2006]. Heterotrophic respiration is a continuous process throughout the year, but peak rates occur during the summer months, when soil moisture and temperature levels are optimal for microbial activity [Hatfield and Parkin, 2012]. The rates of heterotrophic respiration are also sensitive to soil texture, microbial biomass populations, and nitrogen availability [Richardson et al., 2006; Wilson and Al-Kaisi, 2008].

Additionally, management practices have been shown to influence soil respiration, specifically through tillage events, which break apart soil aggregates, thereby exposing the protected, but labile forms of carbon to microbial uptake processes. Studies have reported an order of magnitude increase in soil respiration that lasts for weeks after a tillage operation [e.g., Reicosky and Lindstrom, 1993; Hatfield et al., 2006].

2.2.3 Stabilization (M4)

SOC can be categorized into different pools based on its residence time in the soil [Burke, 2007]. Carbon exists in both a labile form, which is broken down more readily for uptake by the microbes and plants, as well as the more recalcitrant forms of carbon, which are broken down more slowly and hence it is the more abundant form in the soil. Turnover times of these conceptual carbon pools reportedly range from a few months for the more labile or active, to decades and centuries for the decades for the slower, more recalcitrant forms [Paustian et al., 2002; Parkin et al., 2007].

Stabilization of the SOC from the labile form to the recalcitrant forms occurs within the active layer and is treated as a continuous process. The stabilization processes include not only chemical stabilization of labile SOC from root exudates, residue leachates and the decayed portions of incorporated residue and roots, but also the physical stabilization as these byproducts are locked inside soil aggregates [Six et al., 2002; Olchin et al., 2008].

In terms of management, the labile pool is controlled by plant and microbial activity, which was shown in the previous sections as being influenced by tillage. Tillage not brings fresh litter in contact with the microbes, it also breaks apart the aggregates exposing the carbon inside. In terms of the more recalcitrant stocks, erosion/ deposition is the primary control. Large erosion events can remove en masse large amounts during a single event [Wilson et al., 2016]

2.2.4 Soil Organic Carbon Redistribution (M1)

SOC redistribution on the landscape surface is the focus of this dissertation since it is often neglected in many biogeochemical models, especially those that look at only

the soilscape. The erosion process begins with the disassociation of soil aggregates either through rain drop impacts or tillage. In terms of rainsplash, the kinetic energy of the raindrop is transferred to the soil surface, breaking down soil aggregates and dislodging soil grains from interrill areas [Julien and Simmons, 1985; Tayfur and Kavvas, 1994]. The finer soils and less dense organic matter are then transported to rill and gully networks via sheet flow [Foster et al., 2007]. Soil roughness and vegetative cover have been found to be restrictive of certain size fractions of material entering the rill/gully for a given rainfall event [Papanicolaou et al., 2010].

Once within the rill or gully, mobilization of finer soil particles and associated SOC occurs when the applied shear stress of the runoff exceeds the critical erosion strength of the soil [Papanicolaou, 1997; Poesen et al., 2003; Papanicolaou et al., 2010]. The shear stress acting upon the soil is governed by gradient, rill/gully width, and roughness [Foster, 1982], while the resistance offered by the soil is product of its physical (texture, structure) and chemical composition (organic matter content, pH, cation exchange capacity) [e.g. Sutarto et al. 2014].

The rill/gully can behave as both a conveyor and source of material, depending on the transport capacity of the flow, defined here as a specific system's ability to carry and deposit excess material under a wide range of storm events [Yalin, 1977; Foster et al., 1995; Mancilla, 2004]. If the transport capacity of the flow is not exceed by the current flux of entrained sediment and incipient conditions are exceeded, then incision (erosion) of the rill/gully can occur. Conversely, if the flux of transported sediment exceeds the transport capacity, then deposition occurs [Flanagan and Nearing, 2000].

2.2.4.1 Enrichment Ratio

Selective entrainment of the lighter size fractions affects the enrichment ratio (ER), which is a unique measure of change in available SOC through the enrichment or depletion of the finer size fraction of organic rich soils [Palis et al., 1990; Wang et al., 2013; Papanicolaou et al., 2015]. However, many biogeochemical models do not adequately incorporate the effects of selective entrainment and deposition of the finer size fraction of organic rich soils by the flow [Van Oost et al., 2005; Dlugoß et al., 2010, 2012]. The ER is often assumed to be equal to unity [Teixeira and Misra, 1997] or to obtain a constant value greater than unity. On the contrary, it is anticipated that the range of ER values may vary depending on hillslope location and the magnitude of the hydrologic event [Kuhn et al., 2009; Thompson et al., 2010; Hu et al., 2013]. Since Enrichment ratio values have been reportedly used to convert soil loss through erosion events into SOC losses [e.g., Jacinthe et al., 2004; Papanicolaou et al., 2009; Wilson et al., 2009], its oversimplification can lead to an overestimation of the SOC displaced [Papanicolaou et al., 2015].

The capacity of a particle to bind soil carbon has been shown to be proportional to the particles surface area [Palis et al., 1997; Wang et al., 2013], where finer particles (e.g., clay) have larger specific surface areas. In addition soil aggregates, which encapsulate organic material, have been shown to have higher carbon content then bulk soil characteristics [e.g., Tisdall and Oades, 1982; Six et al., 2002]. Therefore, to provide accurate fluxes of carbon via redistribution processes, it is essential to have information regarding the fractions of material and enrichment being transported along the downslope. Studies have estimated ER values either through concentration differences

between the sediment and soil [Quinton et al., 2006; Kuhn, 2007; Zheng et al., 2012] or through textural variations (Papanicolaou et al., 2015):

$$E_R = \frac{C_{sed}}{C_{soil}} \text{ or } \frac{SSA_{sed}}{SSA_{soil}} \quad \text{[Eq.2.1]}$$

where C_{sed} is the carbon content of the eroded sediment; C_{soil} is the carbon content of the in situ soil; SSA_{sed} is the specific surface area of eroded sediment; and SSA_{soil} is the specific surface area of the in situ soil.

High-intensity storms can mobilize and transport larger size fractions and aggregates, which is reflected in lower ER values [Abaci and Papanicolaou, 2009; Jacinthe et al., 2009; Papanicolaou et al., 2015]. It has been reported that ER values commonly vary due to soil types and the timing and magnitude of erosion events [Palis et al., 1990], making the ER a dynamic parameter especially in intensely managed agricultural landscapes.

2.2.4.2 Soil Aggregate Dynamics

The size distribution of soil aggregates and their " stability", defined here as the ability to retain their volumetric structure or arrangement of solids and pores [Diaz-Zorita et al., 2002], have been widely used as proxy measures reflecting the role of management practices on soil structure and health [Kemper and Rosenau, 1986; Bronick and Lal, 2005; Idowu et al., 2008; Pulido Moncada et al., 2013], as well as the resistance to soil erosion [Farmer, 1973; Farres, 1980; Coote et al., 1988; Shouse et al., 1990; Bryan, 2000]. Moreover, the manner in which an aggregate breaks down can dictate the size fractions of the material that is mobilized [Polyakov and Lal, 2004; Wang et al., 2015], and hence the redistribution of organic matter [Hu et al., 2013; Papanicolaou et al., 2015]. Following the Oades and Waters [1991] hierarchical classification of soil aggregates, which consists of microaggregates (0.053-0.250mm), small macroaggregates (0.25-

2.0mm), and large macroaggregates (2.0-5.0mm), it is the small macroaggregates that have been found to be most reflective of changes in management practices [Beare et al., 1994a,b; Franzluebbers and Arshad, 1997; Amezketa, 1999; Blanco-Canqui and Lal, 2004; Moebius et al., 2007].

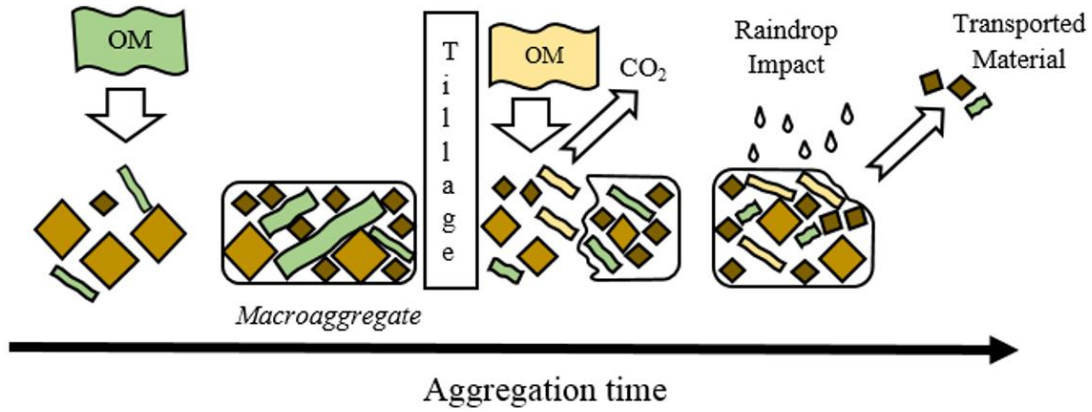

Figure 2.3 Conceptual model of aggregate formation within intensely managed landscapes. Figure modified from Six [2000].

Potential mechanisms in the soil column to store carbon include stabilization, either chemically in organic-clay complexes [Sorenson, 1972; Hassink, 1997] or physically within aggregates [Tisdall and Oades, 1982; Olchin et al., 2008]. But in intensely managed landscapes (IMLs), conventional management practices have been shown to negatively influence soil aggregate dynamics (Figure 2.3), both directly through "defragmentation" of aggregates and indirectly through alteration of physical, pedologic, and biogeochemical factors within the soil, such as organic matter, soil microclimate, and pH [e.g., Six et al., 2000; Olchin et al., 2008; Kara and Baykara, 2014; Papanicolaou et al., 2015]. Furthermore, tillage, in conjunction with rainsplash/runoff erosion, induces

along a hillslope higher spatial heterogeneity and temporal variability in aggregate characteristics, such as size distribution and stability, relative to more established and stable grassland systems [Van Oost et al., 2000; Rieke-Zapp and Nearing, 2005; Kuhn et al., 2009; Abaci and Papanicolaou, 2009; Stavi and Lal, 2011].

CHAPTER 3. ENRICHMENT RATIO EXPERIMENTS

3.1 Experimental Design and Reasoning

Chapter 2 of this dissertation highlighted the need for developing a landscape oriented approach to capture the spatial heterogeneity and temporal variability of SOC stocks within IMLs, which has been enhanced by redistribution from rainsplash/runoff erosion. To provide estimates of SOC fluxes transported along a downslope due to rainsplash/runoff erosion, it is essential to know not only how much material is eroded but also which fractions are mobilized, respective to the carbon composition, and how this selective transport enriches the eroded material. To address these fundamental questions, as well as to understand better the role that management and landscape position have on enrichment ratio (ER) dynamics within IMLs, a series of rainfall simulation experiments were conducted to capture runoff, sediment, and carbon fluxes from experimental plots, which were analyzed for their size fraction availability and carbon contents. These experiments not only promote our fundamental understanding of the dynamics of top soil SOC redistribution but also provide some guidance about aggregate proxy measures such as aggregate size distribution and stability (Chapter 4), as well as help us identify the key processes that affect the differential modes of soil erosion including aggregate mobilization. The latter information is lacking and is used here to provide crucial data for developing an improved ER modulation that can simulate selective size fraction mobilization and active layer updates to more accurately simulate changes in SOC stocks by incorporating the aforementioned landscape processes (Chapter 5).

3.1.1 Study Site Selection

As mentioned in Chapter 1, this study is conducted in southeastern Iowa, within the 270-km^2 Clear Creek watershed, which is part of the Intensely Managed Landscapes Critical Zone Observatory network (http://criticalzone.org/iml/about). Clear Creek can be divided into three distinct zones: (i) an upland, eroding zone with steep slopes that is located in the headwaters; (ii) a transfer zone where the stream begins to widen due to higher lateral contributions; and (iii) a lowland, depositional zone where the system begins to dissipate and gradients flatten out [Figure 3.1].

Mollisols and Alfisols are the dominant soil orders found in the watershed and the most common soil associations are the Tama-Downs, Fayette-Downs, and Colo-Nevin-Nodaway associations (Dideriksen et al. 2007). Tama-Downs and Fayette-Downs soils are both upland associations that are well drained, while the Colo-Nevin-Nodaway soils are formed in either stream terraces or flood plains and the drainage class ranges from poorly drained to moderately well drained (Highland and Dideriksen 1967). Moving downstream, the dominant soil texture changes from silty clay loam in the headwaters to a silt loam near the mouth of Clear Creek.

Daily temperatures reach an average high of 30°C in July, while daily low temperatures drop to -10°C in February. Average annual precipitation is approximately 880 mm/year with convective thunderstorms prominent in late spring and summer and snowfall in the winter [Iowa Environmental Mesonet, 2015].

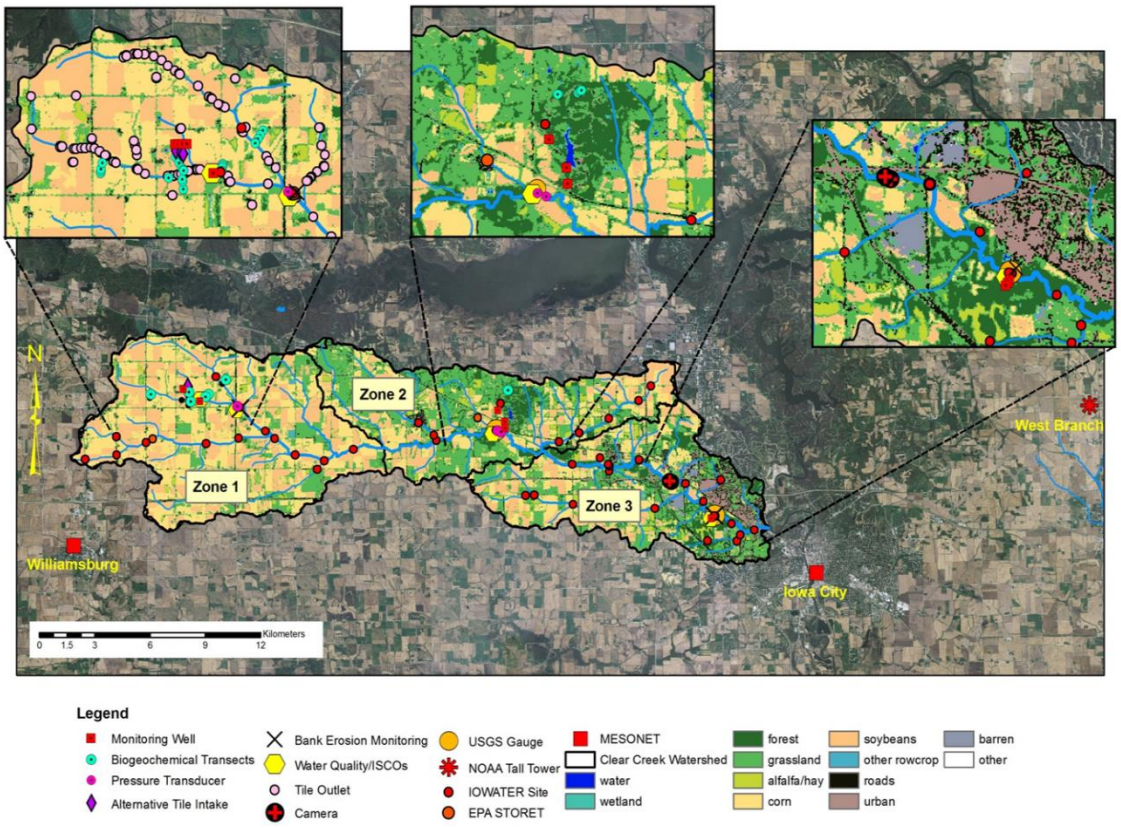

Figure 3.1 Clear Creek watershed

A total of 4 study sites were selected within Clear Creek where the ER rainfall simulation experiments were performed. Sites were selected to be representative of hillslope gradient, curvature, texture, and management practices, which included corn-soybean rotations under conservation tillage, as well as a restored grassland prairie. Study sites under agriculture (i.e., Sites Z1-P1; Z1-P3; Z1-P4) consisted of a 3-yr crop rotation of corn-corn-soybeans (C-C-B), with anhydrous fertilizer applications being applied in late fall followed by conservation, reduced, ridge tillage in the spring before the corn planting. The grassland site (Z2-P2) is a restored prairie, with a 5-yr burn frequency. It has been out of ag-production for over two decades.

Within each study field, hillslope flow pathways were first identified using geospatial analysis to determine experimental locations along a downslope and ensure connectivity between hillslope elements. Site Z1-P1 is located at a midslope section (6.5% gradient) with contour ridge tillage oriented *perpendicular* to flow pathways. Site Z1-P3 is also located at a midslope (8.4% gradient), with light contour tillage oriented *parallel* to flow pathways. Site Z1-P4 is located at the toeslope section (2.5% gradient). It is downslope of Site Z1-P1. Site Z2-P2 is found within a midslope section with a gradient of 15.4%. A summary of experimental conditions of the plots is provided in Table 3.1. Figure 3.2 provides a snapshot of each of the study sites.

Table 3.1 Enrichment ratio experiment study site characteristics

Parameter	**Site Z1-P1**	**Site Z1-P3**	**Site Z1-P4**	**Z2-P2**
Management	Contour, reduced strip tillage. Plot oriented perpendicular to flow pathways	Reduced strip tillage. Rows perpendicular to flow direction	Contour reduced tillage. Rainfall simulators oriented parallel to rows.	Restored prairie grassland
Hillslope Location	Midslope	Midslope	Toeslope	Midslope
Canopy Height (cm)	3	2.5	3	7
Slope (%)	6.5	8.4	2.5	15.4
Surface Cover	Dense cover of corn litter within rows	Medium cover of corn litter	Sparse corn litter within rows	Patchiness of vegetation, mixture of live and dead grasses
Rainfall Intensity (mm/hr)	60	60	60	60
Topography	Large oriented roughness and mallow soil from spring cultivation.	Large oriented roughness and mallow soil from spring cultivation. Interrow provides preferential network for flow development	Oriented roughness much less than upslope sections. The line of planted crops causes initial conduit for material to transport.	Localized depression present in top section of the plot.
Experiment Duration	150 min (3:10 to 5:40 pm)	105mins (1:05-2:50pm)	107mins (3:33 to 5:20pm)	110mins (11:40 to 1:30pm)
Key Features of the experiments	-Water accumulation occurs in small depressions between rows. -A sequence of steps and pools formed as the network began to connect. -Splash erosion is the dominant process.	-Runoff achieved almost immediately. -Large amounts of litter were transported (about 60%)	-Runoff achieved almost immediately. -Sparse litter transported during the test. -Looking upslope, the right hand row of corn had much higher flow than left row due to gradient. -Interrill areas appeared to feed rills.	-Vegetation patches promoted depression storage.

Figure 3.2 Enrichment Ratio (ER) experimental study sites

3.2 Enrichment Ratio Experiments: Methodological Considerations and Design

The design of the enrichment ratio (ER) experimental work is presented below, focusing first on the construction of the experimental plots. This is followed by a description of the sampling protocol, which discusses first the static sampling (*in situ*) performed before the rainfall was applied, followed by the dynamic sampling, which involved collecting the runoff and sediment fluxes while the rainfall was applied. Lastly, the characteristics of each experimental plot are described.

3.2.1 Experimental Plot Construction

At each sampling site, plots were constructed over a 2 to 3 day period to determine ER values [Figure 3.3]. These experimental plots had a width of 2 m and a downslope length of 7m, which defined the effective area that was impacted by the supplied rainfall from 3 Norton Ladder Multiple Intensity Rainfall Simulators [Norton, 2006] set in series over the plot. The simulators provide rainfall through a series of oscillating VeeJet type nozzles. These nozzles have been calibrated to provide natural distributions of raindrops observed in Iowa [Elhakeem and Papanicolaou, 2009]. Figures 3.4 & 3.5 provide example photos showing the layout of the enrichment ratio experiments.

At the outlet of each plot, a wooden weir, with side boards was installed to direct the runoff and sediment to a V-notch weir. The V-notch weir had a 20° angle opening to facilitate measurement of the runoff during the experiments. A high-resolution ruler was attached to the weir to read corresponding flow depths. The flow depths were used to quantify the flow discharge with a calibration-equation from Brater [1996] for a V-notch weir.

A large, 1500-gallon storage tank and a system of gas-powered, water pumps supplied water to the rainfall simulators. Water was supplied from a mixture of local fire departments, municipal facilities, or local farmers based on practicality and closeness to study sites. A series of gas generators were needed to supply power, because the plots were located in the middle of the fields far from a constant power source.

A series of valves were used to adjust the water pressure to match the desired rainfall intensities. For all rainfall tests, a 60-mm/hr intensity was selected as it is

representative of a heavy thunderstorm occurring in the region. This intensity also matches the conditions for the rainfall experiments used to develop the Universal Soil Loss Equation (USLE) relation [Stone and Paige, 2003]. The rainfall intensity was kept constant during the runs to provide the same hydrologic forcing, allowing us to focus on the effects of management and hillslope position. Finally, soil moisture probes were installed within the effective area of the plots to monitor changes in moisture content throughout the experiment.

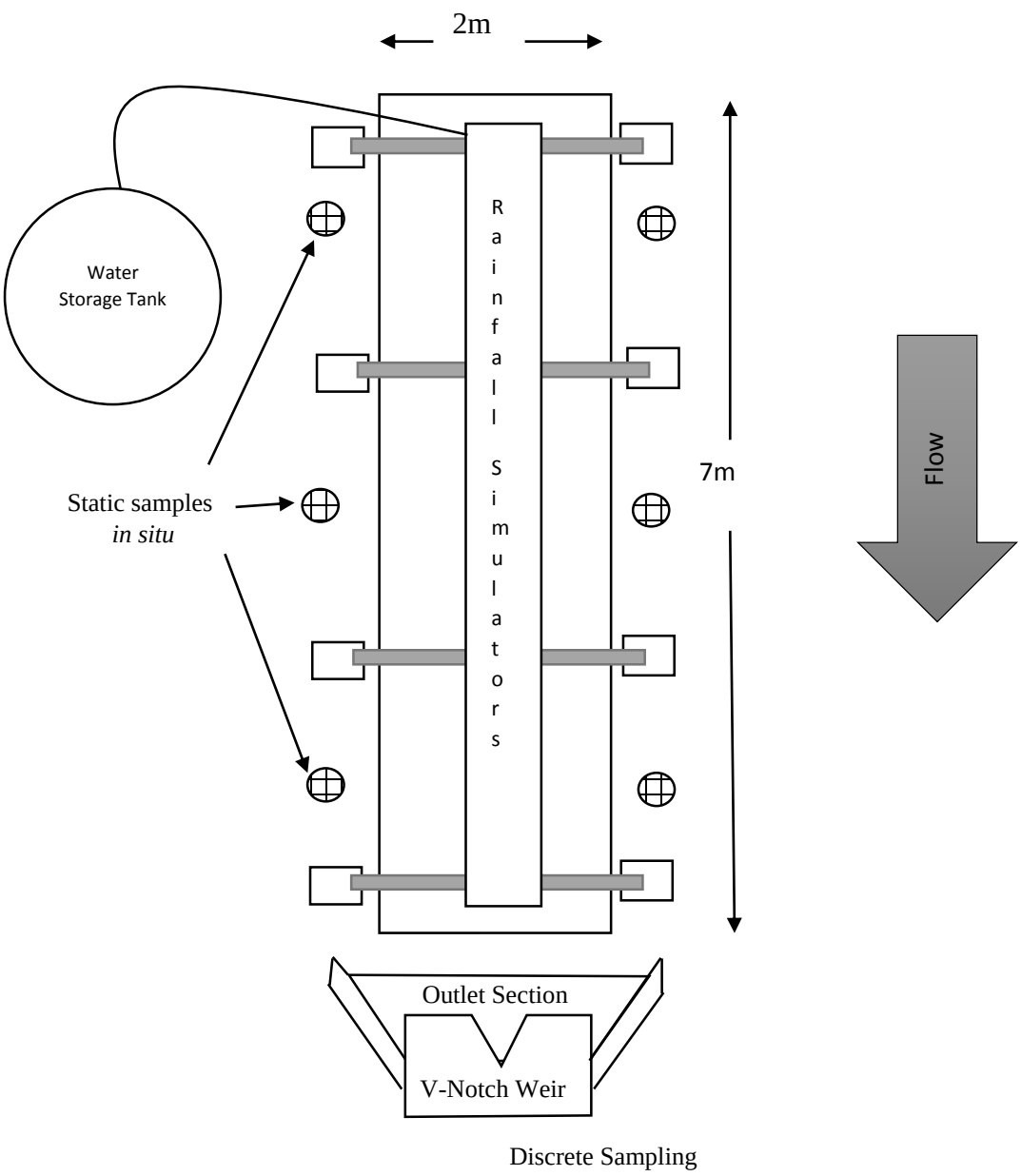

Figure 3.3 Schematic of the enrichment ratio experimental setup

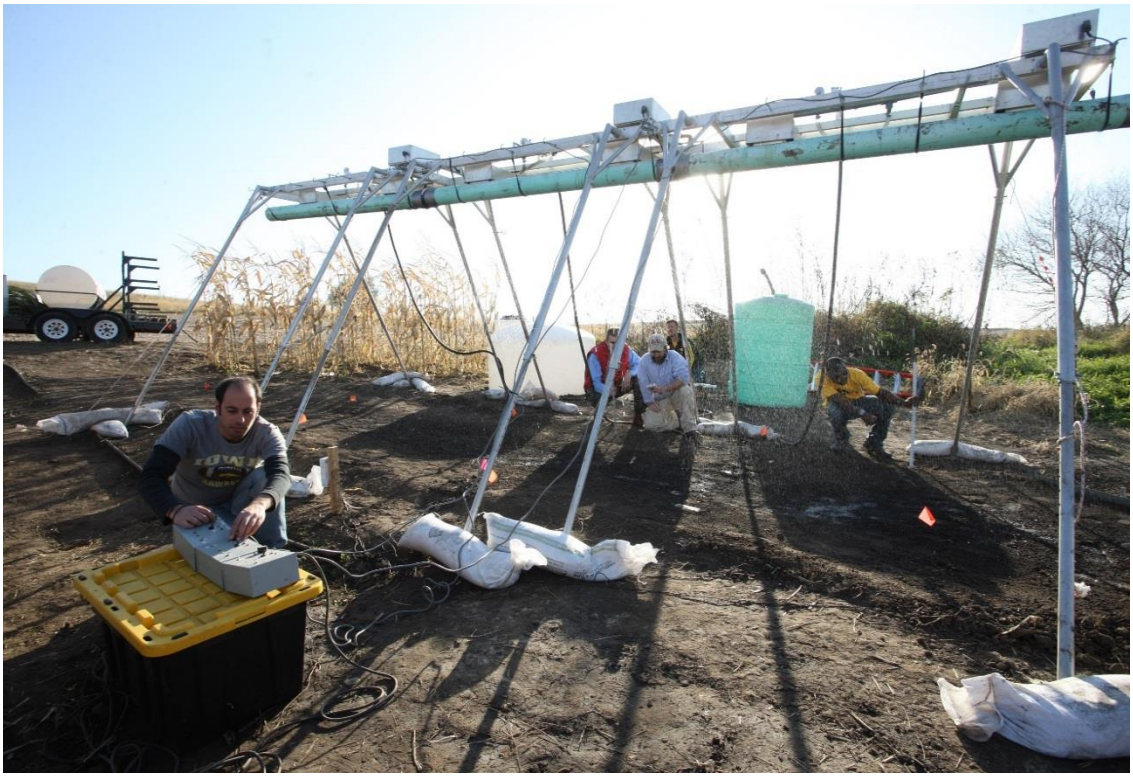

Figure 3.4 Rainfall simulators set up at an experimental plot

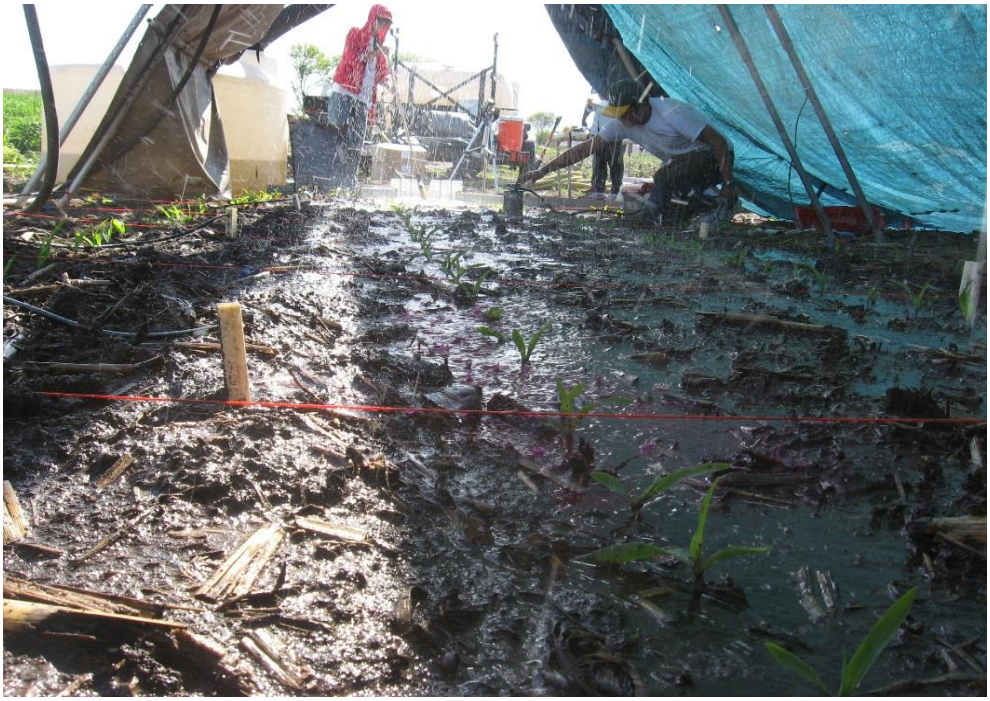

Figure 3.5 The experimental plot becomes saturated during a test

3.2.2 Static Sampling- Collection before Rainfall Experiments

Before the rainfall was applied to the plots, surface soil samples were collected to a depth of 0-10 cm just outside of the effective areas for each experimental plot to determine static properties of the in situ soil [Figure 3.3]. These samples will provide the baseline carbon content of the soils. Disturbing the effective area within the plots was avoided to prevent any artificially induced incision. The collected soil samples were brought back to the lab in a field moist state and passed initially through an 8mm sieve to remove coarse litter fractions. They were allowed to air dry over a period of 2 weeks.

The collected static soil samples were analyzed for their size distributions. First, the bulk samples were passed through a sequence of 0.25-mm and 2-mm sieves to partition it into a three distinct aggregate size classes, namely the small microaggregates, called herein the finer fractions (< 0.25mm), small macroaggregate (0.25-2.00mm) and large macroaggregate (>2.0mm) fractions, which follow the hierarchical classification of Oades and Waters [1991]. The masses of each of the size fractions were compared to the total sample mass to provide measure of size class availability [Figure 3.6].

Sub-samples from each of the size classes were collected for further particle size analysis. A sediGraph 5100 particle size analyzer [Micrometics Company] was used to determine the particle size distributions that are used to estimate the specific surface area [Figure 3.7]. The sediGraph was selected for this purpose as the sampling size was quite small (a few grams) dealing with runoff samples. Procedure steps for this analysis can be found in Appendix D [Bettis, personal communication].

In addition to particle size, the samples were analyzed for total carbon and nitrogen contents using an elemental analyzer following methods proposed by Cambardella and Elliot [1992].

Figure 3.6 Size class availability using a series of sieves. Shown here are large macroaggregate portions of the sample

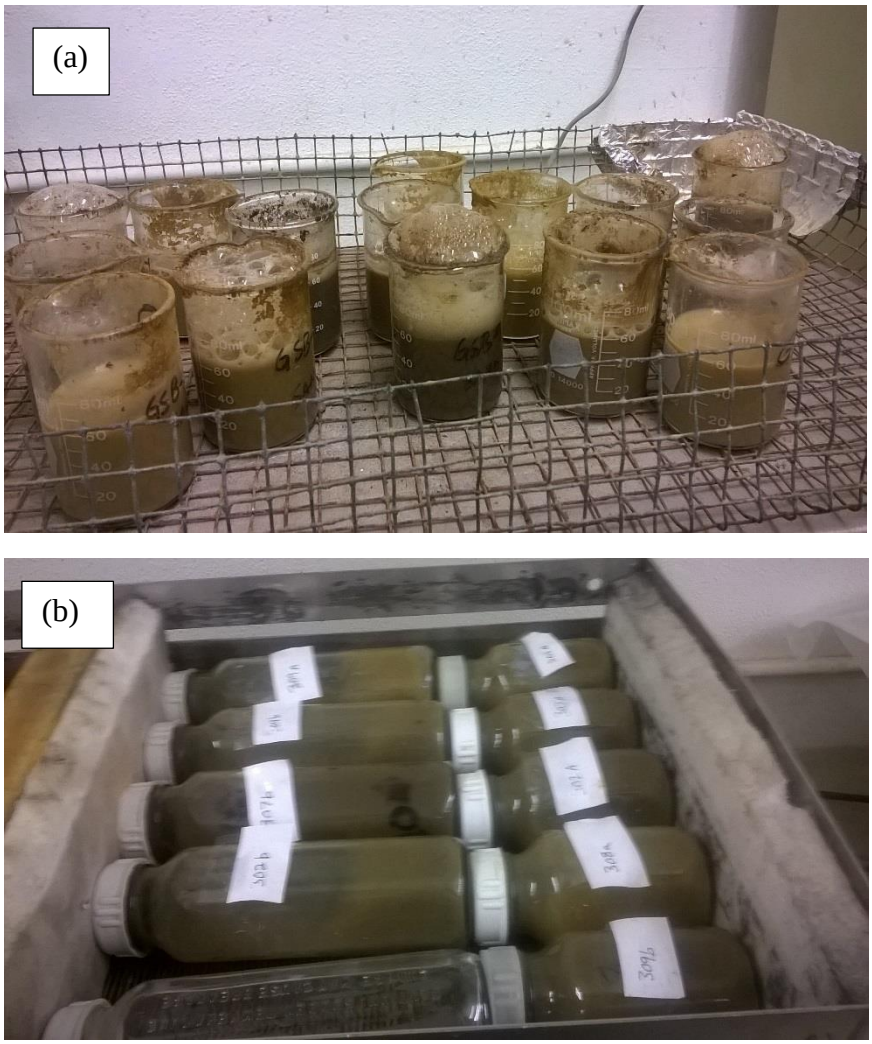

Figure 3.7 Pre-processing steps for sediGraph analysis. Here shown boiling of samples (a) and shaking table (b), both of which are used in determining particle size analysis [See full steps in Appendix D]

3.2.3 Dynamic Collection during Rainfall Experiments

Rainfall experiments were run for 2-3 hours to ensure the pseudo-equilibrated conditions were achieved for both runoff and sediment fluxes. Flow depths readings were taken at the weir at approximately 10-min intervals once runoff was generated. A sample of the runoff was collected following each flow depth reading, labeled and time-stamped. Pseudo-equilibrium for was identified when the flow depth readings became constant and the sampling continued for another 2 hours, because it was difficult to determine

equilibrated sediment concentrations directly in the field. The 2-hr time frame was based on past experiments. Once both the flow and sediment had reached a pseudo-equilibrated state, the experiment was stopped.

In the lab [Figure 3.8], the runoff-sediment samples were passed through a series of 0.25-mm and 2-mm sieves to partition the sediment into three aggregate size fractions, similar to the static *in situ* soil samples. Analyses for particle size, carbon content, and specific surface area were performed the same manner as static *in situ* samples.

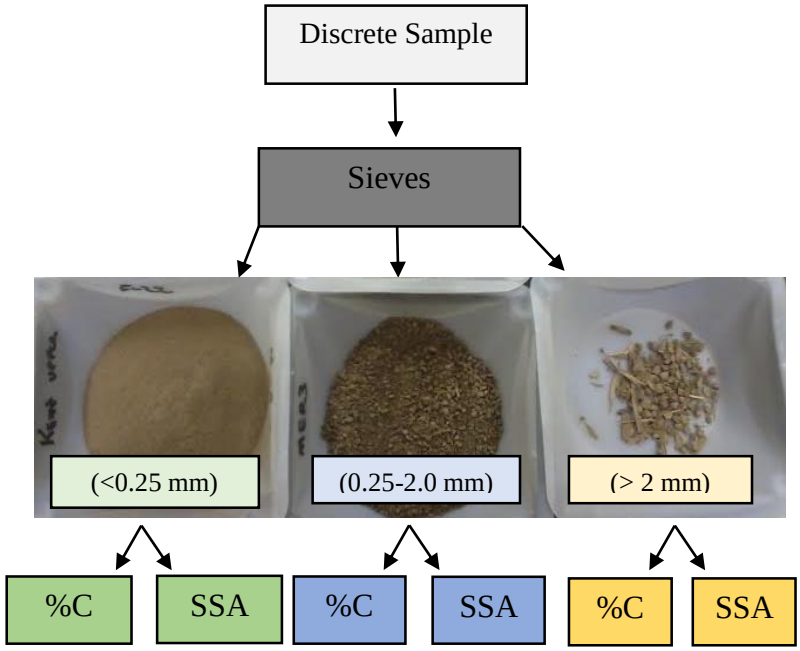

Figure 3.8 Flow chart of analysis for discrete runoff samples

3.3 Enrichment Ratio Experiment Results: Static Properties

The information gathered from the static properties and described below is used as input conditions and verification for the loosely coupled numerical framework (WEPP-CENTURY) to be presented in detail in Chapter 5. This data is also used to assess aggregate size distribution for hillslope location and management practice, which is important for understanding the functionality between aggregate proxy measures with

the 2 pre-described factors (see Chapter 4). The partitioning of the bulk samples into the aggregate size fractions (<0.25mm, 0.25-2mm, and >2mm) is summarized in Figure 3.9. In all cases, sites under agriculture are dominated by the small macroaggregates (0.25 - 2 mm). The size fractions for the midslope site with rows oriented parallel to flow pathways (Z1-P3) are skewed towards the finer fractions when compared to the other midslope site with contour tillage (Z1-P1). The differences can be explained by the added roughness controls that the ridge tillage provides which limit the preferential removal of the finer fractions [Hatfield et al., 1998]. The size fractions for the toeslope site, Z1-P4, were skewed towards the coarser fractions, which may be caused by lower gradient and the accumulation of aggregates eroded from upslope sections [Papanicolaou et al., 2015]. The grassland site Z2-P2 is dominated by large macroaggregates, followed by small macroaggregates. This may be due to longer aggregation periods from a lack of tillage disturbance [Wacha et al., 2016 In prep].

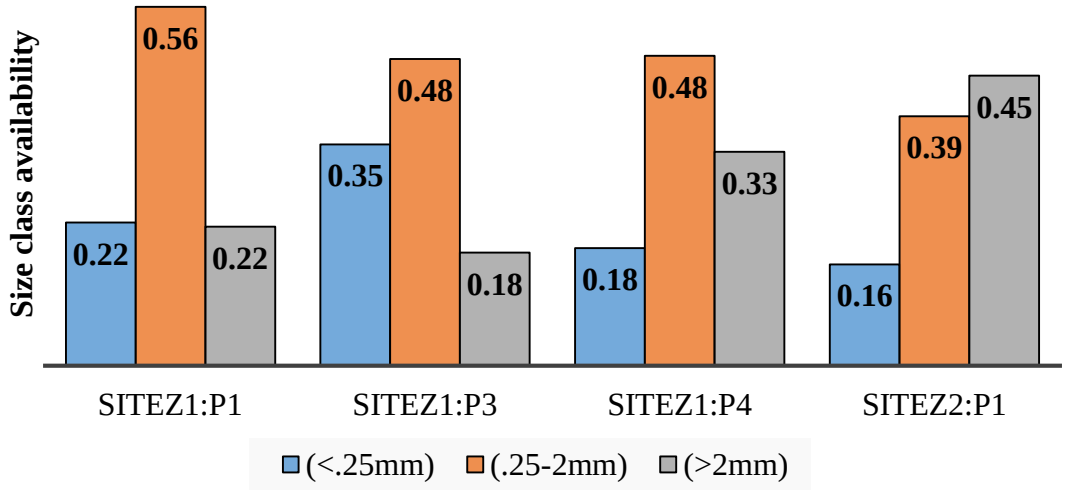

Figure 3.9 Size class availability for *in situ* soil samples

Figure 3.10 provides the SSA of the in situ soil samples. As a reminder, smaller particles have higher SSA then coarser particles [Palis, 1990; Foster et al., 1995]. Looking at the weighted averages for each site in Figure 3.10, the samples from Site Z1-P1 have the highest SSA followed by the soils from Z1-P4 and Z2-P2. The soils from Site Z1-P3 have much smaller SSA values, especially in the finer fraction (<0.25mm). This may be caused from the preferential removal of clay size particles through rainsplash. The soils from the toeslope site Z1-P4 have the highest SSA in the large macroaggregate fraction, which may be reflective of clay accumulation either within the soil aggregates or accumulation on the outside of the aggregate, reminiscent of a "snowball effect".

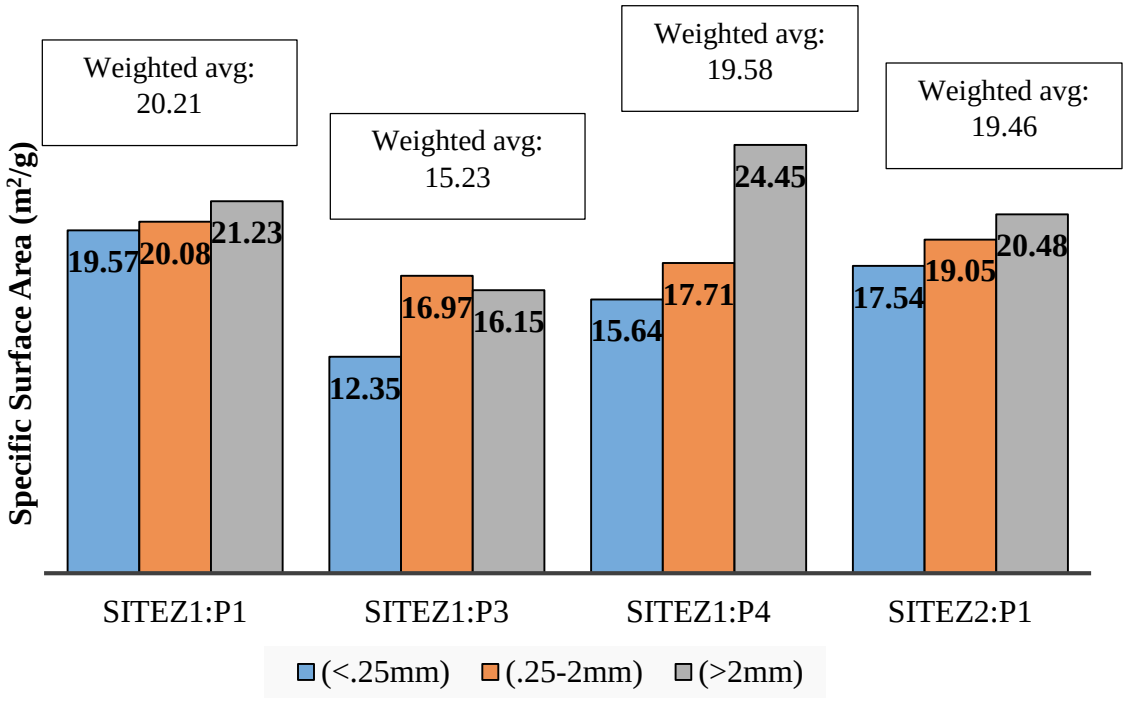

Figure 3.10 Specific Surface Area (SSA) of *in situ* soil samples

Figure 3.11 provides the carbon contents for the in situ samples. The carbon content was highest in the soil samples of restored prairie site for all size classes, while

all other sites were found to be comparable amongst themselves. Of the sites under agriculture, the soils of the toeslope site Z1-P4 have the highest carbon content, which has been found in other studies [Mabit et al., 2008; Dlugoβ et al., 2010; Du and Walling, 2011; Papanicolaou et al., 2015].

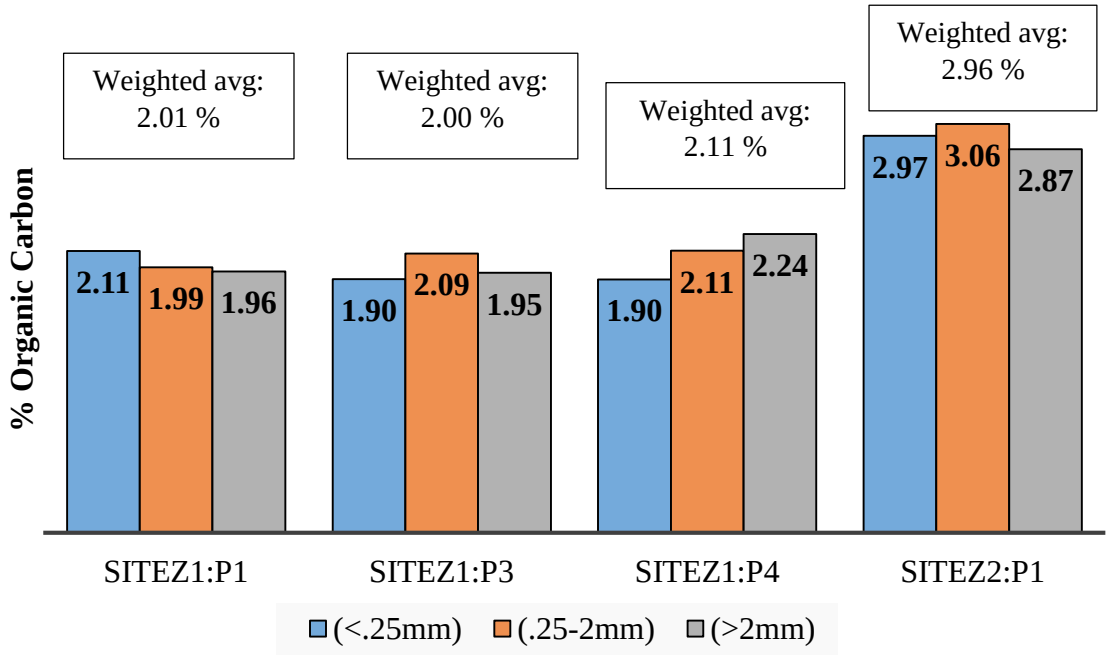

Figure 3.11 Size class availability for *in situ* soil samples

3.4 Enrichment Ratio Experiment Results: Dynamic

This section will focus on the dynamic analysis from the ER experimental plots. The analysis will be categorized as follows:

- Runoff analysis: time series are provided for: (i) weir depth readings; (ii) runoff coefficients, defined here as the ratio of runoff to rainfall; and (iii) sediment fluxes exiting the plot outlet.
- Sediment characteristics: time series are provided for: (i) size class availability; (ii) specific surface area of the various size fractions; and (iii) carbon content of each of the size fractions within each sample.
- Enrichment Ratio: time series are provided for: (i) ER values estimated using SSA relation; and (ii) ER values estimated using concentrations %C.

3.4.1 Runoff Analysis

Figure 3.12 provides the time series of weir height readings collected for all ER rainfall experiments. Highlighted in the description below are the time of runoff initiation and when flow conditions reached a pseudo-steady state.

Runoff was produced the fastest in the restored midslope grassland site (Z2-P2) after around 4 min, possibly due to a steeper gradient, which is at least double that of the other sites, limiting infiltration. The site which took the longest to produce runoff was Z1-P1 (midslope conservation), which is most likely due to the higher oriented roughness from the contour ridge tillage management It has been reported that when the rows are perpendicular to the flowpath, runoff and erosion processes are limited [Hatfield et al., 1998].

The highest flow depth was recorded at Z1-P3 (midslope conservation) at around 5 mm. Site Z1-P3 has rows oriented parallel to flow pathways, providing a longer path of unobstructed flow to promote higher runoff generation. The toeslope site (Z1-P4) had the second highest runoff depth, followed by the grassland midslope site Z2-P2. The grassland site with its established root structure would have higher infiltration and plant uptake limiting runoff. The lowest runoff was found at Z1-P1, due to previously mentioned added roughness controls by ridge tillage, which minimizes the flow pathway length and treats the hillslope as a series of steps and pools [Papanicolaou et al., 2015; Abban et al. in prep].

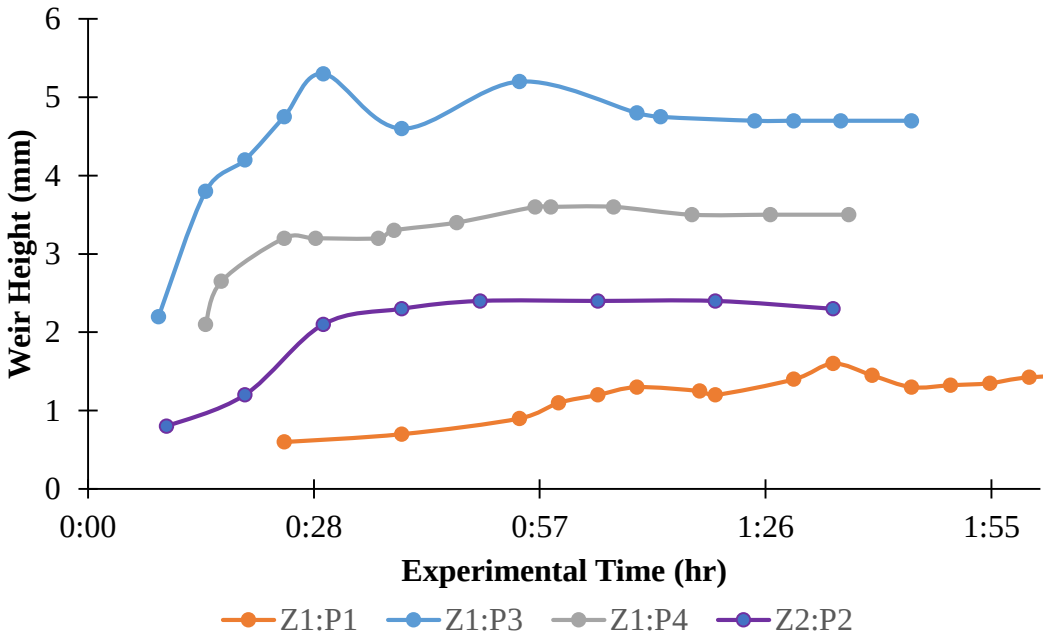

Figure 3.12 Weir height time series for experimental runs

Figure 3.13 provides the runoff coefficients for the experimental runs. When looking at the runoff coefficients at pseudo-steady state, the runoff coefficients were highest at Z1-P3 (0.52), followed by the Z1-P4 (0.20). The smallest runoff coefficients

were at the restored grassland (0.08) due to higher infiltration and Z1-P1 (0.03) due to the step-pool pattern of the ridge tillage.

The time series of the sediment concentrations in the collected runoff samples are in Figure 3.14. Highest concentrations were found at site Z1-P3, as the higher runoff volumes entrained more sediment. Site Z1-P1 had large fluctuations within the concentration values at the start of the test, which then damped by the end of the tests. The fluctuations in sediment concentration at site Z1-P1 may be caused by the contour ridges, which have high oriented roughness elements that can affect the transport of flow and sediment [Papanicolaou et al., 2015]. In the end it had similar concentrations as the toeslope site. As expected the sediment concentration and the restored grassland were the lowest due to the permanent vegetation.

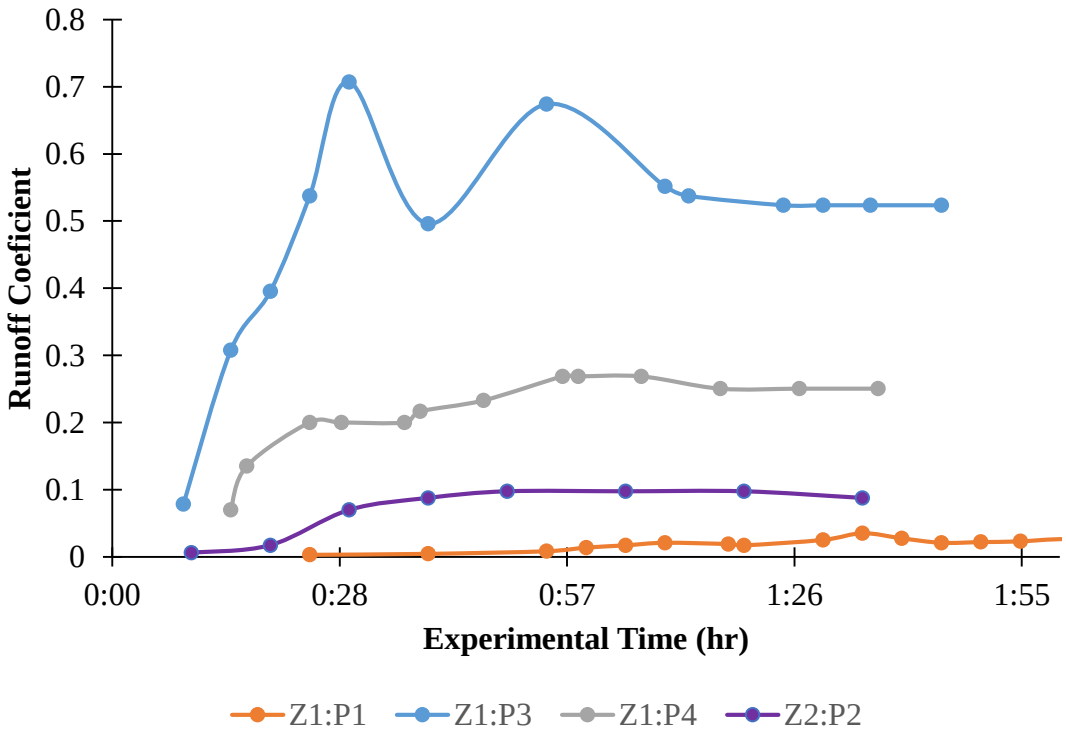

Figure 3.13 Runoff coefficient time series for experimental runs

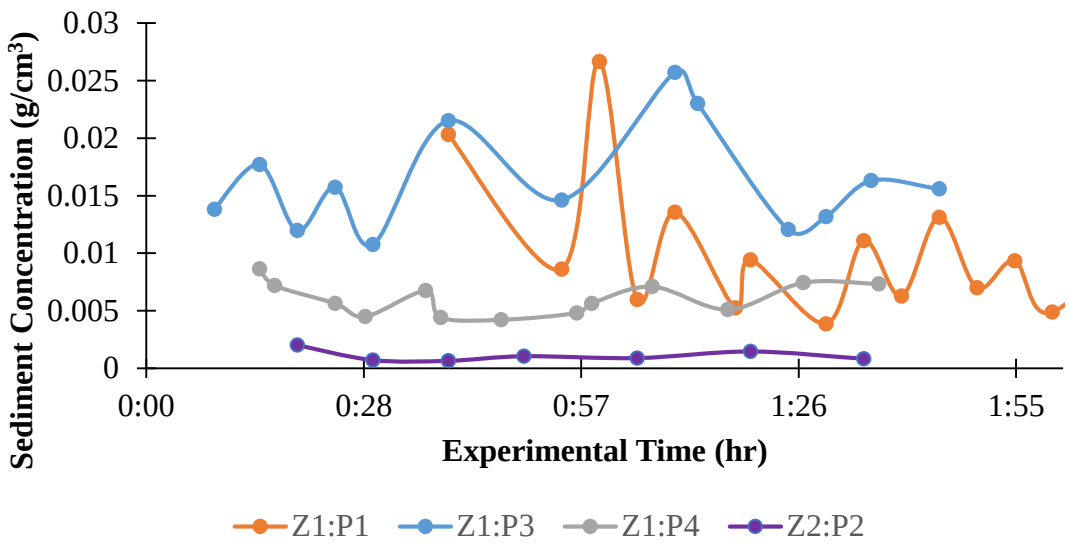

Figure 3.14 Time series of sediment concentrations in discrete samples for all experimental plots

The time series of sediment fluxes for the experiments is provided in Figure 3.15. The sediment fluxes were determined using the corresponding discharge rate at the time of collection for the discrete sample, as well as the total mass of the collected sample.

Site Z1-P3 recoded the highest sediment fluxes of all the experimental sites, as it had the highest runoff and sediment concentrations (Figures 3.12&3.13). The increased runoff generated within the Z1-P3 plot could have led to more incision taking place, reflected in the rising fluxes. Sediment fluxes peaked at a value of approximately 3500 mg/s in little over an hour. After hitting the peak, sediment fluxes declined and dipped to reach a pseudo-steady state of 2000 mg/s after 100 minutes due to either exhaustion of available material and/or a decline in sediment carrying capacity [Papanicolaou et al., 2010].

Because the fluxes in Z1-P3 were on the order of 5-10 times higher than other sites, Figure 3.15 is included to show the remaining sites. The next highest sediment

fluxes were recorded in Z1-P4 (toeslope conservation), which followed a similar increasing trend as Z1-P3, but leveling off at around 460 mg/s. The remaining sites had similar rising and leveling off trends but experienced much lower sediment fluxes. High variability in fluxes is seen in Z1- P1, as a remnant of the variable sediment concentration attributed to intermittency in material caused from the step and pool dynamics imparted by the contour ridge tillage.

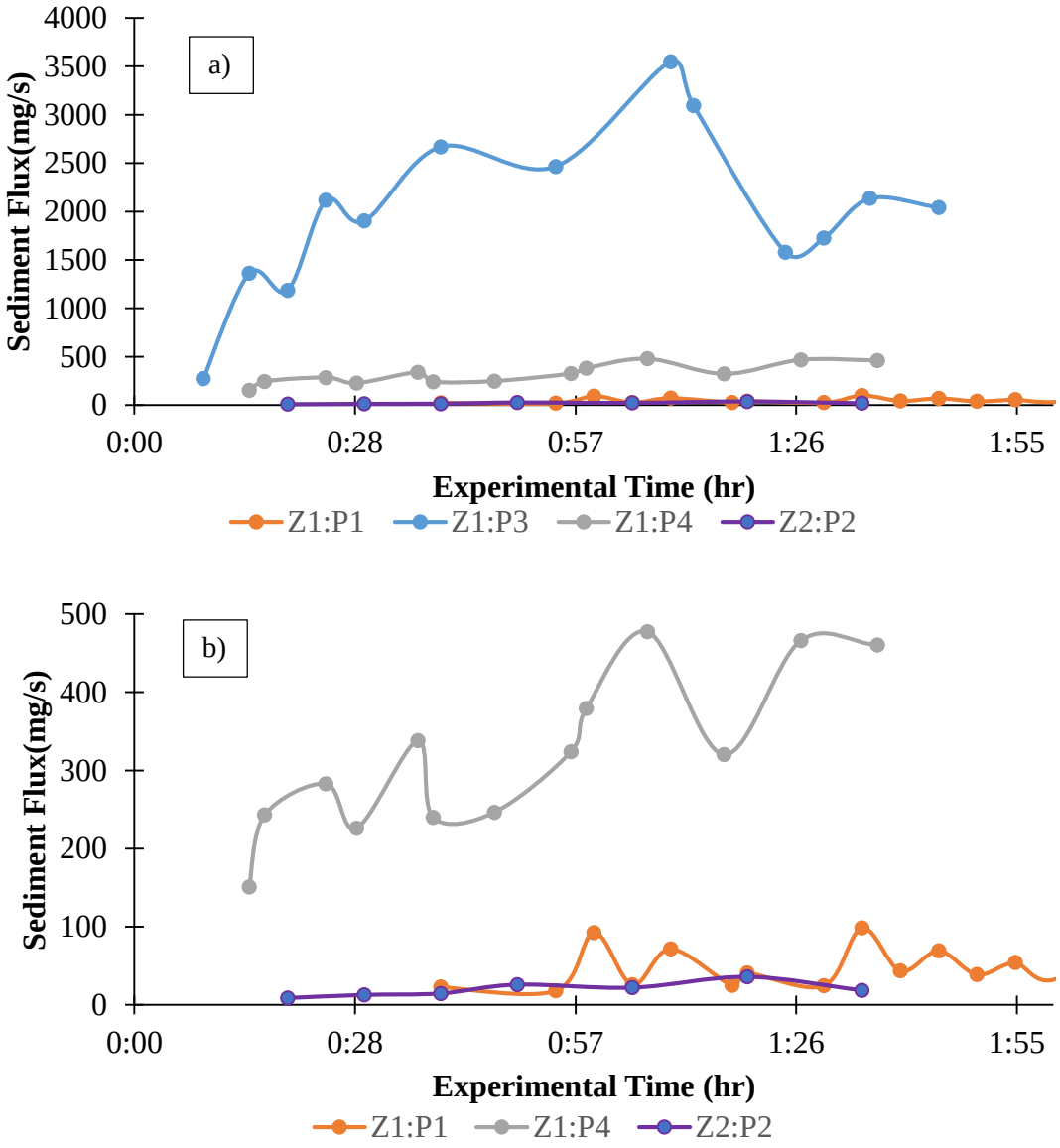

Figure 3.15 Time series of (a) sediment fluxes from all experimental plots, and (b) sediment fluxes focusing in on sites Z1-P1, Z1-P4, and Z2-P2

3.4.2 Sediment Characteristics

Further analysis was performed on the collected samples to determine size class availability within the runoff. Size fraction availability is provided for the agricultural sites, namely Z1-P1, Z1-P3 and Z1-P4; however, due to the limited masses of eroded sediment in the discrete samples collected from grassland sites, further partitioning of these samples was not possible.

3.4.2.1 Site Z1-P1 (Midslope Conservation Ridge Till)

Figure 3.16 provides three time series showing how sediment size fractions change in (a) availability; (b) specific surface area; and (c) carbon content. The x-axes in all plots denote the experimental time in hours and minutes, with the start time being the initiation of the rainfall. During the course of the experiments, the finer fraction (<0.25mm; blue) of the collected material increased in availability starting at around 40% and ending at about 64%. The small macroaggregate fraction (0.25-2mm; orange) decreased throughout the experiment. Large macroaggregates (>2mm; grey) are found in the first sample.

A sharp fluctuation is seen at 1:40, where the fine fraction of the sediment approaches 80%. This corresponds with a sudden increase in the sediment flux (plotted with a yellow line and using the right hand, secondary axis), possibly due to the intermittency of flow and material caused by the contour ridge tillage, which forces the runoff and sediment through a series of steps and pools. Fluctuations in availability may also be attributed to the breakdown of aggregates due to raindrop impacts, which exposes finer material to entrainment by flow. Note the difference in sediment fractions

compared to the static in situ samples collected near the plot (22%-fines, 56%-small macroaggregates, 22%-large macroaggregates).

The specific surface area (SSA) of the size fractions are shown in Figure 3.16b. SSA values for the finer fraction (blue) are around 21 m^2/g at beginning of the test, but increase to around 35 m^2/g after an hour and then decrease to around 15 m^2/g. For the small macroaggregates (orange) SSA values rose similarly from 26 to 32 m^2/g during the beginning of the test and then decreased to values around 15-20 m^2/g. The SSA values for the large macroaggregates (grey) are much larger than the other size fractions as they begin around 87 m^2/g during the first portion of test and then hit a maximum of 94 m^2/g after an hour of testing. The weighted average of SSA values from the *in situ* static samples was approximately 20 m^2/g, which is show as the black dashed line in Figure 3.16b.

The carbon content (%C) of the size fractions are shown in Figure 3.16c. In general, the %C was highest in large macroaggregates (grey), followed next by small macroaggregates (orange). The finer fraction had much less %C than the larger aggregate fractions. Over the course of the event, the %C for the finer fraction stays rather consistent, starting at an initial peak value of 2.18%, and then leveling off around 1.91%. The %C of the small macroaggregates decreased linearly throughout the experiment, starting at 3.77% and ending at 3.29%. The %C of the large macroaggregates were notably higher with initial values over 4.00%. The %C of the in situ soil collected near the plot averaged around 2%, thus showing the level of enrichment due to the selective entrainment.

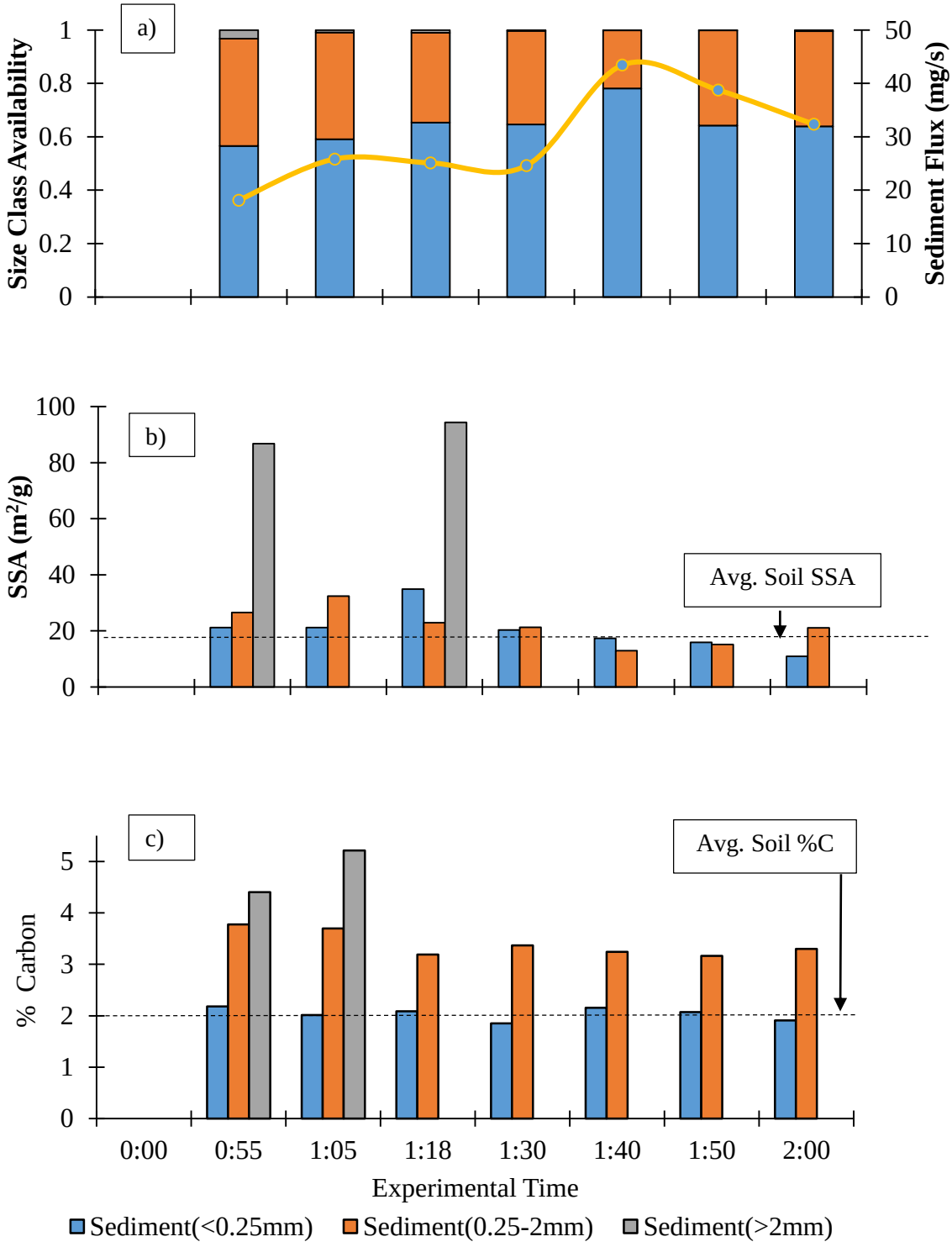

Figure 3.16 Z1-P1 time series of how sediment size fractions change in (a) availability; (b) specific surface area; and (c) carbon content

3.4.2.2 Site Z1-P3: (Midslope Conservation, No Ridges)

Figure 3.17a provides the time series of size fraction availability within the collected samples, as well as the sediment fluxes for site Z1-P3. This site had both higher runoff and sediment fluxes than the other sites, which translated to the general movement of all three aggregate size fractions experimental run. The higher runoff conditions provided the extra energy needed to move the coarser material. This is best seen with the sediment fluxes which were nearly 50 times higher than the other midslope site with ridge tillage, Z1-P1.

The finer fraction (blue) comprised around 59% of the initial samples, and decreased to around 56% as the larger fractions were entrained in the increasing sediment fluxes. The small macroaggregate fraction of these samples (orange) stayed consistent around 38%, with the highest availability correlated to the peak sediment flux of 3000 mg/s at 1:13. The large macroaggregate (grey) availability hovered around 5-7% of the sample. There was a marked difference in sediment fractions compared to the static in situ samples collected near the plot (35%-fines, 48%-small macroaggregates, 18%-large macroaggregates) with an increase in the finer fraction and decrease in the larger fractions, which reflects the breakdown of the larger aggregates and selective entrainment of the finer fractions.

The specific surface area (SSA) of the size fractions are shown in Figure 3.17b. SSA values for the finer fraction (blue) have a general increase throughout the experiment, starting around 12 m^2/g and ending at 18 m^2/g. The small macroaggregate (orange) SSA values remained rather consistent around 19 m^2/g, with the exception of the sample collected at 1:25. The SSA values for the large macroaggregate fractions were

larger than the other size fractions. An extreme case is seen in the first sample where the SSA was over 256 m^2/g. Aside from that extreme value, the SSA values increased to around 65 m^2/g and then decreased back to 27 m^2/g during the test. The weighted average of SSA values in the *in situ* static samples was much less, averaging 15 m^2/g, which is shown as the black dashed line in Figure 3.17b.

The carbon content (%C) of the size fractions are shown in Figure 3.17c. The carbon contents were only slightly higher in the larger aggregate fractions compared to the finer fraction, which is different from what was observed at site Z1-P1, where the larger aggregate sizes had considerably higher values. The time series of the %C for the finer fraction declined consistently throughout the test (2.25% to 1.86%), except for a punctuated sharp increase to 2.78% at 1:13, corresponding to the peak sediment flux. The %C values of the small macroaggregates decreased throughout the first hour of the experiment (2.48% to 1.48%), and then increased to a maximum 3.29% at the 1:13 mark when sediment peaked, while the %C values of the large macroaggregates decreased throughout the test to an end value of 2.41%, which was equivalent to the small macroaggregate %C value. The %C of the in situ soil collected near the plot averaged round 2.00%, which was also seen in Z1-P1.

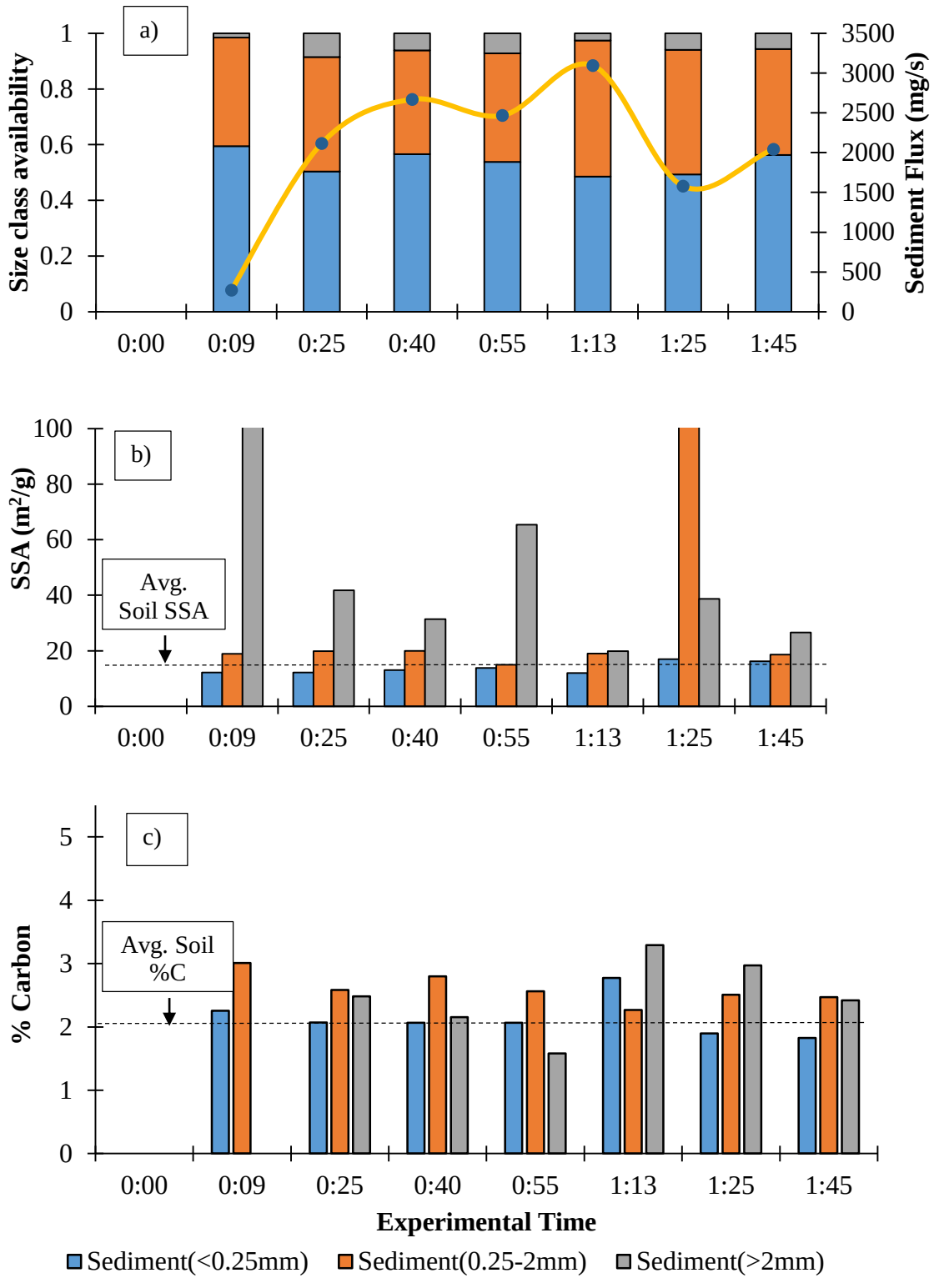

Figure 3.17 Z1-P3 time series of how sediment size fractions change in (a) availability; (b) specific surface area; and (c) carbon content

3.4.2.3 Site Z1-P4: (Toeslope Conservation)

Figure 3.18a provides the time series of sediment fraction availability and sediment fluxes for those samples collected at site Z1-P4. The finer fraction (blue) consistently comprised 53-56% of these samples, with fluctuations found throughout the experimental run. The small macroaggregate fraction (orange) increased throughout the first half of the test to a value of around 50%, and then decreased as the sediment fluxes increased with a final value of 43%. The availability of large macroaggregates (grey) were much less at this toelsope site, with initial values around 2% and then dropping off to negligible values. Again, these availabilities are starkly different from the static in situ samples collected near the plot (18%-fines, 48%-small macroaggregates, and 33%-large macroaggregates) following the similar pattern of the other agricultural sites, namely the breakdown of the larger aggregate sizes and increase in the finer fractions.

The specific surface area (SSA) of the size fractions are shown in Figure 3.18b. The SSA for the finer fraction (blue) portion of these samples increased during the first portion of the experiment, starting around 16 m^2/g and reaching 22 m^2/g, but then dropped to 12 m^2/g at the time of the peak sediment flux (478 mg/s). SSA values for the finer fraction then increased to a final value of 24 m^2/g. The SSA values of the small macroaggregates (orange) slightly increased during first part of the test and then leveled off to values around 25 m^2/g; however, the final value dropped to 12 m^2/g. The SSA values for the large macroaggregate fractions were found only in the first collected sample with an extreme value of 54 m^2/g. The weighted average of SSA values from the *in situ* static samples were comparable to Z1-P1, averaging 20 m^2/g, which is show as the black dashed line in Figure 3.18b.

The carbon content (%C) of the size fractions are shown in Figure 3.18c. The carbon contents were higher in the larger aggregate fractions compared to the finer fractions, which is the similar trend found at site Z1-P1. The % C for the finer fraction rose initially from 2.63% to 2.84%, and then declined consistently to an ending value of 2.25%. The %C values of the small macroaggregates were also shown to decrease throughout the test from 3.50% to 2.96%. The %C values of the large macroaggregates decreased as well from 3.74% to 2.85%. In comparison, the %C values of the *in situ* soil collected near the plot averaged around 2.11%, which was higher than upslope positions, a trend that has been reported in other agricultural studies [Papanicolaou et al., 2015].

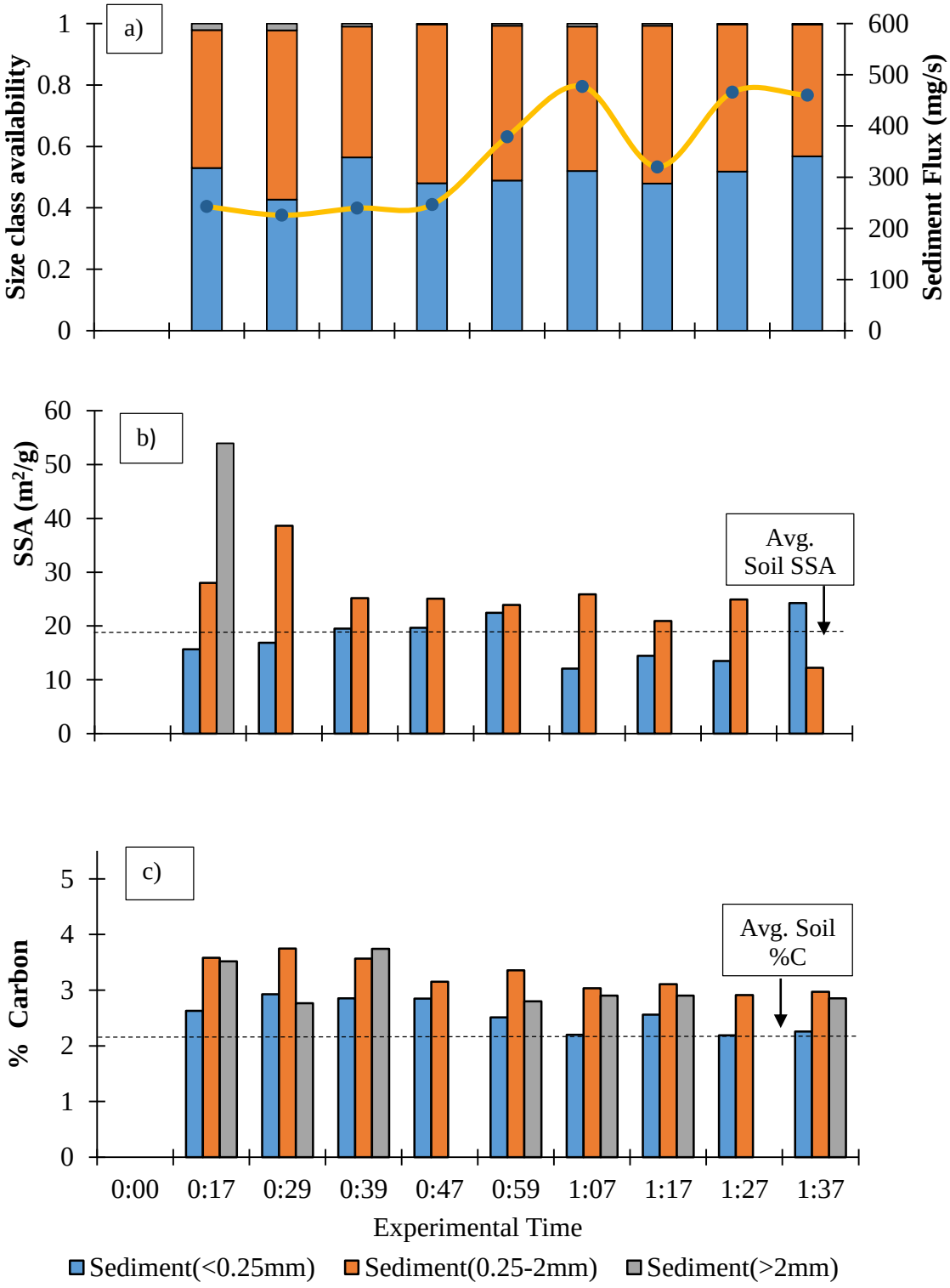

Figure 3.18 Z1-P4 time series of how sediment size fractions change in (a) availability; (b) specific surface area; and (c) carbon content

3.4.2.4 Site Z2-P2: (Midslope-Restored Grassland)

Figure 3.19a provides the time series of changes in specific surface area and sediment fluxes for the samples collected at site Z2-P2. SSA values for the sediment decreased slightly as the experiment progressed, from 32 m^2/g to 29 m^2/g. Decreases in the SSA of sediment were seen as the sediment fluxes peaked at approximately 35 mg/s around 1:20. For comparison, the SSA of the static in situ soil samples was 19 m^2/g, shown with the black dashed line in Figure 3.19a. The carbon content (%C) of the sediment is shown in Figure 3.19b. Looking at the time series, the %C rose initially to 5.80% and 6.00% during the first half hour of the test, and then sharply dropped to 2.66%, before leveling off at around 4.32%. The higher %C values were seen with the lower sediment fluxes. The %C of the *in situ* soil collected near the plot averaged around 2.96%, which was higher than ag-production sites.

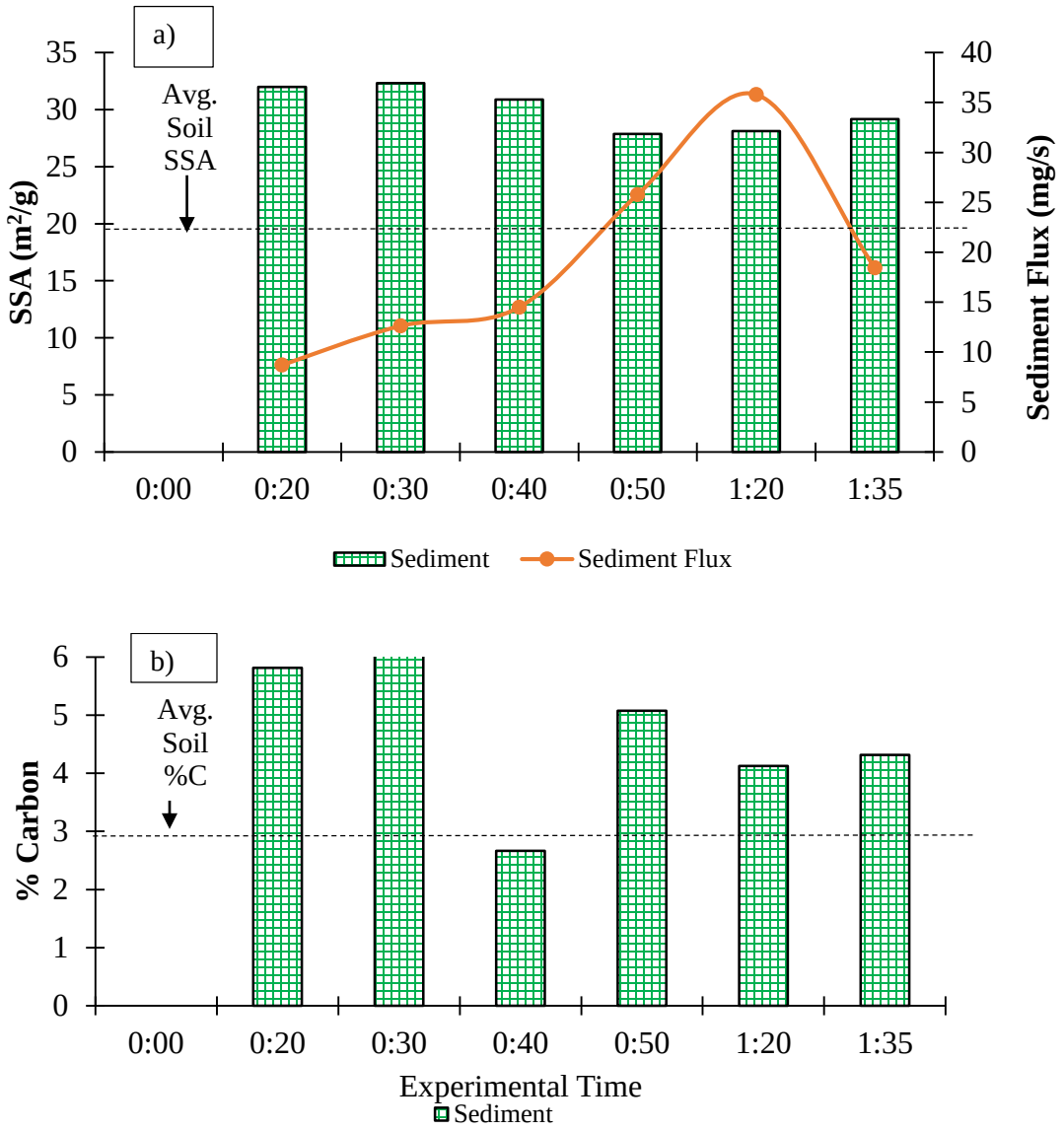

Figure 3.19 Z2-P2 time series of sediment changes in (a) specific surface area and (b) carbon content

3.4.3 Enrichment Ratio

The time series of enrichment ratio values from the rainfall experiments are presented below. Each study site has a separate figure displaying the ER values estimated using the specific surface area and the %C of the various size fractions seen above. A weighted average for the ER is also plotted (shown as black crosses in the

figures below) that considers the availability of the size fractions. As a reminder, ER values greater than 1.00 (unity) suggest the samples are enriched in carbon.

3.4.3.1 Site Z1-P1 (Midslope Conservation Ridge Till)

Figure 3.20 provides the ER time series for site Z1-P1. Using first the SSA of the collected samples (Figure 3.20a), the finer fraction (blue) was more enriched (>1.00) during the first part of the test. The enrichment then decreased considerably to an ER of 0.55. This decrease in ER corresponded to the peak sediment fluxes around 1:40. The ER values of the small macroaggregates (orange) followed a similar trend as the finer fraction, but for the most part were higher. The large macroaggregate fractions had extremely high ER values, which were 3-4 times higher in most cases. Overall, the weighted ER values using SSA increased during the first portion of the test and then decreased to a consistent value around 0.75.

Using the %C, the ER values of the finer fractions (blue) remained relatively unchanged throughout the experiment, slightly declining from ~1.0 to 0.90 (Figure 3.20b). The ER values of the small macroaggregates (orange) also declined throughout the test, from 1.90 to 1.66. With the large macroaggregates (grey), the ER values at the beginning of the test were around 4.0. In summary, the weighted ER using %C showed a decrease as the experiment progressed, with initial values of 1.42 and a final value of 1.17.

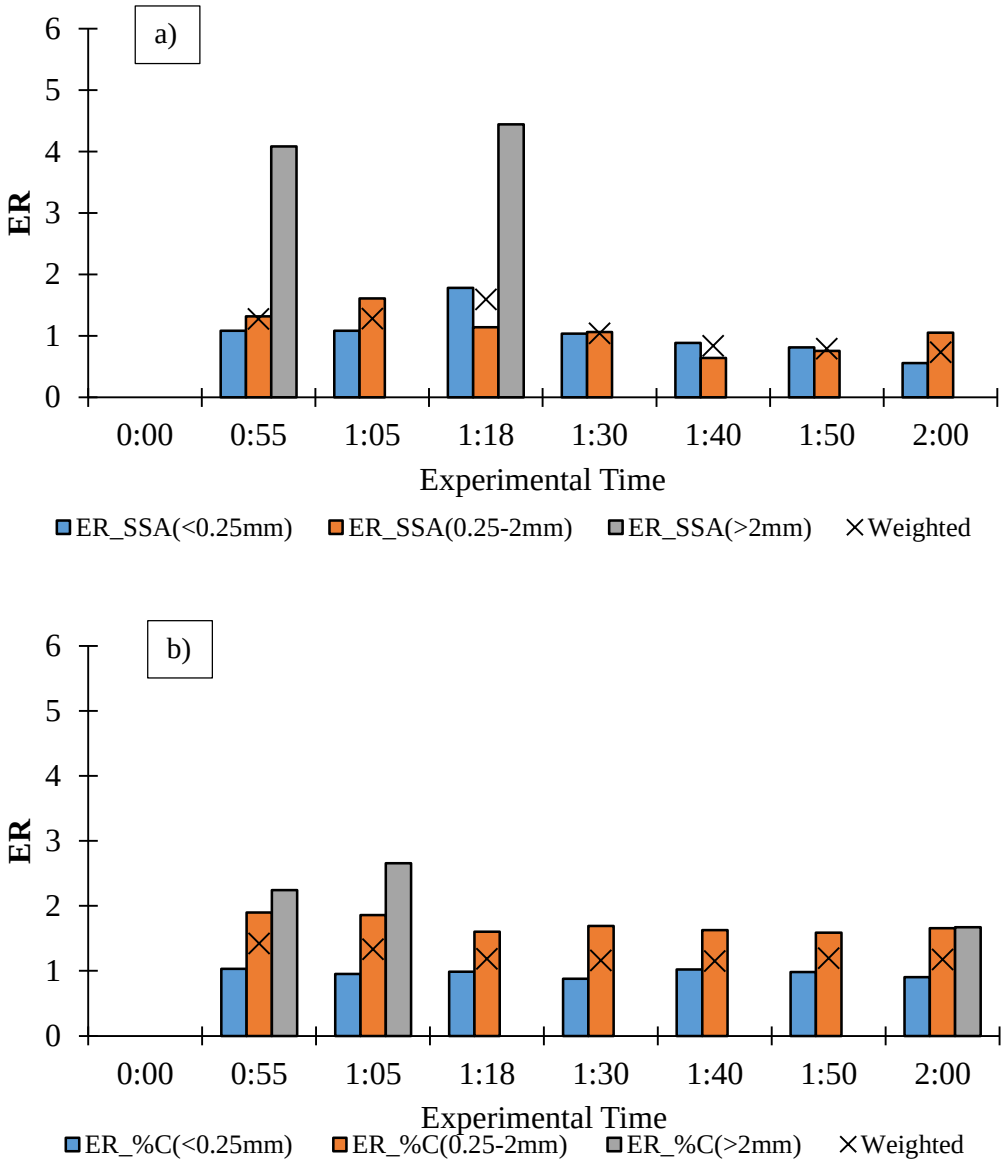

Figure 3.20 Time series of ER values from site Z1-P1 calculated with (a) specific surface area and (b) carbon content

3.4.3.2 Site Z1-P3: (Midslope Conservation, No Ridges)

Figure 3.21a shows the ER time series for site Z1-P3 using SSA (Figure 3.21a). For this case, the finer fraction (blue) became more enriched as the experiment progressed, starting off with values below unity and ending with a value of 1.3. The small macroaggregates (orange) for the most part also remained constant throughout the experiment around 1.10; however, there was an extreme ER value over 12 at 1:25, which has and ER (value not shown to keep axis same). The large macroaggregates (grey) had highly variable ER values, ranging between 1 and an extreme value of 15 (not shown on axis), ending with a value of 1.64. Excluding the extreme ER value at 1:25, the weighted ER values using the SSA (black crosses) were relatively consistent throughout around 1.25.

With the ER values determined using the carbon contents (Figure 3.20b), the values for the finer fraction (blue) declined slightly throughout the test from 1.18 to 0.96. The ER values of the small macroaggregates (orange) were generally higher than finer fractions, but they similarly decreased throughout the test from 1.43 to 1.18. The ER values of the large macroaggregates (grey) decreased during the first part of the test (1.27 to 0.87), and then spiked to 1.69 at the 1:13 mark, before decreasing to 1.24. The weighted ER values using %C followed the same trend as the finer and large macroaggregate fractions with initial values of 1.27 and ending at 1.06.

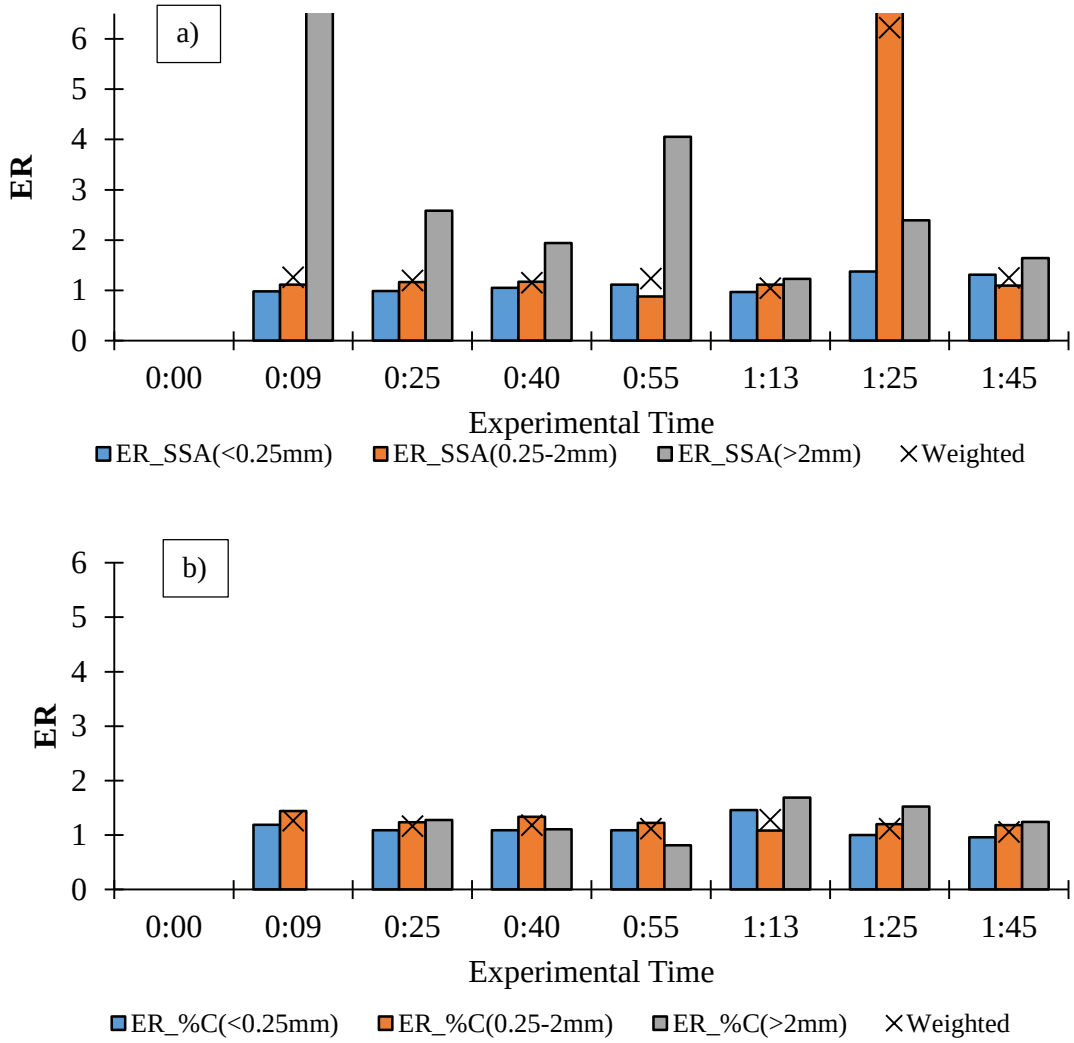

Figure 3.21 Time series of ER values from site Z1-P3 calculated with (a) specific surface area and (b) carbon content

3.4.3.3 Site Z1-P4: (Toeslope Conservation)

The ER time series for site Z1-P4 using the SSA is in Figure 3.22a and the values for the finer fraction (blue) ER increased from 1.0 to 1.43 during the first hour of the experiment, but then dipped below unity (0.77). The values then increased to 1.55. The small macroaggregates (orange) in all samples had higher ER values than the finer fractions. The ER values increased to 2.18 during first half hour the test and then declined to 1.40 before dropping off to a low point of 0.69 at the end of the test. The one

sample of the large macroaggregates for this test had ER value of 2.20. The weighted ER values using SSA (black crosses) increased to 1.66 during first half hour of the test and then decreased to an average value around 1.18.

For the ER values using %C (Figure 3.22b), the values for all size fractions increased during the first 40 minutes of the test and then declined for the remainder of the test. The finer fractions (blue) ER values increased to 1.50 and decreased to 1.19, while the small macroaggregates (orange) ER values, which were the highest at this site, increased to 1.77 and ended at 1.41. The ER values of the large macroaggregates (grey) peaked at 1.67 and declined to 1.28. The weighted ER values using %C followed the same trend as the size fractions, hitting a maximum of 1.66 and leveling off at 1.28.

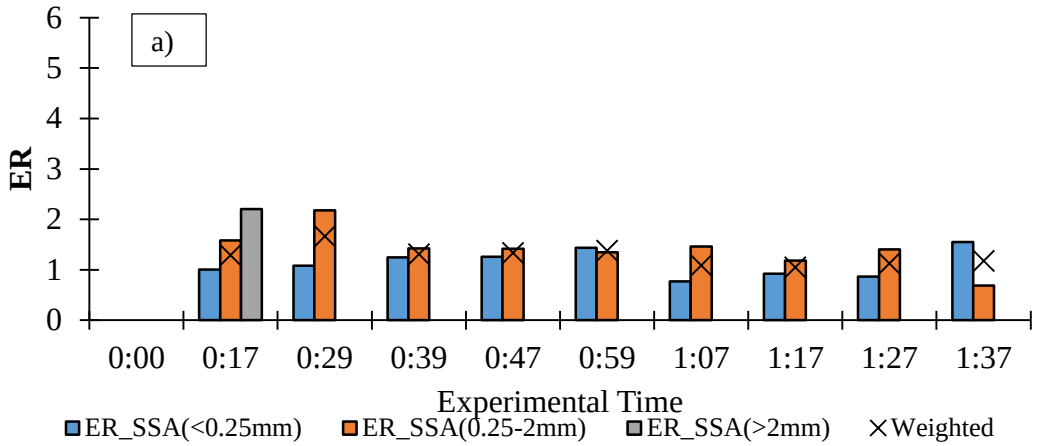

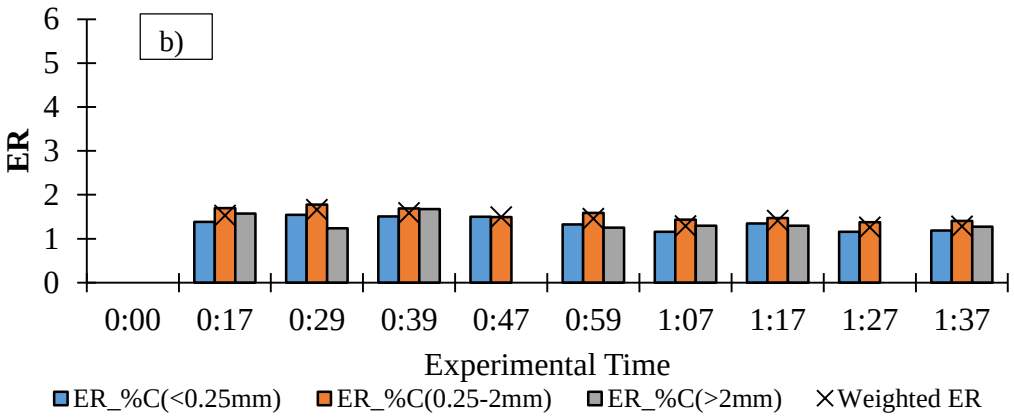

Figure 3.22 Time series of ER values from site Z1-P4 calculated with (a) specific surface area and (b) carbon content

3.4.2.4 Site Z2-P2: (Midslope-Restored Grassland)

Figure 3.23 provides a comparison of ER values determined using SSA and %C for the restored grassland site. Overall the ER values using SSA followed a linear decrease from 1.96 to 1.50. For the ER using %C, the ER values followed a similar decay, with initial ER values of around 2.00 and ending at 1.46.

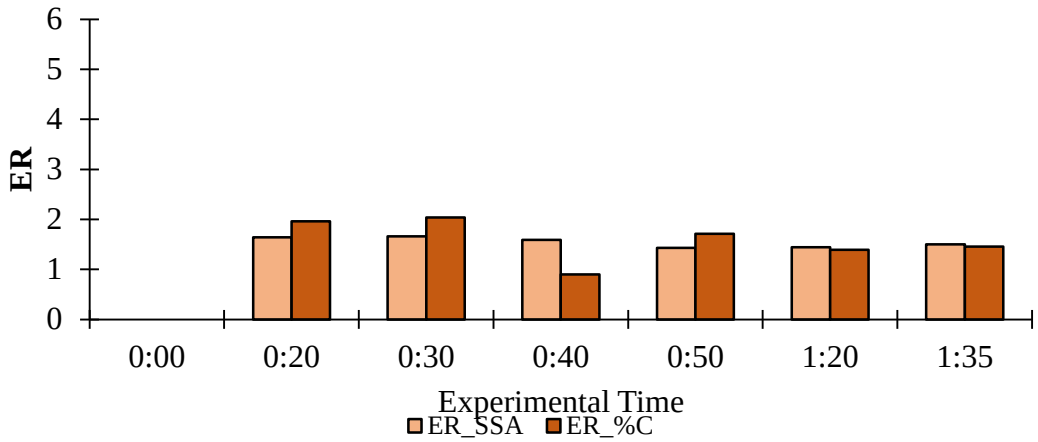

Figure 3.23 Time series of ER values from site Z2-P2 calculated with respect to specific surface area (SSA) and carbon content (%C)

3.5 Enrichment Ratio Experiment: Conclusions

In summary, the key findings of the ER experiments are methodological but also fundamental process oriented. From the methodological point of view this study highlights the need for a dual-level approach that involves both static and dynamic assessment of size fraction availability before and during each test. The findings suggest that there is a unique correspondence between size fraction availability, management practice and hillslope position. This correspondence is revisited and further examined in Chapter 4, with the focus being placed the distribution and stability of small macroaggregates, which has been found to be the aggregate class most reflective of changes in management [Beare et al., 1994a,b; Amezketa, 1999; Moebius et al., 2007].

The second major finding is the enrichment ratio is strongly related to composition and therefore hillslope location. A systematic examination of the ER changes with management and hillslope positon is further examined in chapter 5 through numerical simulations. These simulations are performed with models calibrated and verified for the prevalent conditions of the study site.

Third, there are differential modes for soil mobilization between rill and interrill areas. The differences between the two modes are either exacerbated or dampened depending on the prevalent management practice, the gradient of the site and landscape position. There is a correspondence between enrichment, %C, and SSA, and this correspondence suggests that soil derived from interrill areas vs rill areas may contribute differently to carbon mobilization and storage potential. This necessitates the use of different capacity transport formulas for rill and interrill areas. This need is further addressed in chapter 5 where tested formulas for transport capacity (i.e., the max capacity of soil to be transported by runoff/rainsplash during steady state conditions) are considered in the newly developed ER-module.

Below are some additional specific takeaway findings from these experiments.

- Methods used to estimate ER (SSA vs %C) provide similar values (Figure 3.24). The largest deviation between the methods was seen at the grassland and ridge tilled conservation sites.

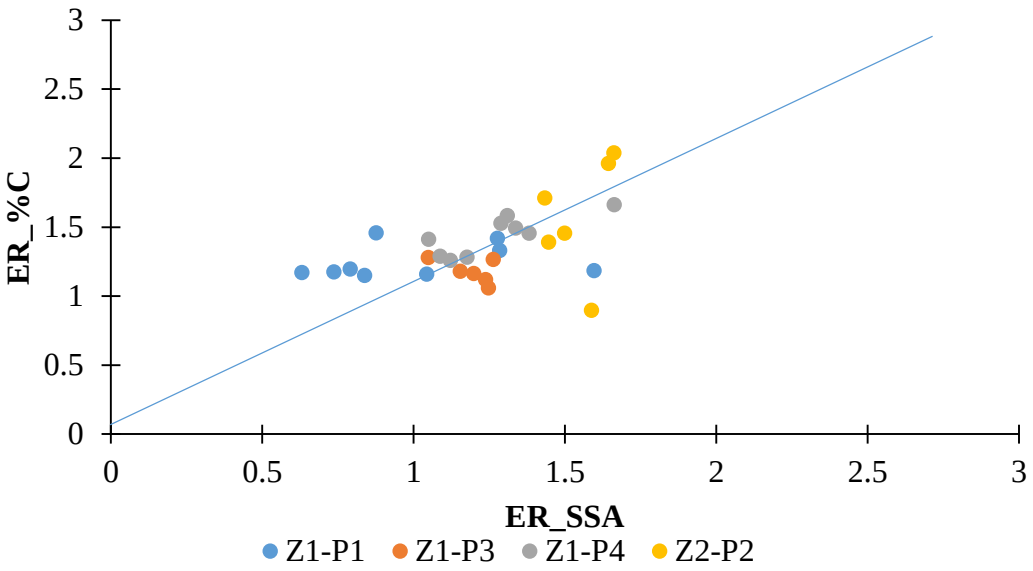

Figure 3.24 Comparison of weighted ER values using SSA and %C

- Management and hillslope position both impacted ER. The highest ER values at pseudo-steady were present at the restored grassland site (1.50), with the lowest values found at site Z1-P3 around 1.06. The higher runoff and sediment fluxes at site Z1-P3 entrained all size fractions allowing the SSA and %C between the in situ soil and entrained sediment to be almost identical. This has been found in other ER studies as a function of sediment concentration (see Figure 3.25). Data from Wang (2010) are plotted along with the experimental data from this study and show a similar decay in ER as sediment loading increases.

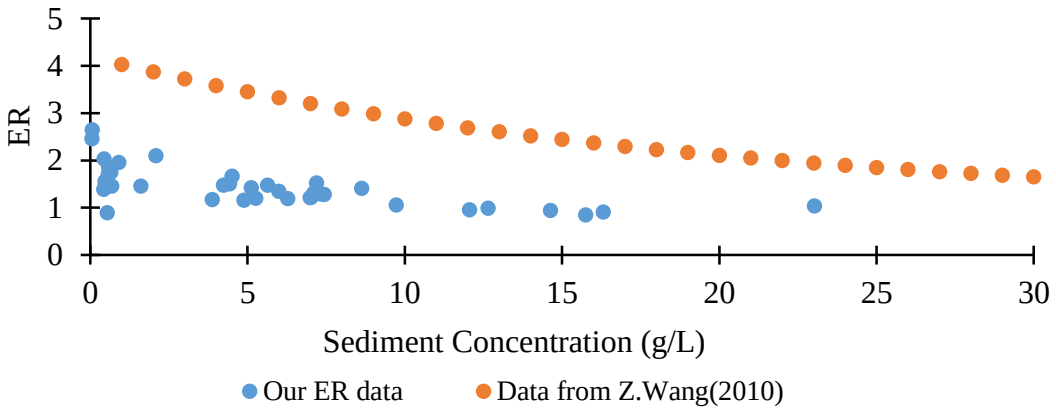

Figure 3.25 Relation between ER and sediment concentration

- Oriented roughness impacted both flow and sediment. Although Z1-P1 and Z1-P3 are both located at a midslope location and are under conservation management, the contour ridges at site Z1-P1 retarded flow and sediment mobilization [Hatfield et al., 1998]. As a result, the ER values in Z1-P1 were higher (1.17) compared to Z1-P3 (1.06), while the sediment fluxes were only a fraction of Z1-P3.

Overall, these experiments provided valuable insight, highlighting the necessity to account for the selective mobilization of different size fractions and corresponding enrichment when exploring carbon redistribution along the downslope of an IML. It is

essential to incorporate the enrichment of the different size fractions (clay, silt, sand, aggregates) into a numerical modeling framework to simulate correctly the biogeochemical and landscape interactions affecting the SOC stocks in IMLs.

The size fractions analyzed in these experiments were found to have varying levels of carbon associated with them, especially the larger aggregates, which encapsulate organic material. For this reason, the next chapter (Chapter 4) looks more closely the role of aggregates in IMLs, specifically identifying how aggregate stability varies with respect to management and hillslope position, through controlled experiments.

Incorporating the findings of both the ER and aggregate stability experiments, Chapters 5 of this dissertation describes the initial set up of a modeling framework (Chapter 5) that couples a hillslope transport model, a biogeochemical model, and a newly developed enrichment ratio module to simulate selective mobilization along a downslope and provide updated SOC additions and/or removals in the soil active layer. The developed model is then used to simulate a historic timeline of local management and climatic conditions to assess changes in SOC stocks.

CHAPTER 4. AGGREGATE STABILITY

Chapter 3 presented the ER experiments and highlighted the need to account for the different aggregate size fractions when determining SOC fluxes. Sediment size fractions were shown to vary with respect to specific surface area (SSA) and carbon content (%C), with the larger aggregate fractions having higher carbon content. By neglecting the larger aggregate fractions in SOC redistribution studies, large errors in carbon budgets are possible at the hillslope scale and beyond. Therefore, the role that soil aggregates play in influencing SOC dynamics is investigated in this chapter by assessing the stability of aggregates against raindrop impact and how the stability varies with respect to hillslope position and management.

4.1 Introduction

Potential mechanisms in the soil column that store carbon include stabilization, either chemically in organic-clay complexes [Sorenson, 1972; Hassink, 1997] or physically within aggregates [Tisdall and Oades, 1982; Olchin et al., 2008]. But in intensely managed landscapes (IMLs), conventional management practices have been shown to negatively influence soil aggregate susceptibility (Figure 4.1), both directly through mechanical breaking known also as "defragmentation" of aggregates, and indirectly through alteration of textural and biogeochemical factors within the soil, like soil composition, organic matter, soil microclimate, etc. [e.g., Six et al., 2000; Olchin et al., 2008; Kara and Baykara, 2014; Papanicolaou et al., 2015]. Furthermore, tillage, in conjunction with rainsplash/runoff (i.e., fluvial) erosion, induces along a hillslope higher spatial heterogeneity and temporal variability in the aforementioned aggregate properties relative to more established and stable grassland systems [Van Oost et al., 2000; Rieke-

Zapp and Nearing, 2005; Kuhn et al., 2009; Abaci and Papanicolaou, 2009; Stavi and Lal, 2011]. The focus here is on the mechanical breaking of aggregates due to fluvial and tillage-driven erosion under different management practices.

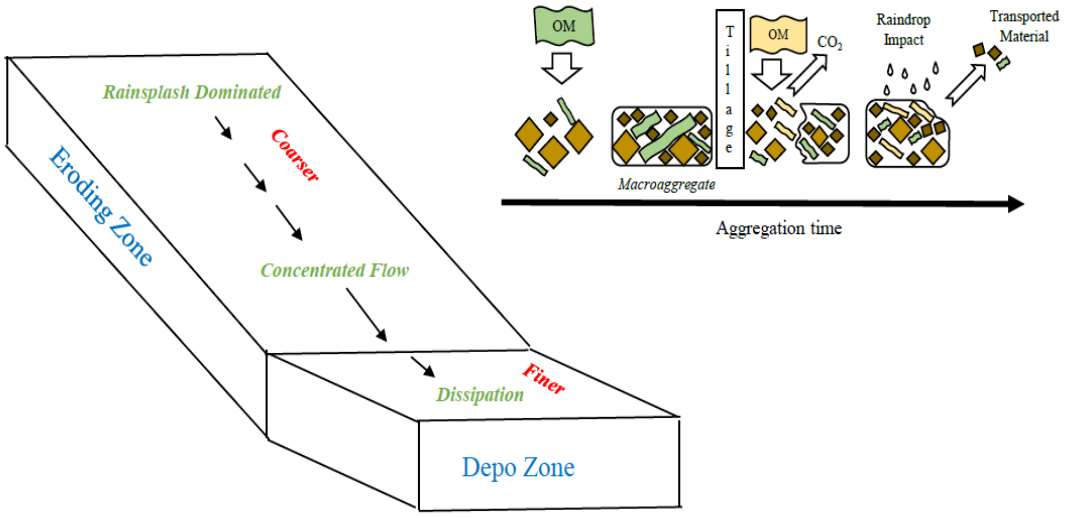

Figure 4.1 Conceptual model of aggregate formation within intensely managed landscapes. Figure modified from Six [2000]

The size distribution of soil aggregates and their " stability" - defined here as the ability to retain their volumetric structure or arrangement of solids and pores; Diaz-Zorita et al., [2002] -have been widely used as proxy-measures reflecting the role of management practices and hillslope location on soil structure and health [Kemper and Rosenau, 1986; Bronick and Lal, 2005; Idowu et al., 2008; Pulido Moncada et al., 2013], as well as the resistance to fluvial and tillage-driven erosion [Farmer, 1973; Farres, 1980; Coote et al., 1988; Shouse et al., 1990; Bryan, 2000]. Moreover, the manner in which an aggregate breaks apart can dictate the size fractions of the material that are mobilized [Polyakov and Lal, 2004; Wang et al., 2014], and hence the redistribution of organic matter [Hu et al., 2013; Papanicolaou et al., 2015]. Following the Oades and Waters

[1991] hierarchical classification of soil aggregates, which consists of microaggregates, or what was called the finer fraction in chapter 3 (0.053-0.250mm), small macroaggregates (0.25-2.0mm), and large macroaggregates (2.0-5.0mm), it is the small macroaggregates that have been found to be most reflective of changes in management practices [Beare et al., 1994a,b; Franzluebbers and Arshad, 1997; Amezketa, 1999; Blanco-Canqui and Lal, 2004; Moebius et al., 2007].

Previous studies have suggested different methods to assess soil aggregate proxy-measures, i.e., size distribution and stability, which tend to vary based on the type of the "disruptive force" being applied [Kemper and Rosenau, 1986; Amezketa, 1999]. Methods that rely on mechanical breaking of dry aggregates use the size distribution of the aggregates to make inferences regarding aggregate stability. In these methods, the size distribution of dry aggregates indicates the degree of abrasion or perturbations to the soil [Wang et al., 2014], which may reflect varying tillage intensities [Yoder, 1936; Youker and McGuiness, 1957]. Alternative methods, though, have been developed that reflect better the influence of fluvial processes like raindrop impact to the breakdown of soil aggregates [van Es et al., 2006; Moebius et al., 2007].

Raindrops transfer different levels of kinetic energy into the aggregate structure. If the kinetic energy exceeds a threshold related to the internal molecular bond strengths, then the aggregate will break [Farres, 1980]. As raindrops continue to "pound" the aggregate, the water eventually penetrates into the aggregate structure and occupies the air voids, thus further instigating the internal breakdown [Loch and Foley, 1994].

While the described studies have offered useful ways of assessing aggregate stability under either mechanical breaking or fluvial impact, the use of each method

separately as a standalone approach does not provide a complete assessment of aggregate susceptibility in IMLs where tillage and fluvial erosion usually coevolve [e.g., Papanicolaou et al., 2015]. Few studies have considered the interplay of fluvial and tillage on aggregate size and distribution [e.g., Barthes and Roose, 2002; Papanicolaou et al., 2015] while systematic examination of these drivers on aggregate susceptibility under different management practices and hillslope position (erosion vs. deposition zones) remains. We posit that in IMLs a coupled methodological approach is needed that includes examining both the dry aggregate size distribution (to reflect the mechanical breaking), as well as wet aggregate stability tests (to capture the effects of fluvial erosion). It is hypothesized herein that different tillage regimes (no till, conservational tillage, and conventional tillage) will affect the tailing skewness of the aggregate size distribution. Size distributions that are back-tailed or comprised of mostly coarser size fraction reflect an armored, or sealed, soil surface. Size distributions that are front-tailed are indicative of the mobile, finer size material. Further, it is hypothesized that the degree of influence that the management changes have on aggregate size redistribution and stability may vary depending on the hillslope location. Aggregate proxy-measures such as size and stability may be significantly different in erosion-dominated (i.e., upslope) areas of a hillslope versus deposition-dominated (i.e., downslope) areas.

The goal of this research is to examine the functionality of aggregate size and stability with hillslope position and management practices (tillage intensity) through controlled experiments in the laboratory of a representative number of soil samples collected from fields with distinct management practices and hillslope locations (see specifics in section 2). A systematic examination of this functionality is undertaken by

developing a coupled, two level approach. First, we look at the aggregate size distribution a priori to wet aggregate stability tests in order to reflect the effects of mechanical breakdown through various intensities of tillage. Second, we perform rainfall simulation experiments on sieved soil samples which were collected from fields with different management practices and hillslope locations. The focus of the two level approach in this study is on the small macroaggregates (0.25-2.0mm) because they best reflect the role of management on the aggregate size distribution and stability. We use the acronym SMAGGs to refer to the small macroaggregates (0.25-2.0mm) hereafter. A definition for the dry mean weight diameter (DMWD) is therefore adopted and modified in order to be applicable to the SMAGG fraction. Moreover, the wet aggregate stability methodology of SMAGG samples builds on the Mobieus et al., [2007] method using the kinetic energy of rain drops. The same testing conditions as those of Mobieus et al. [2007] and Gugino et al., [2009], are considered here with the goal of applying nearly identical kinetic energy to facilitate comparison with the conditions reported in the literature.

In summary, the specific objectives of this study are (i) to determine the stability and size distributions of SMAGG topsoil samples (from the top 10 cm) collected under a range of management practices and hillslope positions; and (ii) to identify how these key controlling parameters in (i) impact SMAGG susceptibility.

4.2 Materials and Methods

4.2.1 Study Site and Design

Samples were collected from field sites in Clear Creek (Figure 4.2) that are representative of hillslope gradients, curvature, texture, and management. They included corn-soybean rotations under conventional and conservation tillage, as well as restored grassland prairie. Table 4.1 provides a summary of the general characteristics for each of the field sites. Within each study field, flow pathways along the dominant downslopes were first identified using Archydro tools 10.3 to determine sampling locations that ensured connectivity between hillslope elements. Collecting samples within defined locations (i.e., crest, midslope, toeslope) of the same flow pathway ensured connectivity between the samples, which takes into account landscape processes, e.g., topographic curvature, changes in roughness and as a result heterogeneous soil conditions along the downslope. At each sampling location, 5 soil samples (~200g) were collected from the top 10 cm of the soil surface in early spring (April 2014) before any perturbations to the soil, specifically spring tillage or fertilizer applications, planting, or burning events. The sampling depth of 10 cm was selected as this is the depth primarily impacted through tillage and water interactions and hence known as the active layer depth [Papanicolaou et al., 2015].

Three of the sampling sites were collected from the Clear Creek headwaters, namely sites Z1-P1, Z1-P3, and Z1-P5. Sites Z1-P1 and Z1-P3 are the same downslopes used in Chapter 3. They are under a 3-yr crop rotation of corn-corn-soybeans (C-C-B), with reduced ridge tillage and anhydrous fertilizer applications being applied in late fall before the corn planting and no-till for the soybeans. Site Z1-P1 has rows oriented

perpendicular to the flow pathway (contour ridges), while site Z1-P3 has rows oriented parallel to the flow. The average hillslope gradient for site Z1-P1 is 6.5%, while Z1-P3 it is slightly steeper with an average slope of 8.4%. At site Z1-P5, a 2-yr corn-soybean rotation (C-S) under conventional tillage is used. The average hillslope gradient of site Z1-P5 is 5.7%, which is comparable to sites Z1-P1 and Z1-P3.

Site Z2-P2 is located in the middle of Clear Creek. It was taken out of intensified agricultural corn-soybean production nearly 50 years ago and was reseeded as a restored grassland prairie about a decade ago. It has the highest average hillslope gradient of all sites at 15.7%. A 5-year burn frequency is used for invasive species control, and last occurred 2 years before sample collection. This was an important consideration in order to avoid water repellency (hydrophobicity) impacts on aggregate stability [Fox et al., 2007].

Near the mouth of Clear Creek, sites Z3-P1 and Z3-P2 also are in a 2-yr corn-soybean rotation (C-S) under conventional tillage, with these sites experiencing higher tillage intensity in terms of frequency than at site Z1-P5. The average hillslope gradients of sites Z3-P1 and Z3-P2 are less than 1%, since it is closer to the watershed mouth.

Figure 4.2 Clear Creek study site locations. Management practices include conservation tillage (sites Z1-P1, Z1-P3), conventional tillage (sites Z1-P5, Z3-P1, Z3-P2) and restored prairie (site Z2-P2). Note: C=corn, S=soybean

Table 4.1 General Site Characteristics

	Site Locations					
	Z1-P1	Z1-P3	Z1-P5	Z2-P2	Z3-P1	Z3-P2
Management						
Tillage	Reduced ridge till		Conventional tillage	n/a	Conventional tillage	
Crop Rotation	C-C-B		C-B	Restored Grassland	C-B	C-B
Soil Properties						
Sand(%)	1.87	3.87	4.10	2.63	19.10	7.85
Coarse Silt (%)	43.57	45.29	41.95	42.32	33.09	33.64
Fine Silt (%)	27.43	26.41	27.58	29.25	25.61	33.41
Clay (%)	27.13	24.43	26.38	25.80	22.20	25.11
Bulk Density (g/cm^3)	0.95	1.04	0.95	1.12	1.14	0.85
Landscape						
Slope (%)	6.5	8.4	5.7	15.2	0.07	0.57

4.2.2 Soil Sample Processing

The collected soil samples, while still being field moist, were initially passed through an 8-mm sieve to remove coarse litter fractions. Soil samples were then allowed to air dry over a period of three weeks [Pansu et al., 2001]. Once dried, SMAGG were

partitioned from the bulk sample using a nest of sieves bracketed by the upper and lower limit size ranges of 2 mm and 0.25 mm, respectively [Moebius et al., 2007].

4.2.3 SMAGG Size Distribution

The dry soil samples were passed through a nest of sieves with square openings of 2.00, 1.70, 1.40, 1.18, 0.85, 0.60, and 0.25 mm, to allow six size classes within the SMAGG range to be obtained (Figure 4.3). The sieves were placed on a shaker table and ran for 120 seconds. The masses of soil retained in each sieve were weighed. The characteristic dry mean weight diameter (DMWD) was determined for the SMAGG samples using a definition adopted from Youker and McGuiness [1957]:

$$DMWD = \frac{\sum_{i=1}^{j} X_i W_i}{W_s} \qquad \text{[Eq. 4.1]}$$

where X_i is the mean diameter of each size class i (mm); W_i is the mass of each size class i (g); and W_s is the total dry mass of the SMAGG sample (g).

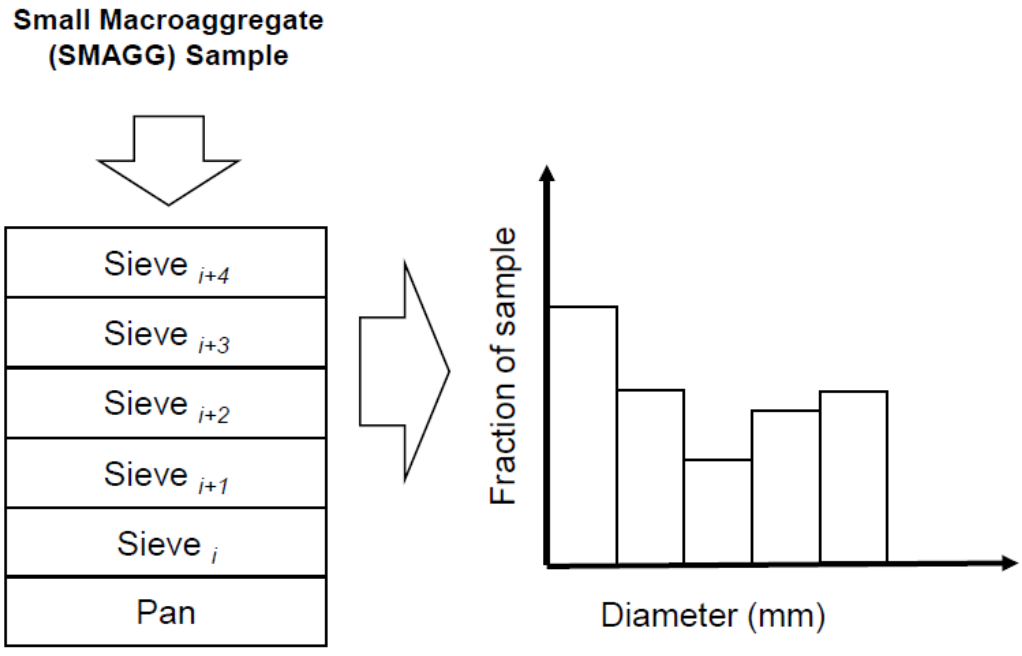

Figure 4.3 Dry aggregate analysis to determine size distribution for SMAGG samples

4.2.4 Aggregate Stability Testing

Moebius et al. [2007] established a method for determining wet aggregate stability that considers the effects of raindrop impact. In this method, SMAGG sub-samples were placed atop a 0.25-mm sieve under a drip mechanism that was at a height of 0.15 m. The drip mechanism provided fixed drop diameters of 4 mm that fell on the sample for a duration of 300 seconds, equating to the forcing of a heavy thunderstorm event. Building on this method, careful attention was placed herein to incorporate the natural distribution of raindrops for southeastern Iowa [Elhakeem and Papanicolaou, 2009] while matching the kinetic energy Moebius et al. [2007] found as a threshold to break the aggregate.

4.2.4.1 Implementation-Rainfall Simulator Experimental Setup

A Norton Ladder Multiple Intensity Rainfall Simulator with dimensions of 2.5 (h) x 1.5 (w) x 2.7 (l) m, which was designed by the U.S. Department of Agriculture – Agricultural Research Service National Erosion Research Laboratory, was used in this study to simulate the effects by raindrop impact [Norton, 2006]. The experimental setup included the simulator, as well as a 1500-gal water tank connected to a series of valves and pumps that allows the internal water pressure and therefore rainfall intensities to be adjusted (Figure 4.4). Special care was placed on the calibration of the rainfall simulator, which used a disdrometer to verify drop size distributions, spatial uniformity, and fall velocities [Elhakeem and Papanicolaou, 2009]. The simulator was set at a height of 2.5 m above the surface to allow uniform spherical raindrops to be applied through oscillating V-jet type nozzles [Elhakeem and Papanicolaou, 2009]. The size distribution of raindrops generated with the simulator was shown to agree well with the Marshall-

Palmer distribution, a commonly accepted distribution for natural raindrop sizes [Marshall and Palmer, 1948; Elhakeem and Papanicolaou, 2009].

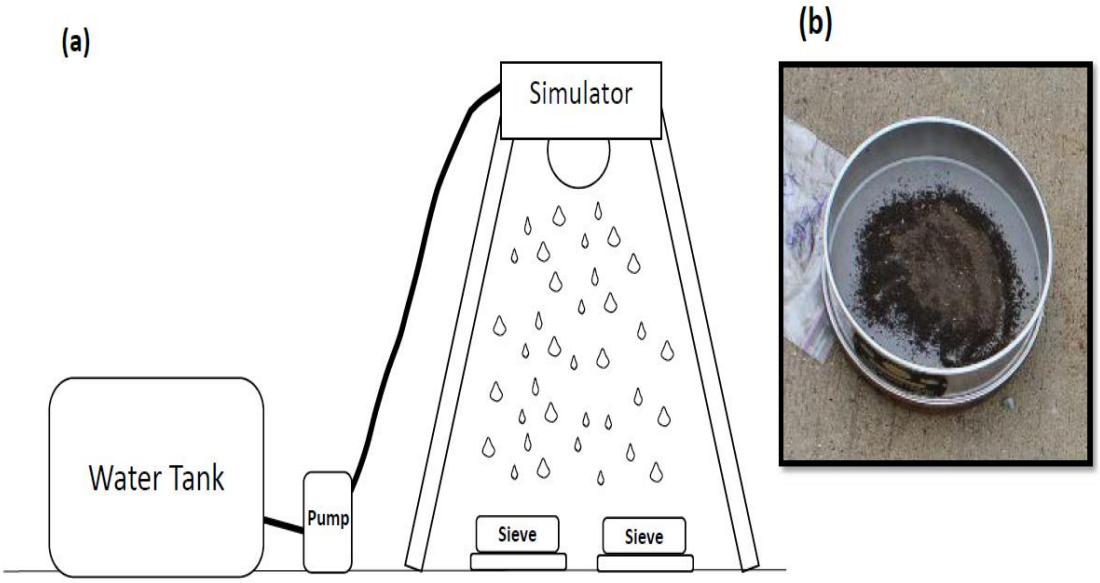

Figure 4.4 Aggregate stability test setup. (a) Setup for running aggregate stability test, including the variable intensity Norton ladder rainfall simulator, water tank, and pump. Below the simulator small macroaggregate samples were placed atop 0.25mm sieves (b)

A rainfall intensity of 60 mm/hr was used in this study, which is not only the intensity used in developing the Universal Soil Loss Equation relation, but also the intensity that matched the kinetic energy of 0.789 J and the rainfall volume applied to the SMAGG samples in Moebius et al. [2007]. This was determined by estimating the volume of rainfall supplied during the 300 sec testing period to an effective testing area, here the area of the circular sieve of which the SMAGG samples were placed atop. The volume of raindrops was used to determine the drop size distribution that is needed to calculate the terminal velocity and corresponding kinetic energy supplied from the individual drops.

To calculate the wet aggregate stability, SMAGG samples were placed on top of a 0.25-mm sieve, which represents the lower size limit for SMAGG. The sieves were placed under the rainfall simulators, which were run for 300 seconds using 60-mm/hr rainfall. Catch pans were placed under each sieve to collect the slaked portions during the tests (Figure 4.4). After each test the slaked material in the catch pan and the material retained atop the sieve were dried and weighed masses. Wet aggregate stability for the SMAGG samples was determined using relation by Moebius [2007]:

$$WSA = \frac{m_{stable}}{m_{total}} = \frac{m_{total} - (m_{slaked} + m_{stones})}{m_{total}} \quad \text{[Eq. 4.2]}$$

where m_{stable} is the mass of stable aggregates; m_{total} is the mass of total aggregate sample; m_{slaked} is the mass of aggregates slaked through sieve; and w_{stones} is the mass of stones/sand after test remaining in sieve.

4.3 Results

The results of this study are organized as follows. First, results of the size distribution analysis are described to assess how SMAGG size distributions and DMWD are influenced by management and hillslope position. Next, the aggregate stability of the SMAGG follows by again examining the role of management and hillslope position, which is used to establish a correspondence with the size analysis.

4.3.1 SMAGG Size Distribution

4.3.1.1 The Role of Management

Figure 4.5 provides a 3-axes plot summarizing the average fractions of the total SMAGG masses in each size range for each study site (horizontal *y*-axis). The horizontal *x*-axis represents the mean diameters of the SMAGG size classes, and the vertical *z*-axis provides the fraction the given diameter represents of the total SMAGG sample. Overall,

the size distribution of SMAGG varied amongst the study sites. Two dominant trends can be seen in Figure 4.5: (i) study sites under conventional tillage (namely Z1-P5, Z3-P1, and Z3-P2) display comparable long tailed distributions toward smaller size fractions. This is due to repeated intensified tillage that breaks apart the soil structure. The continuous perturbations do not allow time for the aggregates to coalesce and grow [Castro Filho et al., 2002]; and (ii) the restored prairie (i.e., site Z2-P2) and the conservation management sites (namely Z1-P1 and Z1-P3) display more even distributions with increasing skewness towards coarser material found especially in the grassland site [Dal Ferro et al., 2014]. A slight bimodality is observed at these sites, which are steeper, the reasons for which are explained below as they relate to different hillslope positions.

The DMWD values Eq. [4.1] for SMAGG are provided in Figure 4.6 in the form of an interval plot with upper and lower 95% confidence intervals of samples represented as error bars. In Figure 4.6, outliers in data are represented as crosses, and are determined as samples greater than 1.5 times the InterQuartile Range from the 1st and 3rd quartiles, assuming a normal distribution [Hubert et al., 2008]. The largest average DMWD values were in samples from the restored prairie (site Z2-P2) with 1.16 mm, followed next by the samples from the conservation sites of Z1-P3 and Z1-P1measured at 1.10 mm and 1.03 mm, respectively. The DMWD of sites under conventionally managed sites were notably smaller with values of 0.99, 0.98 and 0.95 mm for sites Z3-P2, Z3-P1,

and Z1-P5, respectively. The smallest variability of DMWD values was seen in the conventional sites Z3-P1 and Z3-P2, which may be attributed to a much lower gradient.

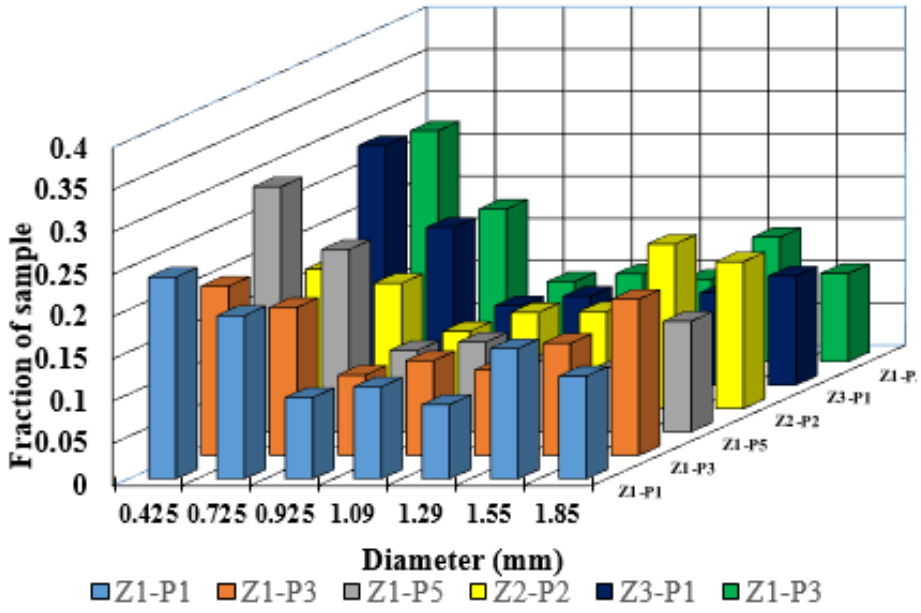

Figure 4.5 Average size distribution values for SMAGG samples

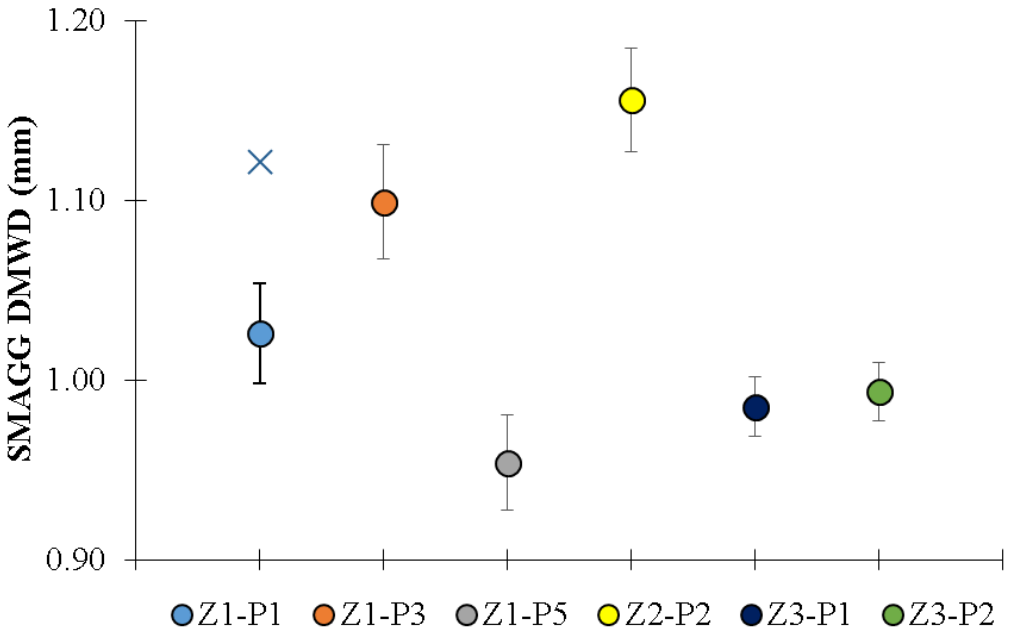

Figure 4.6 Interval Plot showing 95% confidence intervals (shown as error bars) for dry mean weight diameter of SMAGG samples. Outlier samples are represented as crosses (X)

4.3.1.2 The Role of Hillslope Position

Figure 4.7 provides the average DMWD of SMAGG collected from four different hillslope positions along the downslope flow pathways at each study sites, (namely, crest = T1, midslope1 = T2, midslope2 = T3, and toe = T4). For the majority of sites, the DMWD decreased in size from the crest to the toeslope. In general, coarser size fractions of material were found at the top portions of the hillslopes, which may have been left behind due to selective transport [Warrington et al., 2009; Wang et al., 2014]. The anomaly to this trend was conservation site Z1-P3, which had rows oriented parallel to flow pathways. There, DMWD values were rather uniform along the downslope with a slight increase at the toeslope. This trend may be reflecting the deposition of coarser material from eroding upslope sections, as larger material may have settled out of suspension due to changes in gradient [Papanicolaou et al., 2015].

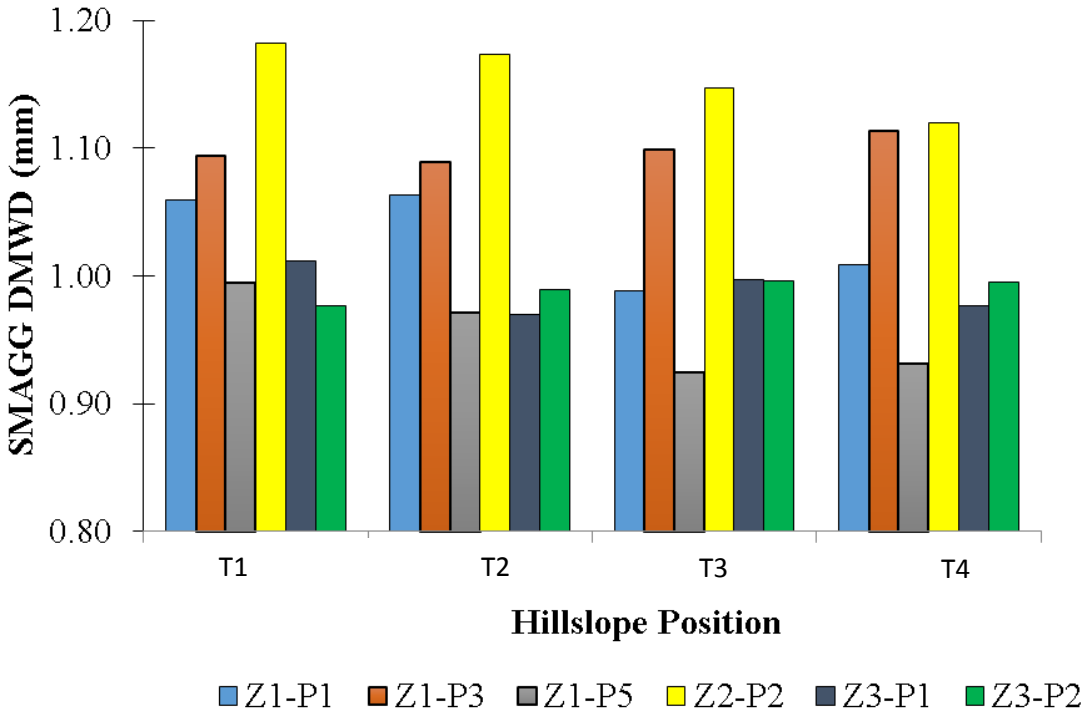

Figure 4.7 Average dry mean weight diameter (DMWD) of SMAGG samples for various hillslope positions. (T1=Crest, T2=Midslope1, T3=Midslope 2, T4=Toe)

4.3.2 SMAGG Aggregate Stability

4.3.2.1 The Role of Management

Figure 4.8 provides an interval plot, displaying the 95% confidence limits of SMAGG stability values for all sites. SMAGG stability values were found to be highest in the samples from the restored prairie (site Z2-P2) with a mean of 0.934. Comparable stability values were recorded from soils in the conservation site Z1-P1 with a mean of 0.930, followed by site Z1-P3 with 0.896. The smallest stability values were found in the conventional sites, with means of 0.873, 0.864, and 0.859 for sites Z3-P1, Z1-P5, and Z3-P2, respectively. These findings follow trends seen in other studies that reported higher stability in soils under no-till compared to those under conventional tillage [Bossuyt et al., 2002; Wang et al., 2015]. The smallest spread (variability) of SMAGG stability values was found in the samples from site Z1-P1, which could be explained through the added controls that reduced contour tillage perpendicular to flow pathways has on erosional, depositional processes that are sensitive to aggregate dynamics [Hatfield et al., 1998; Hajabbasi and Hemmat, 2000]. The highest variability in aggregate stability of SMAGG was found in site Z1-P5 (conventional tillage). Although the mean values were comparable amongst the conventional sites, the higher variability at site Z1-P5 could be due to the higher gradient and more active downslope flow pathway.

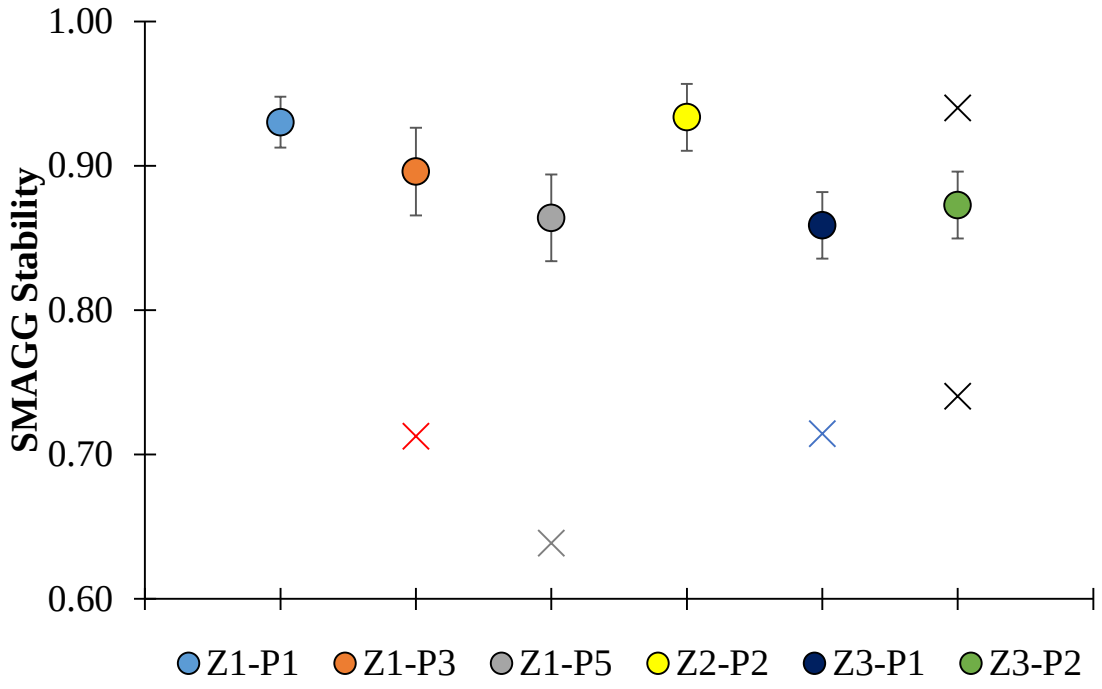

Figure 4.8 Interval Plot showing 95% confidence intervals (shown as error bars) for aggregate stability of SMAGG samples. Outlier samples are represented as crosses

4.3.2.2 The Role of Hillslope Position

Figure 4.9 provides SMAGG stability values for the four hillslope positions at each site. The horizontal *x*-axis represents the various hillslope positions (i.e., T1 = crest to T4 = toe), while the *y*-axis represents SMAGG stability. General trends from Figure 4.9 include higher stability found at the top (eroding) portions of the hillslope compared to the bottom (depositional) sections [Pierson and Mulla, 1990; Hoyos and Comerford, 2005]. This trend is more apparent at the sites with higher slope gradients. The lowland study sites (i.e., Z3-P1, Z3-P2), which have more milder gradients may experience more prolonged rainsplash effects, in contrast to the sites with steeper gradients, due to differences in the formation of rill networks based on topographic curvature and oriented roughness [Favis-Mortlock et al., 2000; Papanicolaou et al., 2010]. This may be explained through variability in soil moisture content along the downslope that dictate

wetting/drying cycles, which have been found to negatively impact the stability of aggregates [Amezketa et al., 1999].

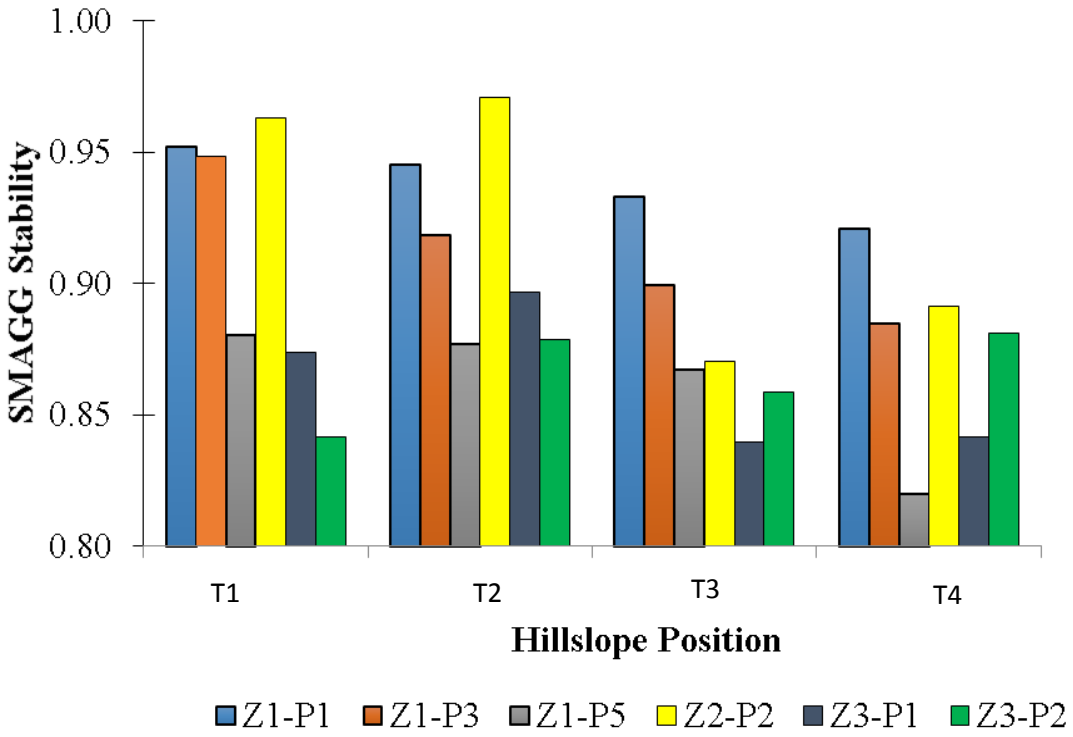

Figure 4.9 Average stability of SMAGG samples for various hillslope positions. (T1=Crest, T2=Midslope1, T3=Midslope 2, T4=Toe)

4.3.3 Aggregate Stability as a Function of DMWD

Figure 4.10 provides a plot of SMAGG stability with respect to size distribution (DMWD). The symbols here are grouped by management, representing the restored prairie, as well as the conservation and conventional tillage sites. There is a positive overall correspondence between stability and DMWD, apparent through the three clusters of points seen in Figure 4.10. As DMWD increases, the aggregate stability increases. The lowest stability and size fractions were found with the aggregates under conventional tillage. The aggregates from the restored prairie had the highest values of stability and largest DMWD. A middle range, consisting of the aggregates from the conservation sites, is present in Figure 4.10. Similar findings have been reported in Weaver and Zink

[1946], Elliot [1986], Perfect et al. [1990], and Ciric et al. [2012], where they documented changes in soil structure in disturbed and undisturbed agricultural systems.

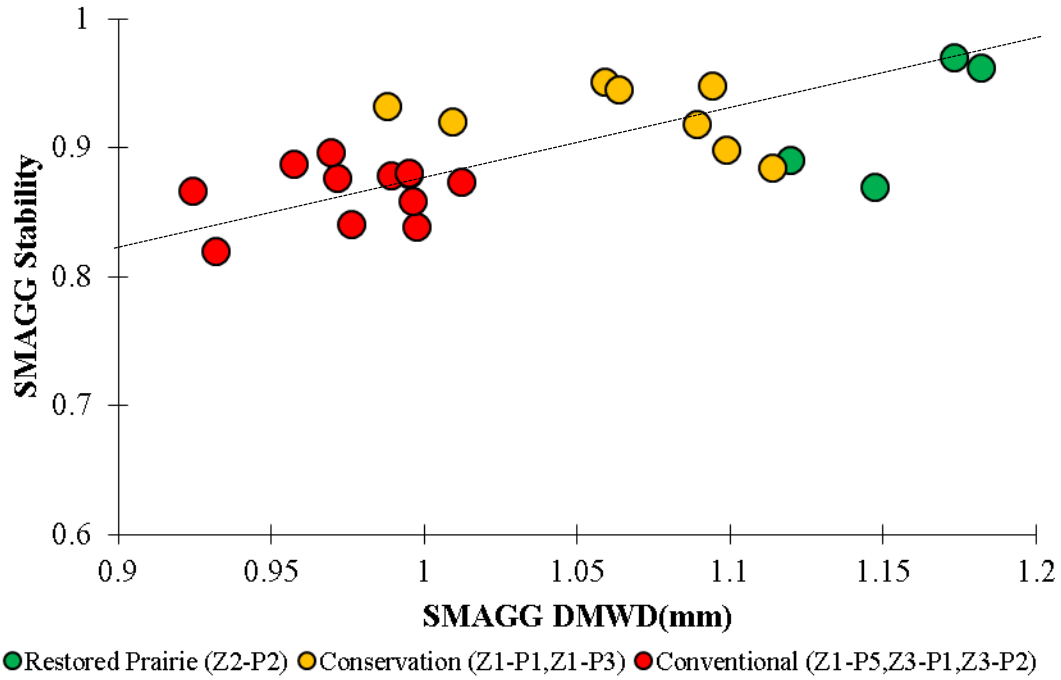

Figure 4.10 Plot of average SMAGG stability values with respect to SMAGG DMWD. Samples are grouped with respect to management. Dashed line represents the positive linear correspondence between the parameters

4.4 Discussion and Conclusions

This chapter assesses aggregate dynamics within IMLs, specifically looking at how size distribution and stability are influenced through management and hillslope position. The method considers a dual assessment of SMAGG by first looking at the aggregate size distribution a priori to wet aggregate stability tests using a calibrated rainfall simulator to apply controlled raindrop forcing (kinetic energy) to the SMAGG sub-samples. Soil samples were collected along the downslope flow pathways of representative hillslopes within the Clear Creek Watershed. At these sites the management consisted of conservation and conventional rotations in corn-soybean

production, as well as a restored prairie. A summary of some key findings in this study follows:

- **SMAGG size distributions are influenced by management.** SMAGG from all conventional sites exhibited long tailed distributions, skewed towards smaller size fractions supporting the hypothesis of this study. The repeated disturbances by the tillage would limit the time needed for the aggregates to grow and stabilize. In contrast, the conservation and restored prairie sites had coarser size aggregates due to the minimized disturbances (Figure 4.5). The DMWD was highest in the restored prairie, followed by conservation sites, and lastly conventional management (Figure 4.6). These findings could be explained in part by tillage intensity, which breaks apart soil structure and chronically disrupts time-sensitive aggregation processes [Castro Filho et al., 2002]. A slight bimodality is observed in these sites, which are steeper and more energetic, the reasons for which are related to the sorting along the downslope flow pathway.
- **SMAGG stability is influenced by management.** The restored prairie soils had the highest stability, followed closely by the soils from both conservation sites (Figure 4.8). The lowest stability was found in the soils from the conventional sites. These findings are supported by Bossuyt [2002], Elliott and Cambardella [1991], and others who reported higher stability under no-till when compared to conventional tillage. Concerning the two conservation sites, smaller variability in stability values are seen at site Z1-P1, which could be explained through the added controls provided by the contour tillage, which would inhibit the sorting and enhanced heterogeneity that would occur with the runoff and erosional/ depositional processes that are highly sensitive to aggregate dynamics [Hatfield et al., 1998; Hajabbasi and Hemmat, 2000]. In terms of the conventional sites, higher variability in stability values were found at site Z1-P5 compared to sites Z3-P1 and Z3-P2. This is possibly explained through the higher hillslope gradient, which relates to more active flow pathways in the downslope [Papanicolaou et al., 2015].

- **SMAGG size distributions are influenced by landscape position.** In general, coarser size fractions were found at the top of the hillslopes, while the bottom positions were more prevalent in the smaller fractions (Figures 4.7). This could be attributed to the preferential removal of finer fractions from eroding portions of the hillslope [Warrington et al., 2009; Wang et al., 2014]. The largest variability in DMWD values was found at the high-gradient, high-energy sites, which would have higher carrying capacities along the downslope [Tucker and Bras, 1998; Papanicolaou et al., 2015].
- **SMAGG stability is influenced by landscape position.** In general, aggregate stability was found to be higher in the eroding sections (crest, midslope) of the hillslope when compared to depositional toeslope (Figure 4.9). Similar findings have been reported within other agricultural systems by Pierson and Mulla [1990], Hoyos and Comerford [2005], and others. This trend is not as pronounced in the low gradient sites of Z3-P1 and Z3-P2, which may experience more prolonged rainsplash effects instead of concentrated runoff generally found in steeper gradients [Favis-Mortlock et al., 2000; Papanicolaou et al. 2010]. This explanation is further supported by the corresponding higher stability and DMWD values in upslope areas which are indicative of the preferential removal of the finer fractions by splash dominated effects.
- **SMAGG size distribution (DMWD) is related to SMAGG stability.** Figure 4.10 provides a positive overall correspondence between stability and DMWD. As DMWD increases, aggregate stability increases. The lowest stability and DMWD are found in the soils under conventional management, with the highest values present in the restored prairie. A middle range exists between these groups consisting of the soils from the conservation sites.

Overall, this study offers some valuable insight into the controls that management, landscape processes, and climate have on aggregate dynamics. Decreasing mechanical breaking (tillage) and kinetic energy from raindrop impacts may enhance

aggregation and size, which can positively affect stability by allowing more time. Soil aggregates have been shown to have higher carbon contents than bulk soil due to encapsulated organic material and preferential binding of clay particles. However, there are some caveats here that need to be addressed. Not accounting for raindrop-induced mobilization and transport of aggregates due to runoff in more realistic settings such as field plots could lead to significant errors in redistribution estimates at the hillslope scale which would propagate at larger extents in the landscape. The mobilization of aggregates due to raindrop and runoff impact may also provide some key insight on available size fractions preferentially entrained in various flow conditions and information needed for modeling. The presented study at this phase, does not consider the role of runoff on SMAGG proxy-measures because as noted such examination may require laborious and extensive in-situ field experimentation with rainfall simulators where dynamic characterization of aggregate proxy-measures can be feasible [Barthes and Roose, 2002; Papanicolaou et al., 2011]. Future studies must address this limitation by performing systematic rainfall erosion experiments in the field that overlap with the management and landscape positions examined here in order to assess the aggregate susceptibility for IMLs in a more dynamic and realistic setting than considered here.

CHAPTER 5. LANDSCAPE ORIENTED MODELING FRAMEWORK

5.1 Introduction

Despite considerable gains in knowledge about SOC processes, most studies have been geospatially limited to the soil profile thereby failing to account for the effects of landscape heterogeneity on SOC redistribution and storage [e.g., Tornquist et al., 2009]. In addition, the majority of these studies has been performed in punctually disturbed ecosystems, such as grasslands and forests, rather than constantly disturbed IMLs [e.g., Li et al., 1997; Yoo et al., 2005; Parton et al., 2007].

Only a handful of models have the capacity to incorporate the effects of rainsplash/runoff and tillage erosion, defined herein as "collective erosion", and deposition on SOC predictions at the watershed scale [Van Oost et al., 2000; 2005]. Rainsplash triggers redistribution of the finer fractions of soil through sheet erosion which provide lateral inputs to rills. Rills, in turn, erode soils and SOC on their own due to concentrated flows. They also convey the total eroded material (e.g., sediment and SOC) downslope from erosion-dominated areas to deposition-dominated areas.

Tillage has several effects on SOC redistribution and storage potential through a series of mechanistic processes [Moore and Burch, 1986; Van Oost et al., 2000; Billings et al., 2010; Lal, 2011]. These include the incorporation of residue within the soil profile and fracturing of soil aggregates which exposes lighter size fractions of carbon-enriched material to selective entrainment by flow [Kuhn et al., 2009; Papanicolaou et al., 2009; Van Oost et al., 2009]. Selective entrainment of the lighter size fractions affects the enrichment ratio (ER), which is a unique measure of change in available SOC through the

enrichment or depletion of the finer size fraction of organic rich soils [Palis, 1990; Wang et al., 2013].

Changes in Land Use/ Land Cover (LULC) and associated management practices in agricultural IMLs can lead to a higher degree of spatial heterogeneity and temporal variability in SOC redistribution [Parkin, 1993; Abaci and Papanicolaou, 2009; Dlugoβ et al., 2010; Kravchenko and Robertson, 2011; Du and Walling, 2011; Stavi and Lal, 2011; Navas et al., 2012]. These different practices lead to changes in the percentage of bare soil, tillage depth, fertilization, and soil roughness. The degree that these changes influence SOC redistribution and storage may vary depending on the hillslope location and the magnitude of the hydrologic event. In fact, SOC changes may be significantly different in erosion-dominated (i.e., upslope) areas of a hillslope versus deposition-dominated (i.e., downslope) areas, with significant effects on net gains or losses in the SOC stored in these zones [Van Oost et al., 2006; Wang et al., 2015]. It is, therefore, not surprising that most of the available biogeochemical models, being soil profile models or "point models in space", tend to overestimate or underestimate SOC storage predictions in IMLs as they do not account for outputs or inputs of mobilized SOC [e.g., Parton et al., 1987; Paustian et al., 1992; Harden et al., 1999; Manies et al., 2001; Mangan et al., 2004; Jarecki et al., 2008; Tornquist et al., 2009; Wilson et al., 2009; Van Oost et al., 2006; Bortolon et al., 2011; van Groenigen et al., 2011; Vaccari et al., 2012].

Some studies have linked existing biogeochemical models (e.g., ROTH-C, DNDC, CENTURY) with lumped erosion models, such as those based on the Universal Soil Loss Equation (USLE) or its modifications [e.g., Monreal et al., 1997; Manies et al., 2001; Zhang et al., 2014], to account for losses of SOC along the downslope. These

erosion models tend to provide long term (100-yr. time window) estimates of eroded SOC fluxes, but are neither able to capture the seasonal variability in SOC distribution [Harden et al., 1999; Li et al., 2001; Blaschke and Hay, 2001] nor account for SOC deposition [Gregorich et al., 1998; Van Oost et al., 2006].

Recently, significant modeling efforts have accounted for the dynamics of collective erosion and the role of deposition on SOC redistribution and storage [e.g., Billings et al., 2010; Dlugoβ et al., 2010; 2012]. However, these models do not adequately incorporate the effects of selective entrainment and deposition of the finer size fraction of organic rich soils by the flow [Van Oost et al., 2005; Dlugoβ et al., 2010; 2012]. The ER is currently assumed to be equal to unity [Teixeira and Mishra, 1997] or to obtain a constant value greater than unity. On the contrary, it is anticipated that the range of ER values may vary depending on hillslope location and the magnitude of the hydrologic event leading to an overestimation of the SOC displaced [Kuhn et al., 2009; Thompson et al., 2010; Hu et al., 2013].

The goal of this study is to provide spatiotemporal predictions of SOC stocks at the hillslope scale by accounting for the role of selective entrainment and deposition on SOC redistribution under different hydrologic and LULC conditions. SOC predictions are made following a similar discretization approach suggested by Berhe et al. [2012] where the hillslope is partitioned into two control volumes (CVs): an upslope zone and downslope zone (Figure 5.1). An ER module is developed to account for selective entrainment and deposition in both zones. The backbone of the proposed modeling framework is based on the recognition that (i) interrill splash erosion is of equal importance to rill erosion for soil dislodgement and therefore should not be ignored in

estimating ER for both the upslope (CV I) and downslope (CV II) zones [Hu et al., 2013]; and (ii) ER estimations for CV II are strongly affected by material contributions from CV I which in turn affect the potential for material mobilization or settling in CV II under different hydrologic and LULC conditions.

The proposed landscape-oriented approach is demonstrated at the hillslope scale (0.01 km^2) in a case study site of the U.S. Midwest, namely Clear Creek, IA. The Clear Creek watershed is an ideal location for resolving SOC fluxes due to the data availability on soil, hydrologic, and land use properties [Papanicolaou and Abaci, 2008; Abaci and Papanicolaou, 2009].

We first estimate ER values for both CVs I and II at the hillslope scale for different hydrologic and LULC conditions. Second, using the improved ER estimates for the two CVs we evaluate the effects that management practices with different crop cover, tillage depths, fertilization, and soil roughness characteristics have on SOC redistribution in CVs I and II. The simulations are supplemented with detailed site historic and current management practices as well as climate data (benchmark dates of the different management practices within the simulation period are detailed in section 5.3.2). To assess the predictive capabilities of the newly developed framework, samples collected from representative field locations in Clear Creek for recent years are compared with model predictions.

5.2 Integrative WEPP-CENTURY Models

Two established process-based models, namely, the Watershed Erosion Prediction Project, WEPP [version 2012.8] and the biogeochemical soil-column model, CENTURY [version 4.6] are considered in this modeling framework. Detailed reviews of WEPP and

CENTURY are provided by Parton [1987] and Flanagan [2007], but the emphasis in this dissertation is on the steps involved in the coupling of the two models and an enrichment ratio (ER) module.

The WEPP and CENTURY models are coupled here in a loose sense (see Figure 5.1). The soil profile within a control volume (CV) represents the spatial domain of the CENTURY model. It is made up of a top layer (i.e., active layer), and a lower sub-horizon layer, known as the parent layer. The CENTURY model simulates changes in SOC stocks within the soil active layer through inputs from litter incorporation and losses through microbial decay [e.g., Parton et al., 1987; Jarecki et al., 2008; Tornquist et al., 2009; Wilson et al., 2009; Vaccari et al., 2012; Zhang et al., 2013]. However, the CENTURY model alone cannot explicitly simulate the fluxes of SOC entering or exiting the active layer through collective erosion effects [Campbell et al., 1996; Metting et al., 1999].

The WEPP model is utilized in the study to bridge these missing features found in CENTURY, specifically by incorporating the ability to account for downslope variability in key soil parameters (e.g., roughness, bulk density, critical erosional strength, and hydraulic conductivity) and provide size fraction (textural) updates to the soil active layer [Foster, 1982; Nearing and Nicks, 1998; Pieri et al., 2007], all of which can strongly influence SOC fluxes. WEPP, however, in its present state, cannot adequately distinguish contributions of material from rill and interrill areas when estimating ER [Vásquez et al., 2005; Thompson et al., 2010], or have the ability to simulate the ER of material being deposited, as it only tracks the ER of exiting material [Flanagan and Nearing, 2000].

To address in part these limitations, an ER module was developed, that links the WEPP and CENTURY models. The ER module considers separate formulae for determining the transport capacity for rill and interill erosion [Yalin, 1963; Abrahams et al., 2001] to allow for a better representation of the size fractions of material being redistributed and corresponding SOC enrichment for eroding and depositional sections. For the upslope CV I, the ER is calculated as the ratio of the concentration of eroded fractions contributed by rill and interrill processes to that of the total available concentration found in the active layer prior to an event, e.g., *in situ* soil. The ER for the downslope section (CV II) can be estimated for either a net erosion or deposition event, depending on the direction of the flux (positive direction = net erosion, negative direction = net deposition). The direction of the flux greatly affects the contributions of material from the upslope CV. If net erosion occurs then ER is determined the same as the upslope section. For net deposition, the ER is estimated as the ratio of the concentration of incoming deposited material to the concentration of material eroded from rill and interrill processes in the upslope CV I.

Daily outputs of updated ER values along with the daily net soil fluxes and size fractions from the ER module and WEPP are aggregated to the monthly time scale and are then used as input into CENTURY to provide SOC stocks within a CV. In addition, SOC stocks are continuously updated due to mechanisms of decay and physicochemical stabilization. The next sections describe the assumptions of the proposed landscape oriented approach, as well as the enhanced redistribution mechanism formulation that this framework offers.

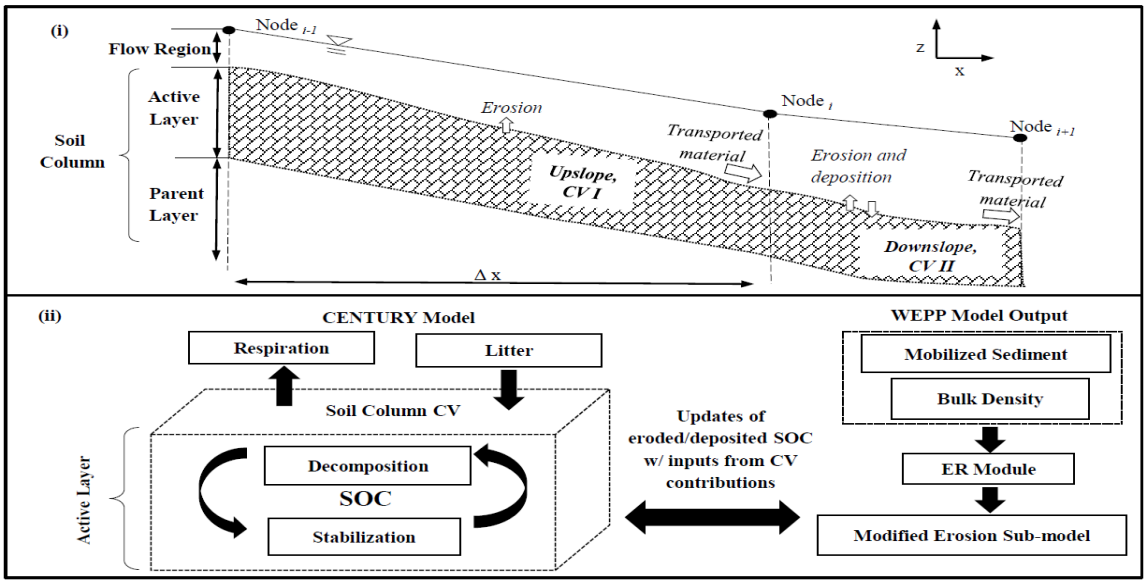

Figure 5.1 Linked WEPP-CENTURY modeling framework. A hillslope is segmented into control volume (CV) sections composed of a flow region, soil active layer, and parent layer. (i) The WEPP model and ER module are used to simulate the mobilization, transport, and deposition of soil size fractions and SOC along the hillslope. (ii) The integrative modeling framework allows the CV active layer to be updated via redistribution (from Figure 5.1i) as well as physical mechanisms (processes) of decomposition, stabilization, and litter incorporation

5.2.1 Modeling Assumptions

The proposed landscape-oriented approach is based on the following eight assumptions:

1. The distribution of rainfall is uniformly applied to the CVs at the hillslope scale [Elhakeem and Papanicolaou, 2009]. Soil properties within each CV are treated as homogeneous but heterogeneous between the two CVs, which are updated during the simulations.
2. The impact of tillage events is to exacerbate the effects of rainfall/runoff erosion on SOC stocks rather than directly displacing soil in the downslope [Quine et al., 1999; Van Oost et al., 2005].
3. A fixed fraction of the SOC transported in runoff is considered to be mineralized so that the C loss due to mineralization of SOC in the transported soil can be estimated by a simple relation. In our study it is assumed that 20% of the mobilized material is mineralized [Lal, 2006; Yadav and Malanson, 2009].

4. Soil is mobilized and transported through both interrill and rill processes [Zhang et al., 2003; Wang et al., 2013], where rainsplash effects dominate the interrill areas [e.g., Gilley et al., 1985; Gabet and Dunne, 2003] and concentrated overland flow is the main driver for soil particle movement in rills [e.g., Römkens et al., 2002; Rieke-Zapp and Nearing, 2005].
5. The capacity of a soil particle to bind SOC is proportional to its surface area and the affinity of its surface to hold carbon [Palis et al., 1997; Thevenot, 2010; Wäldchen et al., 2012; Wang et al., 2013].
6. The soil continuum is composed of both primary particles and aggregates [Foster et al., 1985]. The primary particles (i.e., clay, silt, and sand) are each assigned their median diameters. Aggregates are partitioned into small and large aggregates, with specific gravity values of 1.8 and 1.6, respectively. The size distribution and composition of mobilized soil particles is based on the availability of the range of size fractions found within the active layer of the soil column [Foster et al., 1985]. Rill and interrill areas are source contributors of different size fractions to the active layer. The eroding zone is treated as supply-limited (i.e., no incoming material from upslope sections) [Yalin, 1963; Abrahams et al., 2001].
7. Surface residue is distributed homogenously across the soil surface of each CV, and is incorporated vertically within the soil active layer profile during a tillage event [Salinas-Garcia et al., 2002; Flanagan et al., 2012].
8. SOC biogeochemical stabilization within the active layer is treated as a continuous process that includes not only supply contributions from decayed labile forms of SOC, such as root exudates and residue leachates, but also the decayed portions of incorporated residue and roots, which are relatively more decay-resistant than fresh plant material [Six et al., 2002; Olchin et al., 2008].

5.2.2 Enhanced Model Formulation

In the sub-sections below, we provide the basic relationship used to estimate SOC stocks within the active layer followed by the key formulation for estimating daily soil

fluxes, enrichment ratios, textural updates of the active layer, and related monthly-aggregated SOC fluxes and changes.

Updates in soil flux inputs/outputs along with updates in textural and soil microclimate conditions affect rates of decomposition, stabilization, and respiration within the soil profile [Paustian et al., 2006]. Appendix A provides key formulation for the hydrologic component and Appendix B describes formulation for the decomposition, stabilization and respiration processes. All formulation is presented below in index notation.

5.2.2.1 Estimation of SOC Stocks within the Active Layer

The stock of SOC (g C/m^2) present within the active layer of CV *i* at time *j*, $(SOC_{ACT})_i^j$, is defined as follows:

$$(SOC_{ACT})_i^j = \left(\rho_{Bulk_{ACT}} \left(\frac{M_{Carbon_{ACT}}}{M_{Soil_{ACT}}} \right) D_{ACT} \right)_i^j \qquad \text{[Eq. 5.1]}$$

where $\rho_{\text{Bulk}_{\text{ACT}}}$ is the dry soil bulk density of the active layer at time *j* (g/m^3); $M_{\text{Carbon}_{\text{ACT}}}$ is the mass of carbon in the active layer (g); $M_{\text{Soil}_{\text{ACT}}}$ is the mass of soil within the active layer (g); and D_{ACT} is the active layer depth (m).

Studies in agricultural fields have shown that the dry bulk density values can fluctuate sub-seasonally or seasonally via management and microclimate perturbations [Logsdon and Karlen, 2004; Osunbitan et al., 2005; Burras et al., 2008]. To reflect these changes, we estimate the dry bulk density within the soil active layer, $\rho_{\text{Bulk}_{\text{ACT}}}$, of CV *i* at time *j*, with (assumption 2):

$$\left(\rho_{bulk_{ACT}}\right)_i^j = (\rho_{till})_i^j + \left(\Delta\rho_{rf} + \Delta\rho_{wt}\right)_i^{j-DTE} \qquad \text{[Eq. 5.2]}$$

where ρ_{till} is the dry bulk density value following a particular tillage event (g/m^3); *DTE* is the number of days since the last tillage disturbance; $\Delta\rho_{rf}$ is the increase in density due to rainfall consolidation (g/m^3); and $\Delta\rho_{wt}$ is the increase in density due to weathering consolidation (g/m^3) that is mostly triggered by heavy equipment [e.g., Williams et al., 1984; Flanagan et al., 2007].

5.2.2.2 Estimation of Net Soil Fluxes and ER-"The ER module"

The steps involved in estimating the net soil fluxes and ER for daily rainfall/runoff events via WEPP and the ER module are outlined in Figure 5.2 and are as follows: (i) determination of interrill contributions of different size fractions (five fractions are used in this study) using an improved interrill transport capacity formula, see Eqs. [5.5-5.7]; (ii) determination of rill contributions and routing of the transported soil flux of different size fractions (both interrill and rill contributions) along the downslope, see Eqs. [5.8-5.10]; (iii) updating the composition of the active layer based on the net fluxes of material of each size fraction, see Eq. [5.11], and; (iv) aggregating the daily net fluxes to a monthly scale to estimate losses or gains in SOC stocks, see Eqs. [5.12-5.17].

Size Fractions: We take advantage of existing WEPP features to represent size fractions of soil (denoted by *p*). WEPP employs five size fractions (*p=1,...,5*) representing the soil matrix as both primary particles and aggregates [Foster et al., 1985]. The primary particle diameters d_{clay}, d_{silt}, and d_{sand}, are assigned median values of 0.002 mm, 0.010 mm, and 0.2 mm, respectively. The diameter, d_{smag}, of small aggregates (mm)

is approximated using the following empirical equations where *cl* denotes the clay percentage [Foster et al., 1985]:

$$d_{smag} = \begin{cases} 0.030 & cl < 0.25 \\ 0.2(cl - 0.25) + 0.030 & 0.25 \le cl \le 0.60 \\ 0.100 & cl > 0.60 \end{cases} \quad \text{[Eq. 5.3]}$$

For large aggregates, the diameter, d_{lgag} (mm), is determined as follows:

$$d_{lgag} = \begin{cases} 0.300 & cl \le 0.15 \\ 2cl & cl > 0.15 \end{cases} \quad \text{[Eq. 5.4]}$$

In WEPP small and large aggregates, are assigned specific gravity values of 1.8 and 1.6, respectively. If coarser material fractions were present WEPP can easily incorporate them by modifying the number of soil size fractions *p*.

Interrill Erosion: For each size fraction *p*, the interrill detachment rate, $D_{\text{inte}\,p_i}$ (g/s/m), is estimated as:

$$D_{inte\,p_i} = f_p D_{inte_i} \quad \text{[Eq. 5.5]}$$

where f_p is the mass fraction of size fraction *p* in the active layer and $D_{\text{inte}i}$ (g/s/m) is calculated as $D_{\text{inte}_i} = K_{\text{int}_i} I_{\text{e}} \sigma_{\text{int}_i} R_{\text{int}_i}$ [Foster et al., 1995] where K_{int_i} is the interrill erodibility (g/s/m^4); I_{e} is the effective rainfall intensity (m/s); σ_{int_i} is the interrill runoff rate (m/s); and R_{int_i} is the width of the interrill area.

To estimate soil contributions to rills from interrill areas, we introduce into the ER module the Abrahams et al. [2001] transport capacity formula, rewritten for each size fraction as follows:

$$TC_{intp_i} = \phi \rho_{sp} \left[g\left(SG_p - 1\right) d_p \right]^{0.5} d_p \quad \text{[Eq. 5.6]}$$

where

$$\phi = a\tau^{*}_{int\,p_i}{}^{1.5}\left(1-\frac{\tau^{*}_{c\,int\,p_i}}{\tau^{*}_{int\,p_i}}\right)^{0.5}\left(\frac{u_{int_i}}{u_{*int_i}}\right)^{c}\left(\frac{w_{sp}}{u_{*int_i}}\right)^{-0.5}$$

$$a = 10^{-0.42Cr_{int_i}/Dr_{int_i}^{0.2}}$$

$$c = 1+0.42Cr_{int_i}/Dr_{int_i}^{0.2}$$

where $TC_{\text{int}p_i}$ (g/s/m) is the sediment transport capacity of size fraction *p* in the CV; SG_p is the particle specific gravity (-) of each size fraction *p*; ρ_{sp} is the particle density (g/m^3); d_p is the median particle diameter (m) for each fraction *p*; $\tau^{*}_{\text{int}\,p_i}$ is the dimensionless shear stress acting on size fraction *p* (-); $\tau^{*}_{\text{c int}\,p_i}$ is the dimensionless critical shear stress (-); u_{int_i} is the interrill flow velocity (m/s); $u_{*\text{int}_i}$ is the shear velocity (m/s); w_{sp} is the settling velocity (m/s) of the median particle diameter; and a and c are regression coefficients dependent on the concentration of roughness elements; Cr_{int_i} (-), and the characteristic roughness diameter, Dr_{int_i} (m) in the CV.

If the transport capacity of the size fraction, $TC_{\text{int}p_i}$, is greater than its detachment rate, (i.e., $TC_{\text{int}p_i} > D_{\text{inte}\,p_i}$), then the interrill supply, $D_{\text{int}p_i}$, of the size fraction to the rill (per unit rill area; kg/s/m^2) is determined as:

$$D_{\text{int}p_i} = \frac{D_{\text{inte}\,p_i}}{w_{rill}} \qquad \text{[Eq. 5.7a]}$$

where w_{rill} is the width of the rill (m). On the other hand, if $TC_{\text{int}\,p_i} < D_{\text{inte}\,p_i}$, then $D_{\text{int}p_i}$ (g/s/m^2) is calculated as follows :

$$D_{int\,p_i} = \frac{1}{w_{rill}}\left[D_{inte\,p_i} - \frac{\beta w_{sp}}{\sigma_{int_i}}\left(D_{inte\,p_i} - TC_{int\,p_i}\right)\right] \qquad \text{[Eq. 5.7b]}$$

where β is a turbulence re-suspension coefficient (assigned a value of 0.5) and w_{sp} is the settling velocity for size fraction *p* (m/s) estimated using the approach described in Fox and Papanicolaou [2007].

Rill Erosion and Downslope Particle Transport: A steady-state form of the 1-D sediment continuity equation is used to account for the collective net fluxes contributed in the downslope by the interrill and rill areas. The downslope flux equation for each size fraction is solved along a rill where the contributions of interrill areas are assumed to occur laterally along the rill longitude:

$$G_{ACTp,i} = D_{int\,p_i} + D_{rill\,p_i} \qquad \text{[Eq. 5.8]}$$

where G_{ACTp} (g/m/s) is the transported soil load of size fraction *p* derived from the active layer within CV *i*;[,] implies the derivative of G_{ACTp} in the downslope; $D_{int p_i}$ is the net interrill flux rate of size fraction *p* (g/s/m^2) determined with Eq. [5.7]; and $D_{rill\,p_i}$ is the net rill flux rate of size fraction *p* (g/s/m^2).

For determining whether net erosion or deposition is occurring within CV *i*, the rill flow transport capacity, $TC_{rill\,p_i}$ (g/m/s), is determined using the Yalin [1977] formula:

$$\frac{TC_{rill\,p_i}}{SG_p d_p \rho^{0.5} \tau_{o\,rill\,p_i}{}^{0.5}} = 0.635\left[1 - \frac{1}{\beta_0}\ln(1+\beta_0)\right] \qquad \text{[Eq. 5.9]}$$

where

$$\beta_0 = 2.45\left(SG_p\right)^{-0.4}\left(\tau^*_{c\,rill\,p_i}\right)^{0.5}\delta$$

$$\delta = \frac{\tau^*_{rill\,p_i}}{\tau^*_{c\,rill\,p_i}} - 1$$

$$\tau^*_{rill\,p_i} = \frac{\tau_{o\,rill\,p_i}}{\rho\left(SG_p - 1\right)g d_p}$$

$$\tau^*_{c\,rill\,p_i} = \frac{\tau_{c\,rill\,p_i}}{\rho\left(SG_p - 1\right)g d_p}$$

where SG_p is the particle specific gravity (-) of size fraction p; g is the acceleration due to gravity (m/s^2); ρ is the density of water (g/m^3); d_p is the particle diameter (m) of size fraction *p*; $\tau_{o\,rill\,p_i}$ is the hydraulic shear stress (Pa); $\tau_{c\,rill\,p_i}$ is the critical erosional strength (Pa); $\tau^*_{rill\,p_i}$ denotes the dimensionless shear stress acting on the rill bed; $\tau^*_{c\,rill\,p_i}$ denotes the dimensionless critical shear stress (-), and β_0 and δ are dimensionless parameters that reflect the soil properties [Foster and Meyer, 1972; Alonso et al., 1981; Finkner et al., 1989].

When net erosion occurs for a size fraction (i.e., $TC_{rill\,p_i} > G_{ACTp_i}$) the rill erosion rate, $D_{rill\,p_i}$ (kg/s/m^2), is determined as:

$$D_{rill\,p_i} = K_{rill\,p_i}\left(\tau_{o\,rill\,p_i} - \tau_{c\,rill\,p_i}\right)\left(1 - \frac{G_{ACTp_i}}{TC_{rill\,p_i}}\right) \qquad \text{[Eq. 5.10a]}$$

where $K_{rill\,p_i}$ denotes the rill erodibility (s/m) that is a function of surface roughness and soil textural properties. When there is net deposition (i.e., $TC_{rill\,p_i} < G_{ACTp_i}$), $D_{rill\,p_i}$ is determined as:

$$D_{rill\,p_i} = \frac{\chi w_{sp}}{q_{rill\,i}}\left(TC_{rill\,p_i} - G_{ACTp_i}\right) \qquad \text{[Eq. 10b]}$$

where $q_{\text{rill}\,i}$ is the unit discharge (m²/s) in the rill; w_{sp} is the settling velocity; and χ (~0.5) is a raindrop-induced turbulent coefficient [Lindley et al., 1995].

Active Layer Composition Updates: Eqs. [5.5-5.10] are solved for each size fraction to accommodate textural changes in the soil active layer in CENTURY. At the end of each time step, the updated mass fraction, $f_{\text{ACT}pi}^{j+1}$, of each size fraction *p* in the soil active layer of CV *i* at time *j+1* is determined as follows [Papanicolaou et al., 2011]:

$$f_{ACTpi}^{j+1} = \frac{Mass_{ACTpi}^{j+1}}{\sum_{p} Mass_{ACTpi}^{j+1}} \qquad \text{[Eq. 5.11]}$$

where

$$Mass_{\text{ACT}pi}^{j+1} = Mass_{\text{ACT}pi}^{j} - \left(Mass_{erodpi}^{j} - Mass_{depopi}^{j}\right) \pm A_{\text{CV}i} DZ \rho_{si} f_{PARpi}$$

where $Mass_{\text{ACT}pi}^{j}$ is the mass with size fraction *p* in the active layer at time *j* (g); $Mass_{erodpi}$ is the mass with size fraction *p* (g) that eroded within time interval *DT*; $Mass_{depopi}$ is the deposited mass with size fraction *p* (g) within *DT*; $A_{\text{CV}i}$ is the surface cross-sectional area (m²) of CV *i*; $f_{\text{PAR}pi}$ is the mass fraction of size fraction *p* transferred to (- if under net deposition) or incorporated from the parent layer (+ if under net erosion); ρ_{si} is the bulk density of the parent layer (under net erosion) or the active layer (under net deposition); and DZ_i is the net change in bed elevation (m) for CV *i* accounting for the net flux of material for all size fractions and the soil porosity.

Soil Enrichment and ER Determination: We determine the ER of mobilized and deposited soil in the CVs by determining the specific surface area of the active soil material as follows:

$$SSA = \sum_{p} f_{mp} \left(\frac{fr_{sndp} SSA_{snd} + fr_{sltp} SSA_{slt} + fr_{clyp} SSA_{cly}}{1 + fr_{orgp}} + \frac{fr_{orgp} SSA_{org}}{1.73} \right) \quad \text{[Eq. 5.12]}$$

where f_{mp} is the proportion of size fraction *p* in the material being considered (i.e. active layer, mobilized or deposited material); fr_{sndp}, fr_{sltp}, fr_{clyp}, and fr_{orgp} are the mass proportions of sand, silt, clay and organic matter in each size fraction *p*, respectively; and SSA_{snd}, SSA_{slt}, SSA_{cly}, and SSA_{org} are the specific surface areas of sand (0.05 m^2/g), silt (4.0 m^2/g), clay (20 m^2/g), and organic carbon (1000 m^2/g), respectively [Sposito, 1989; Flanagan and Nearing, 2000]. For in-situ soils, f_{mp} is the proportion of size fraction *p* in the soil active layer, whereas for mobilized and deposited soils, f_{mp} is the proportion of size fraction *p* in the total eroded and deposited soil fluxes, respectively. The value of 1.73 is used to convert the fraction of organic matter to organic carbon [e.g., Neitsch et al. 2002].

The capacity of a soil particle to bind SOC is proportional to the particle's surface area [Palis et al., 1997; Wang et al., 2013] and the soil enrichment ratio of CV *i* at time *j*, $\left(ER_{Erod\,ACT}\right)_i^j$, (assumption 5) can be expressed as:

$$\left(ER_{Erod\,ACT}\right)_i^j = \left(\frac{SSA_{Erod_{ACT}}}{SSA_{SOIL_{ACT}}} \right)_i^j \quad \text{[Eq. 5.13]}$$

where $SSA_{\text{Erod}_{\text{ACT}}}$ is the specific surface area of eroded soil (m^2/g); and $SSA_{\text{SOIL}_{\text{ACT}}}$ is the specific surface area of the in situ soil (m^2/g). To determine the enrichment of the material being deposited within CV *i* at time *j*, $\left(ER_{\text{Depo}_{\text{ACT}}}\right)_i^j$ the following expression is used:

$$\left(ER_{Depo_{ACT}}\right)_i^j = \left(\frac{SSA_{Depo_{ACT}}}{SSA_{Mob_{ACT}}}\right)_i^j \qquad \text{[Eq. 5.14]}$$

where $SSA_{\text{Depo}_{\text{ACT}}}$ is the specific surface area of deposited soil (m^2/g) and $SSA_{\text{Mob}_{\text{ACT}}}$ is the specific surface area of the total mobilized soil from which material is deposited (m^2/g).

Net SOC Fluxes within the Soil Profile: The net flux of material, $\left(G_{\text{ACT}}\right)_i^j$ in g/s, from CV *i* at time *j* is calculated as the sum of the fluxes of all the size fractions (i.e., $\left(G_{\text{ACT}}\right)_i^j = \sum_p \left(G_{\text{ACT}p} \times w_{rill}\right)_i^j$). The calculated $\left(G_{\text{ACT}}\right)_i^j$ values are aggregated for each month to estimate the loss or gain in SOC for the month. For net erosional events (i.e., $G_{ACT} > 0$) the loss of SOC for CV *i* in a given month j, $\left(SOC_{\text{NetErod}_{\text{ACT}}}\right)_i^j$, is estimated as:

$$\left(SOC_{NetErod_{ACT}}\right)_i^j = (SOC_{ACT})_i^j \left(\frac{G_{ACT} ER_{Erod\,ACT}}{\rho_{Bulk_{ACT}} D_{ACT}}\right)_i^j DT \qquad \text{[Eq. 5.15]}$$

where $\rho_{\text{Bulk}_{\text{ACT}}}$ is obtained from Eq. [5.2]; and $ER_{\text{Erod ACT}}$ is the enrichment ratio of monthly-aggregated material leaving the CV (see Eq. [5.13]).

Per assumption 3, the portion of $\left(SOC_{\mathrm{NetErod}_{\mathrm{ACT}}}\right)_i^j$ that is considered to be mineralized during transport, $\left(SOC_{\mathrm{OX}_{\mathrm{ACT}}}\right)_i^j$, is estimated as follows:

$$\left(SOC_{OX_{ACT}}\right)_i^j = f_{OX_i}\left(SOC_{NetErod_{ACT}}\right)_i^j \qquad \text{[Eq. 5.16]}$$

where f_{OX_i} is a fixed fraction assumed to be 20% [Yadav and Malanson, 2009] in this study. For net depositional events ($G_{ACT} < 0$), fluxes of SOC being deposited within CV i in month j, $\left(SOC_{NetDepo_{ACT}}\right)_i^j$ are expressed as:

$$\left(SOC_{NetDepo_{ACT}}\right)_i^j = (1 - f_{OXi-1})\left(SOC_{NetErod_{ACT}}\right)_{i-1}^j \frac{(G_{ACT})_i^j}{(G_{ACT})_{i-1}^j}\left(ER_{Depo_{ACT}}\right)_i^j \qquad \text{[Eq. 5.17]}$$

where $\left(SOC_{NetErod_{ACT}}\right)_{i-1}^j$ is the stock of SOC entering CV *i* from the upslope; and $\left(ER_{Depo_{ACT}}\right)_i^j$ is the enrichment ratio of monthly-aggregated material being deposited within CV *i* (see Eq. [5.14]).

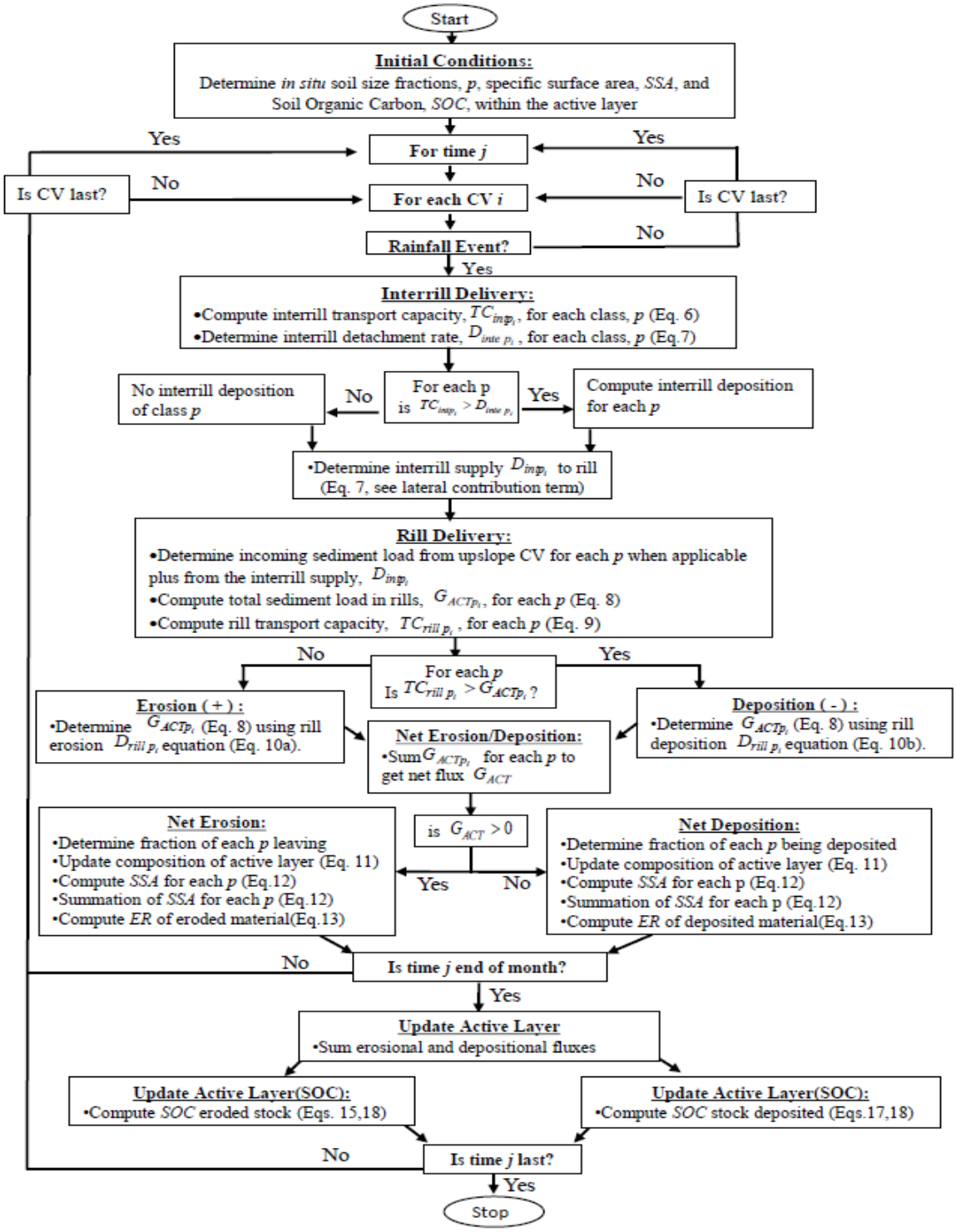

Figure 5.2 ER module and SOC stock updates. The enrichment ratios and SOC stock updates in the upslope and downslope zones are determined taking into account the mobilization and deposition of the different size fractions in both rill and interrill areas. The ER module considers the flow transport capacity in each area of the CV and updates the composition of the active layer with each event

5.2.2.3 Updating SOC Stocks

Using the above outputs from WEPP and the ER-Module as inputs to the CENTURY model, CENTURY is run sequentially for each CV along the downslope, simulating SOC dynamics from the impact of management and climatic events. Stocks of available SOC within the soil active layer are first determined (Eq. [5.1]). At the end of each month *j*, the net change in total SOC in the soil active layer of CV *i*, $(\Delta SOC_{ACT})_i^j$, in g C/m^2, is calculated as follows based on inputs from Eqs. [5.15 and 5.17].

For net erosion:

$$(\Delta SOC_{ACT})_i^j = (SOC_{ACT})_i^j - (SOC_{ACT})_i^{j-1} \cong \left(STAB_{ResD_{ACT}} - R_{HetSOC_{ACT}} - SOC_{NetErod_{ACT}}\right)_i^{j-1} \text{[Eq. 5.18a]}$$

For net deposition:

$$(\Delta SOC_{ACT})_i^j = (SOC_{ACT})_i^j - (SOC_{ACT})_i^{j-1} \cong \left(STAB_{ResD_{ACT}} - R_{HetSOC_{ACT}} + SOC_{NetDepo_{ACT}}\right)_i^{j-1} \text{[Eq. 5.18b]}$$

where $STAB_{ResD_{ACT}}$ is the net amount of SOC that was stabilized from decayed residue and root stocks for the month (g C/m^2; assumption 8; see Appendix B for more detail); and $R_{HetSOC_{ACT}}$ is the heterotrophic soil respiration during SOC decomposition for the month (g C/m^2; see Appendix B for more detail).

5.3 Study Site Characteristics

5.3.1 Topographic Characteristics

The representative hillslope selected here is located within a region of the Clear Creek watershed where the predominant soil series is Tama (Fine-Silty, Mixed, Superactive, Mesic Typic Argiudoll), a mollisol, or prairie-derived soil, that is well-drained and formed from loess [Bettis et al., 2003]. Since European settlement, over 80%

of the watershed has been converted from intrinsic prairie conditions to row crop agriculture.

Although the watershed features a mosaic of convex and concave hillslopes [Dermisis et al., 2010], the selected representative hillslope has a convex, downslope curvature as it represents the worst case scenario in terms of soil and SOC loss [e.g., Huang et al., 2002; Rieke-Zapp and Nearing, 2005; Hancock et al., 2006; Dermisis et al., 2010]. The representative hillslope has an elevation drop of 22.5 m along a downslope length of 430 m yielding a declination of 5%, which is the approximate average gradient for the watershed [Dermisis et al., 2010].

For the case study, both upslope and downslope zones (CVs) have the same soil series, which is Tama. The representative hillslope does not extend all the way to the floodplain where the dominant soil series is Colo. The length and average gradient of the upslope were 320 m and 5.8%, respectively, and of the downslope, 110 m and 3.5%, respectively.

5.3.2 Management Practices

A detailed time series of local, historical management practices is provided in Table 5.1. The first cultivation practices were introduced around 1930 following a final burn and intensive breakup of prairie sod with the moldboard plow [Hart, 2001]. A 5-yr diverse crop rotation of corn-corn-oat-meadow-meadow (CCOMM) w/organic fertilizer was then adopted. In years 1 and 2 of that rotation, corn (*Zea mays*) was planted and the moldboard plow was used for both spring and fall tillage. Oats (*Avena sativa*) and alfalfa (*Medicago sativa*) were planted simultaneously in year 3 of the rotation with the oats acting as a companion crop to protect the alfalfa from excessive sunlight exposure and

weed competition. Grain harvest of the oats was performed in late summer of year 3 while in years 4 and 5, the alfalfa was cut and baled for hay twice per year. In each year of this 5-yr rotation, manure applications were applied in both spring and fall. However, in 1951, these manure applications were replaced with inorganic fertilizers [Keeney and Hatfield, 2008].

During the early 1970's, grain prices and demand began to surge, which prompted shifts of many bio-diverse crop rotations (e.g., CCOMM) to more intensified production of other commodity crops [Rupnow and Knoox, 1975; Trautmann et al., 1985]. From 1976-1990, soybeans (*Glycine max*) replaced oats and alfalfa grasses in a 3-yr rotation of *corn-corn-beans*, *CCB*. The CCB management period consisted of larger fertilizer applications and higher tillage intensity with the use of the chisel plow [Reicosky et al., 1997; Keeney and Hatfield, 2008].

In the 1990's intensified practices were replaced with more conservative tillage practices, including the 2-yr corn-soybean rotation of *spring till corn/no-till bean*, *STC-NTB* [Abaci and Papanicolaou, 2009]. During corn production in the 1st year of the rotation, a field cultivator performed reduced spring tillage prior to planting. In the 2nd year of the rotation, soybeans were planted under no-till conditions, with only minor disturbances to the soil from ripple coulters to chop up and remove residue stubble when planting. Fertilizer applications of anhydrous ammonium were knifed into the soil following soybean harvest when soil conditions were favorable [Keeney and Hatfield, 2008].

Table 5.1 Local Historic Management Practices Used in Model Simulations [a]

Time Period	Management	Rotation(yr.)	Crop	Tillage	Fertilizer
1930-1975	C-C-O-M-M (*Diversity*)	1	Corn	MP	Manure, inorganic
		2	Corn	MP	
		3	Oats	-	
		4	Alfalfa	-	
		5	Alfalfa	-	
1976-1990	C-C-B (*Intensification*)	1	Corn	CP	Broadcast urea
		2	Corn	CP	
		3	Soybean	CP	
1991-2010	STC-NTB (*Conservation*)	1	Corn	FC	Anhydrous ammonium
		2	Soybean	-	

[a] *MP, moldboard plow; CP, chisel plow; FC, field cultivator.*

5.3.3 Climatic Conditions

Due to the mid-continental location of Iowa, the climate for Clear Creek is characterized by hot summers, cold winters, and wet springs [Highland and Dideriksen, 1967]. Daily high temperatures reach an average July maximum of 30°C, while daily low temperatures reach an average minimum of -10°C in February [Markstrom et al., 2012]. Average annual precipitation is approximately 876 mm/yr with convective thunderstorms prominent in the early summer and snowfall in the winter [Iowa Environmental Mesonet, 2015]. For site specific information, the observed data from a neighboring weather station found in Williamsburg, IA was used [Arnold and Williams, 1989; Gete et al., 1999; Abaci and Papanicolaou, 2009]. We focus on the period of 1930-2010 as this is the period coinciding with the different management periods described earlier (see Table 5.1).

The time series of historic monthly precipitation for the period of 1930-2010 highlights a sequence of seasonal Gaussian distributions, with the peak rainfall in the

watershed being received in May and June of each year [Abaci and Papanicolaou, 2009]. In addition to the seasonal variability, several notable extreme climatic events, namely floods and droughts, have occurred throughout this time period, with implications to the overall carbon cycle [Reichstein et al., 2013]. Two major flooding events occurred in years 1982 and 1993 [Heinitz, 1986; Mutel, 2010] and an intensive drought period in 1988 [Handler, 1990].

5.4 Methodological Procedures

5.4.1 Model Initialization and Calibration

Prior to performing model simulations, the initialization and calibration steps of the loosely-coupled models were conducted. Careful attention was first placed on the initialization of CENTURY to ensure that the initial stocks of SOC adequately represented the conditions found within the active layer (top 20 cm) before introducing cultivation practices. The model was run for an extended period of time prior to 1930 to allow key biogeochemical processes and recalcitrant pools of SOC within CENTURY sufficient time to reach the *pseudo-equilibrated state* conditions where conditions do not change in an average sense with time [Metherell et al., 1993]. The year 1930 is considered a benchmark date to our modeling efforts as this is the year that the first cultivation practices were introduced.

Calibration was needed for both models. Topographic data (section 5.3.1) as well as longitudinal data of changes in management practices (section 5.3.2) and climate records (section 5.3.3) helped us perform the calibration procedures. Next, a description of initialization and calibration steps follows.

During the initialization period, intrinsic prairie conditions were considered, as a tall grass has been historically found throughout much of Iowa and the Midwest with minor grazing from free-range buffalo, and a 10-year fire frequency [Table 5.2; Hart, 2001; Weaver, 1968; Delucia et al., 1992; Macha and Cihacek, 2009; Kaiser, 2011]. For the representative hillslope, an initial stock of SOC (at t = 0) was first estimated as 5,500 g C/m^2 using the semi-empirical relation developed by Burke [1991], which considers average annual climatic and soil texture conditions as input parameters. Then, assuming the presence of the Big Bluestem (*Andropogon gerardii Vitman*), the model was run until the SOC stocks reached pseudo-equilibrated values of 4,520 g C/m^2 after approximately 4,000 years. This pseudo-equilibrated value of SOC agrees with the ranges of the reported field measured SOC stocks found within the Dinesen prairie, a remnant, native tallgrass prairie, the closest "undisturbed" location with SOC measurements to the study site [Harden et al., 1999; Manies et al., 2001]. No initialization of WEPP was needed since it was reasonable to assume that SOC mobilization due to erosion during the prairie period was insignificant other than some episodic events.

Typically, the calibration procedure for WEPP starts with flow (i.e., the driving mechanism for upland erosion) and continues with the sediment component [Santhi et al., 2001]. Additional information is needed in the model for key state variables such as the effective hydraulic conductivity, critical erosional strength, and residue cover which is available for the study site (see Tables 12 and 13 in Abaci and Papanicolaou, [2009]). Because the procedural steps for calibrating WEPP have been extensively described in the literature [e.g., Flanagan et al., 2007; Papanicolaou and Abaci, 2008; Abaci and

Papanicolaou, 2009; Dermisis et al. 2010] an emphasis here has been placed on the calibration for CENTURY.

The plant production sub-model of CENTURY was calibrated to ensure accurate inputs of plant material into the soil active layer. Based on prior studies the CENTURY model must be first calibrated using reported ranges of aboveground Net Primary Production (NPP) in this region, defined here as the total net carbon stored in above-ground vegetation (i.e., stems, leaves, grain) [e.g., Chapin et al., 2002]. Having the NPP estimated values within the measured ranges was deemed important for ensuring that CENTURY incorporates the correct inputs of above-ground C allocation for simulating below-ground C allocations and stocks.

The first step of the calibration process involved the collection of historic corn and soybean grain yield data (1930-2010) from Iowa County, where is the study location [NASS, 2012]. Yield data were converted to total grain mass and corrected for seed moisture, which is commonly assumed to be 15.5% [Lauer, 2002]. Using unique harvest indices, defined here as the ratio of grain to total plant mass [Huehn, 1993; Prince et al., 2001], the grain mass was used to estimate above-ground biomass. The above-ground biomass and grain mass data were then converted to a carbon density, namely NPP, by utilizing vegetative carbon contents of corn and soybean plants (i.e., leaves, stems, and grain) collected within the study site [unpublished data, Papanicolaou, 2014]. Measured values of corn and soybean plant carbon contents were found to be in good agreement (correlation above 90%) with reported literature values [Latshaw and Miller, 1924; Machinet et al., 2009].

A sensitivity analysis revealed that precipitation and temperature data were sensitive parameters within the CENTURY plant production sub-model [Xiao et al., 2004; Schurgers et al., 2011]. For this reason, local climate data from the Williamsburg site was used to simulate the time series of NPP from 1930-2010. The simulation period was partitioned into the following key crop rotations: CCOMM from 1930 to 1975; CCB 1976 to 1990; and STC-NTB 1991 to 2010 (see Table 5.1), with soybeans present in years 1976-2010, and corn present throughout the entire simulation. During the calibration efforts the reported statewide nitrogen fertilizer application rates for Iowa were adopted [NASS, 2012].

Comparisons of NPP values estimated using the above-mentioned methods and simulated NPP from 1930 to 2010 are shown in Figure 5.3. In terms of corn, there is an overall upward trend in simulated NPP from 1930 to 2010 which agrees well with the estimated NPP values. During this time period, NPP increases from 350 g C/m^2 to around 1,400 g C/m^2. Large variability in NPP occurs during CCB management, between the years 1980 to 1993, due to reported extreme climatic events, namely droughts and flooding [Rosenzweig et al., 2012].

For soybeans (1976-2010), simulated values increase from 288 g C/m^2 to around 450 g C/m^2. Overall, the simulated and estimated NPP appear to be in an agreement (R^2 value=0.84) for the entire period 1930 to 2010.

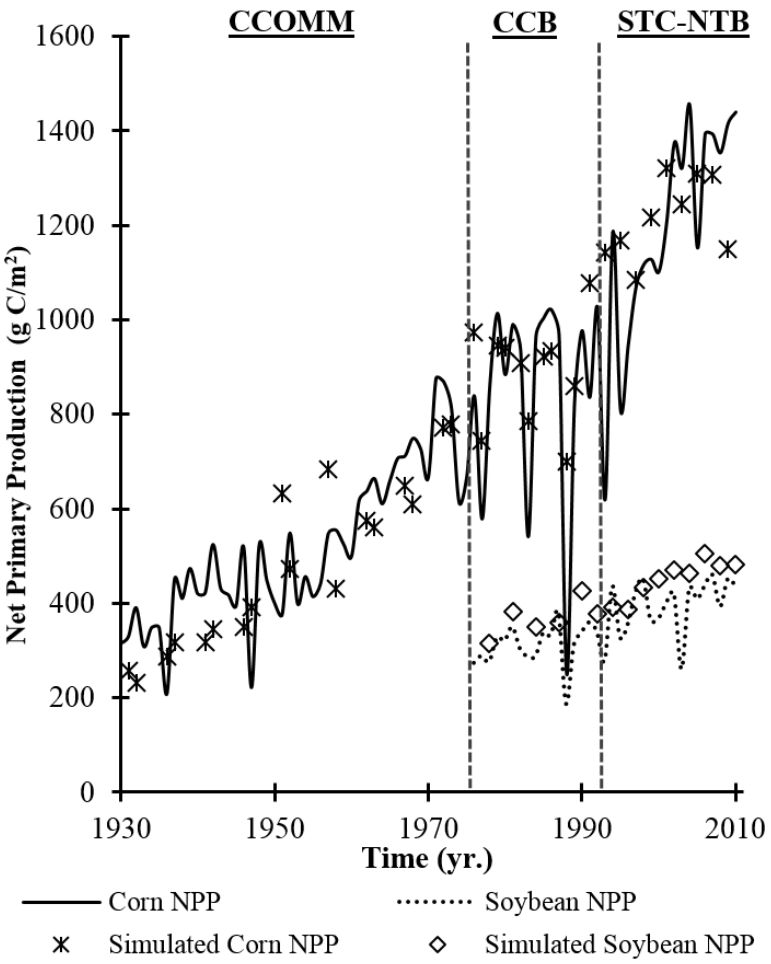

Figure 5.3 Model Calibration. Local corn and soybean grain yield data, field-measured values of vegetative carbon content as well as harvest indices were used to generate a times series of estimated aboveground Net Primary Production (NPP) values of corn (solid green line) and soybeans (solid blue line) from 1930 until 2010 as well as simulated values of corn NPP (green dot) and soybean NPP (blue dot). The simulated values of NPP are the average of the upslope and downslope zones

5.4.2 Verification

To assess the predictive capabilities of the newly developed framework, samples (n = 250) were collected from representative field locations in 2005, 2007, and 2010 and tested for SOC using an elemental analyzer following methods in Martinotti [1997] and Pansu et al. [2001]. Sampling locations were determined based on results from Papanicolaou et al. [2009] and literature found in Fox and Papanicolaou [2007; 2008].

Factors hypothesized to induce variation of SOC stocks in the study site (e.g., depth, soil type, management, gradient) were used to fine tune the sampling locations in both eroding and depositional areas. Comparisons of the measured and the simulated values are presented in section 5.5.4.

5.5 Analysis of Results

In this section, we present estimates of net erosion/deposition and dry soil bulk density generated from WEPP, as well as ER values generated from the ER module for the upslope and downslope CVs for the period of 1930-2010. These estimates are generated by accounting for rill and interrill contributions and are utilized to generate, via CENTURY, SOC trends where long-term changes in SOC stocks are assessed as a function of historic management practices and climatic conditions for 1930-2010.

5.5.1 Spatial Heterogeneity and Temporal Variability of Net Soil Fluxes

Figure 5.4i provides a time series of the daily precipitation, color coded with simulated daily runoff coefficients (RC) from 1930-2010 to discern the effects of rainsplash from concentrated flow on the magnitude and direction of the soil fluxes. Figures 5.4ii-5.4iii illustrate the corresponding net erosion and net deposition fluxes for the different management practices.

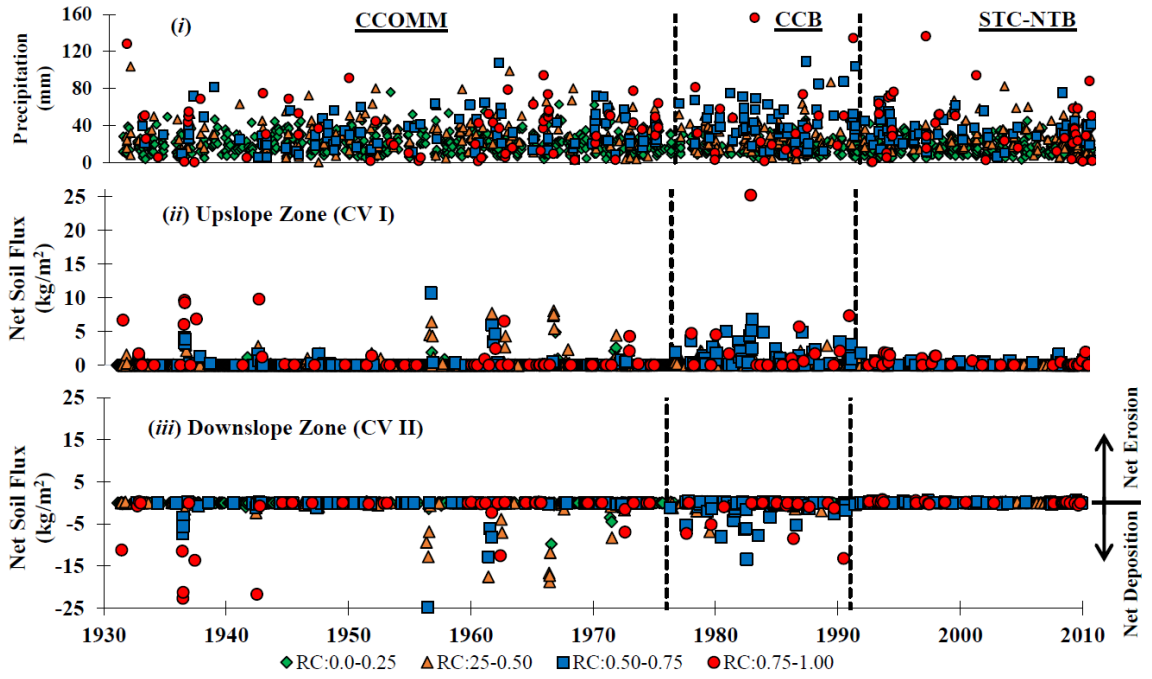

Figure 5.4 Time series of simulated runoff coefficient and soil redistribution. A time series of simulated runoff coefficients (RC) is shown in Figure 5.4i, with corresponding net erosion rates for the upslope (Figure 5.44ii) and downslope (Figure 5.44iii) zones of the representative hillslope. The net erosion plots (Figure 5.4ii-5.4iii) are color coded with the following corresponding RC intervals (0.00-0.25=green diamond; 0.25-0.50=orange triangle; 0.50-0.75=blue square; 0.75-1.00=red circle). The time series covers the years 1930 to 2010, reflecting CCOMM, CCB, and STC-NTB management practices

The RC values throughout the CCOMM management period (1930-1975) averaged 0.18. During the corn production years of the CCOMM rotation (years 1-2), however, RC values were found to be 35% higher than years in grass production (years 3-5 of rotation) despite similar precipitation amounts. During the CCB management period (1976-1990), RCs were highest, averaging 0.30. The highest RC during this time period was during the June flood of 1982 [Heinitz, 1986; Barnes and Eash, 1990], which produced a monthly RC value of 0.65. In the management period of STC-NTB (1991-2010), RC values dropped to an average of 0.26, as conservation tillage methods become prevalent. However, extreme events during the flood of 1993 had an average RC of 0.46, which was almost double the average of the entire period.

In CV I (Figure 5.4ii), the net erosion events appeared to be more spread out during the CCOMM period comparatively to the CCB and STC-NTB periods. Significant erosion events occurred for the CCOMM period in only two of the five years of the rotation when corn was grown and attributed to the decreased land cover from tillage activities. The average net monthly erosion for the entire period was estimated as 0.48 kg/m^2/month. The frequency of erosion events intensified during the CCB period due to reduced land cover in each year of the rotation and increased tillage frequency (3 out of 3 yr for CCB vs. 2 out of 5 yr for CCOMM). The 1st year of the rotation generally experienced the highest net erosion rates because fall tillage events performed after harvesting soybeans provided less residue cover than corn [Abaci and Papanicolaou, 2009]. The average net monthly erosion during the CCB management period was 0.99 kg/m^2/month, which was more than double the CCOMM rates. The largest net flux for the entire simulation period, 25.2 kg/m^2, occurred in the CCB period during the recorded flood event in June of 1982, where 15 cm of rainfall fell on top of an already wet year [Barnes and Eash, 1990]. There was a significant reduction in net erosion rates with the introduction of conservation practices in the STC-NTB period, in the form of reduced tillage and no-till practices [Abaci and Papanicolaou, 2009]. Overall, during STC-NTB management, the soil loss in CV I was found to average 0.21 kg/m^2/month, which was less than half the average rate during the CCOMM management. Similar value ranges for STC-NTB management have been reported in this region (although the emphasis has been in Western Iowa) by Bukart et al. [2005] and Karlen et al. [2013].

In the downslope control volume, CV II (Figure 5.4iii), the absolute magnitude of net soil fluxes during all management periods was generally less than the magnitude in

the upslope CV. During the CCOMM and CCB periods, deposition events in the downslope appeared to "mirror" incoming fluxes from the upslope (Figure 5.4ii), suggesting that contributions from the upslope generally exceeded the transport capacity of flow in the downslope, where the unit flow power term - defined as the amount of flow energy available to mobilize and transport material [Yang, 1973] and expressed in Eq. [5.9] through the bed shear stress terms and coefficients as functions of gradient and velocity - was lower comparatively to the upslope. Overall, CV II experienced an average monthly net deposition rate of 0.66 kg/m^2/month in the CCOMM period. Net deposition events continued throughout the CCB management period, with an average net monthly deposition rate of 1.08 kg/m^2/month. This trend was consistent with net fluxes from the upslope during the CCB period being twice as much as the fluxes during the CCOMM period. During the STC-NTB conservation management, net soil fluxes in the downslope switched from net deposition to net erosion, at an average monthly rate of 0.11 kg/m^2/month. The considerably reduced supply of incoming material from the upslope during the STC-NTB period resulted to a supply limited system in CV II and increased mobilization of material derived from the downslope. Hence, although there were still some deposition for certain events, on average, the net flux for each month had generally a positive direction (net erosion). Despite the switch to net erosion, the flux rates in the downslope were less than half the rates in the upslope due to the lower unit stream power (Eqs. [5.9-5.10]). What is worth noting is that despite the positive net flux in both the upslope and downslope CVs for the STC-NTB period, the average monthly flux of material exiting the hillslope for that period was considerably less than the

CCOMM and CCB periods due to the effectiveness of the STC-NTB management at reducing net erosion overall.

5.5.2 Bulk Density Spatial and Temporal Variability

As seen in Figure 5.5, the dry soil bulk density (BD) decreased directly following a tillage event, and then increased as cumulative rainfall increased. The simulated BD values ranged between 0.92 to 1.40 g/cm^3. This is in good agreement with observed BD values of 0.90 to 1.40 g/cm^3, gathered from a collection of past and current research conducted within the study site. [Oneal, 2009; Papanicolaou et al., 2015; http://criticalzone.org/iml/infrastructure/field-area/clear-creek-watershed].

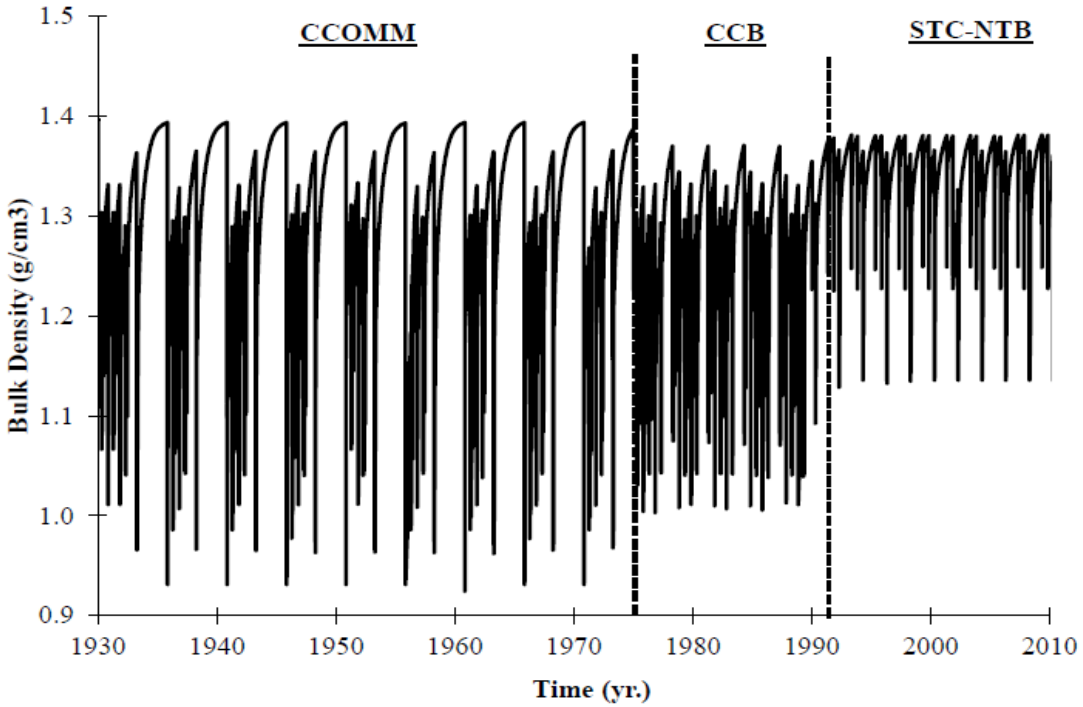

Figure 5.5 A time series of simulated daily soil bulk density values for the representative hillslope (black line) as determined by the WEPP model. The time series covers the period of 1930 to 2010 to reflect initiation of tillage. Field measurements of soil bulk density from the study watershed ranged from 0.90 to 1.48 g/cm^3, which are in good agreement with simulated values (Papanicolaou et al., 2008; O'Neal, 2009)

The introduction of the moldboard plow spurred inter-annual fluctuations in BD, decreasing values from 1.40 to 0.92 g/cm^3 during the years in which corn was planted in

the CCOMM management period. The BD increased in the months following the tillage events, potentially due to weight consolidation. In rotation years 3-5 when oats or alfalfa was present, the BD increased due to the prolonged absence of tillage events. During the CCB management period, inter-annual variability in BD decreased (1.35 to 1.00 g/cm^3) as less intensive tillage practices were used in the production of both corn and soybeans, and the BD was unable to reach to the maximum values found in CCOMM because the CCB rotation did not have long-enough "rebounding" periods. In year 1 of the 2-yr STC-NTB management practice, fluctuations in BD ranged from 1.38 to 1.13 g/cm^3. The smaller decrease in density was found to be from the reduced spring tillage before corn planting [Abaci and Papanicolaou, 2009]. However, in the 2nd year of the rotation, when no-till was used for soybean production, the even smaller decrease in BD from 1.35 to 1.25 g/cm^3 was due to disturbance of the soil by the planter, which was less intrusive. At the end of the 2nd year, application of the anhydrous ammonia also caused the BD to drop to 1.20 g/cm^3.

Overall, the ~20–40% change in BD supports the need to account for temporally updated values of BD in quantifying transport and deposition rates of soil and SOC. Similar trends and the need to account for the chronosequence in BD changes have been reported in the literature [Lal, 2005; Kuhn et al., 2009; Schwarzel et al., 2011; Celik et al., 2012].

5.5.3 Enrichment Ratio Spatial and Temporal Variability

Figure 5.6 highlights the time series of simulated ER values for the representative hillslope from 1930-2010. Figures 5.6i and 5.6ii represent material leaving the upslope and downslope CVs, respectively, whilst Figure 5.6iii represents material being deposited

within the downslope CV. In all plots, the ER values are categorized into four classes corresponding to those used for the precipitation and net erosion plots in Figure 5.4 based on the four RC classes. The plots reveal three key findings: (i) there are distinct differences in ER between the upslope and the downslope; (ii) ER varies with event magnitude; and (iii) management practices affect the ER.

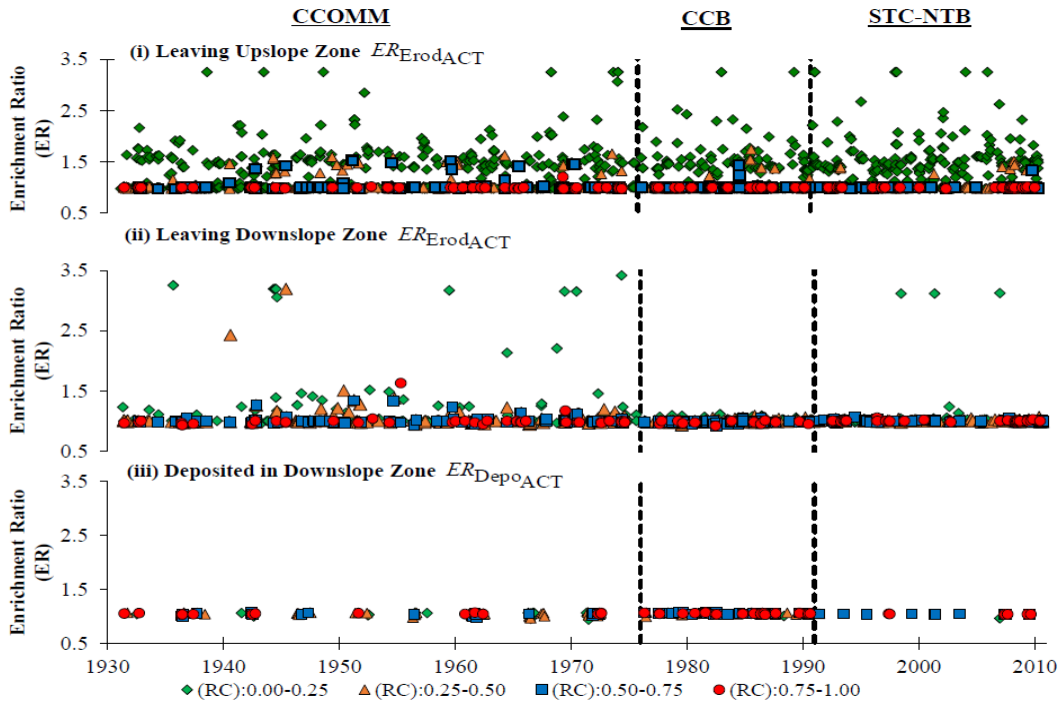

Figure 5.6 A time series of daily simulated enrichment ratios (ER) values of material leaving the upslope and downslope zones of the representative hillslope are provided in Figures 5.6i-5.6ii, respectively. Figure 5.66iii provides the ER values of the material being deposited within the downslope zone, aggregated to the monthly time scale. The ER values are broken into corresponding runoff coefficients (RC), with RC between 0.00-0.25(green diamond); 0.25-0.50 (orange triangle); 0.50-0.75 (blue square); and 0.75-1.00 (red circle)

In the upslope CV (Figure 5.6i), ER values ranged from 0.97–3.25 for all runoff-generating storms, with the maximum value reducing systematically from 3.25 to 1.2 from the smallest RC range (0.00–0.25) to the largest RC range (0.75–1.00). The

minimum ER value, on the other hand, was similar for all RC ranges, falling between 0.97–0.98. Average ER values followed the same trend as the maximum values, also systematically decreasing from 1.27 to 1.00 from the smallest RC range to the largest RC range. The general reduction in ER with increasing RC supports the notion of less preferential mobilization of different size fractions at higher flows where general motion usually occurs [Papanicolaou et al., 2004]. Under these high flow conditions, the composition of the mobilized soil is similar to the composition of the in-situ soil, resulting in little to no SOC enrichment of the transported soil. The results indicated that, on average, mobilized material during CCOMM period was 8% more enriched compared to the in-situ soil, whereas material mobilized during the CCB and STC-NTB periods were only 1% more enriched.

In the downslope CV, the average ER values under net erosion conditions (Figure 5.6ii) were generally lower in magnitude compared to their corresponding values in the upslope CV. Like the upslope, the average ER values in the downslope decreased systematically with increasing RC range from 1.17 to 0.99. The smaller ER values in the downslope compared to the upslope, highlighted the importance of rainsplash in the selective transport of finer material on the upper sections of the hillslope [Nadeu et al., 2011; Hu et al., 2013]. On the lower hillslope sections, concentrated flow effects, which tended to mobilize all fractions, were dominant and overshadowed the effects of rainsplash, leading to the smaller ER values. In the downslope CV, the mobilized material during the CCOMM period was only 4% more enriched than the in-situ soil, implying that the loss in SOC per unit mass of soil eroded was less in the downslope compared to the upslope (for the same initial SOC content).

Under net deposition conditions (Figure 5.6iii), material being transported from the upslope CV was deposited onto the active layer of the downslope CV. Deposition processes were also selective, but, on the contrary, favored heavier, generally larger size fractions. The deposited fraction was found to be either less or more enriched compared to the material being transported, depending on the composition of the deposited fractions. This is seen in Figure 5.6iii, where the range of ER values (from Eq. [5.20]) falls between 0.93–1.07. The depositional patterns in Figure 5.6iii reflect the management practices in each period. There are net-deposition events during the two corn production years of the CCOMM period, net-deposition events during each year of the CCB period, and net-deposition events every other year of the STC-NTB period, reflecting the tillage practices adopted. The ER values for all the management periods suggest that, on average, depositional events resulted in the flux of material that was 3-5% more enriched into the soil. This is consistent with the deposition of larger size fractions containing finer enriched material in their composition [Nadeu et al., 2011].

Overall, the smaller loss in SOC per unit mass of eroded soil in the downslope, combined with the relative enrichment of soil in the active layer, tended to promote higher SOC per unit mass in the downslope relative to the upslope. However, since the ER is concentration ratio, the actual loss or gain in SOC is dependent on the initial stocks of SOC to a large degree [Schiettecatte et al., 2008].

5.5.4 Effects of Long-Term Changes in LULC on SOC stocks

Figure 5.7 provides the time series of simulated monthly SOC stocks within the upslope and downslope CVs of the representative hillslope from 1930-2010. The year 1930 was selected to represent the introductory baseline SOC stock value of 4500 g C/m^2

supplied from the initialization (represented by the black dot in Figure 5.7) right before conversion to agricultural production.

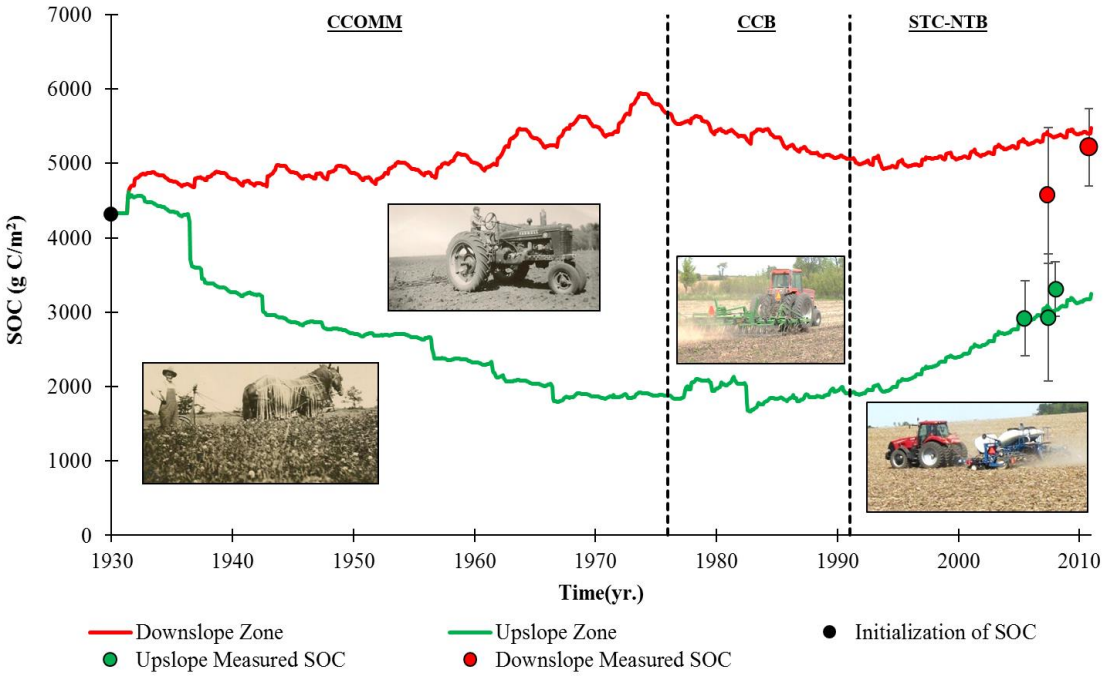

Figure 5.7 Spatial heterogeneity and temporal variability of SOC: A time series of simulated values of SOC is provided for the upslope (green line) and downslope (red line) zones of the representative hillslope. In addition, the baseline stocks of SOC acquired in during model initialization is also plotted (black dot). This figure highlights the variability of SOC throughout historic management practices from 1930 to 2010

In the upslope CV (green colored line), the general trend includes (i) significant losses of SOC following conversion to row crop agriculture during the CCOMM period; (ii) a "plateaued" recovery period during the CCB management period; and (iii) a "rebounding" period during the implementation of current STC-NTB conservation practices. Similar trends have been reported in other assessments of SOC within IMLs [Mann, 1986; Owens et al., 2002; Liu et al., 2003; Tornquist et al., 2009; Brown et al., 2010; Bortolon et al., 2011]. On conversion to row crop production in 1931, there was a sharp, initial spike in SOC stocks due the massive supply of organic material delivered to the active layer through tillage-incorporation of prairie grasses. After the spiked flux,

there were SOC losses attributed to the combined tillage effects with rainfall/runoff erosion events [Stinner et al., 1983; Tivy, 1990]. This is seen in Figure 5.7 with a series of "descending staircases" suggesting losses in SOC with time especially throughout the CCOMM period. Residue incorporation rates (i.e., SOC contributions from residue decomposition; see Eqs. [5.18], and [B3]) during the period averaged 127 g C/m^2/yr, while heterotrophic respiration and net erosional SOC losses were 115 and 67 g C/m^2/yr, respectively.

During the CCB management period, enhanced crop production rates from increased fertilizer usage and genetic seed advancements (see Figure 5.3) began to halt the downward trend of SOC stocks. Residue incorporation rates during this period increased to an average of 237 g C/m^2/yr, while heterotrophic respiration and net erosional losses rose to 131 and 104 g C/m^2/yr, respectively. Overall, SOC stocks kept nearly constant despite a punctuated loss of SOC during the 1982 flood event [Barnes and Eash, 1990].

During the STC-NTB management period, the implementation of conservation practices further decreased erosion rates, while the adoption of high-yield crop hybrids increased plant production such that residue incorporation was greater than the losses due to decomposition and erosion, resulting in SOC stock increases. Here residue inputs averaged 247 g C/m^2/yr, while respiration and erosional losses were 148 and 29 g C/m^2/yr. Loss of SOC due to erosion under STC-NTB was almost 4 times smaller than the previous CCB period. In fact, net erosion fluxes from flooding events in 1993 were "dampened", in part due to the protection offered by increased residue cover from conservation (reduced and no-till) practices [Rhoton et al., 2002]. Toward the end of the

simulation, SOC stocks appear to approach a new equilibrium value [Six et al., 2002; Stewart et al., 2007], building at a rate of 71 g C/m^2/yr, which is comparable to increases reported by Reicosky [1995].

SOC within the downslope net-depositional CV (red colored line) for all periods was found to be much higher than the upslope net-erosional CV, which has been reported in the literature [e.g., Stavi and Lal, 2011; Du and Walling, 2011; Navas et al., 2012; Wang et al., 2015]. Throughout the CCOMM period, the gradient of SOC stocks increased as the frequency of deposition events (Figure 5.4iii) and production rates also increased starting in the late 1950's (see Figure 5.3). Residue incorporation rates during this period averaged 196 g C/m^2/yr, while heterotrophic respiration was 217 g C/m^2/yr. Both of these rates were more than double the values found in the upslope. In addition, SOC losses due to erosion in the downslope were minimized, averaging around 4 g C/m^2/yr, which is over 10 times less than upslope losses. The average annual stock of SOC deposited from CV I contributions was 55 g C/m^2/yr. This finding could have major implications to the overall carbon budget of the system as most of the mobilized material was not actually exiting the hillslope.

During the CCB period, the downslope experienced a constant degradation in SOC stocks. Residue incorporation and heterotrophic respiration rates averaged 226 and 305 g C/m^2/yr, respectively. The rotational switch from grasses to soybean production not only decreased organic inputs (less biomass) into the soil, but also enhanced microbial activity through increased tillage frequency [Stinner et al., 1983; Tivy, 1990]. Average SOC losses due to erosion increased to over twice the CCOMM rates at 12 g

$C/m^2/yr$, while fluxes of deposited SOC from CV I contributions decreased to 50 g $C/m^2/yr$.

In the STC-NTB management period, the SOC stock began to slowly build and continued to rise, but at a slower rate than the corresponding period for the upslope. Residue inputs averaged 291 g $C/m^2/yr$, while respiration losses were 235 g $C/m^2/yr$. Erosional SOC losses in the downslope during this period, however, were the highest of all periods, matching rates in the upslope at 34 g $C/m^2/yr$. Deposition of SOC during this period was negligible due to the reasons outlined earlier (see section 5.5.1).

Lastly, Figure 5.7 also provides a comparison of simulated SOC stocks with field measured values of SOC from a field site in Clear Creek that exhibit nearly identical properties with those selected for the representative hillslope during the simulations (green dot represents values from upslope; red dot represents values from downslope). The figure shows good correspondence between the measured and the simulated values for the representative hillslope. Field values of SOC in the upslope and downslope zones are both increasing over time, with the downslope values higher than the upslope values, which is consistent with the simulation and literature reports [e.g., Liu et al., 2003].

5.6 Discussion and Conclusions

This chapter offers an improved methodological framework to account for the collective effects of soil erosion on SOC redistribution in IMLs by spatially simulating the key processes described in this study, taking into consideration monthly-aggregated changes in ER and BD. The framework loosely couples two established process-based models, WEPP and CENTURY, to incorporate the effects of the described landscape features on SOC stocks. A newly developed ER-module is used to overcome some

important limitations of WEPP by accounting for (i) textural updates of the active layer, (iii) the enrichment of material being deposited on the hillslope, and (ii) explicitly considering the effects of splash-driven interrill erosion on ER estimates.

The framework is applied in Clear Creek to a representative hillslope that is discretized into two CVs, namely an upslope net-erosional zone and a downslope net-depositional zone, to simulate spatial and seasonal changes in SOC stocks due to historical long-term changes in LULC (Table 5.1). Figure 5.8 summarizes the simulation results, illustrating the effects of management practice and hillslope location on changes in net soil fluxes, ER, BD, and associated SOC stocks. In the figure, the hollow arrows represent net soil fluxes, where net erosional fluxes are oriented in the downslope direction and net depositional fluxes are oriented vertically downward into the soil active layer. The sizes of the arrows represent the relative magnitudes of the fluxes; larger arrows indicate greater fluxes (and vice versa). SOC symbols with an upward arrow represent gains in SOC stocks whilst a downward arrow represents loss in SOC stocks. For ER and BD, the sizes of the symbols represent the relative magnitudes of the quantities.

During the CCOMM and CCB management periods, erosion fluxes from the upslope were generally higher than erosion fluxes from the downslope due to a greater supply of material from the upslope to the downslope resulting in a reduced capacity of flow to mobilize material in the downslope. On the contrary, during the STC-NTB period, erosion fluxes from the upslope were lower than the fluxes from the downslope since the supply from the upslope was greatly reduced and the flow in the downslope had a higher capacity to mobilize material. The average deposition rate was largest during

the CCB period due to the highest supply of material from the upslope, attributed to the greater tillage frequency and the lower soil cover. The deposition rate was smallest during the STC-NTB period due to the least supply of material from the upslope attributed to the effectiveness of conservation practices.

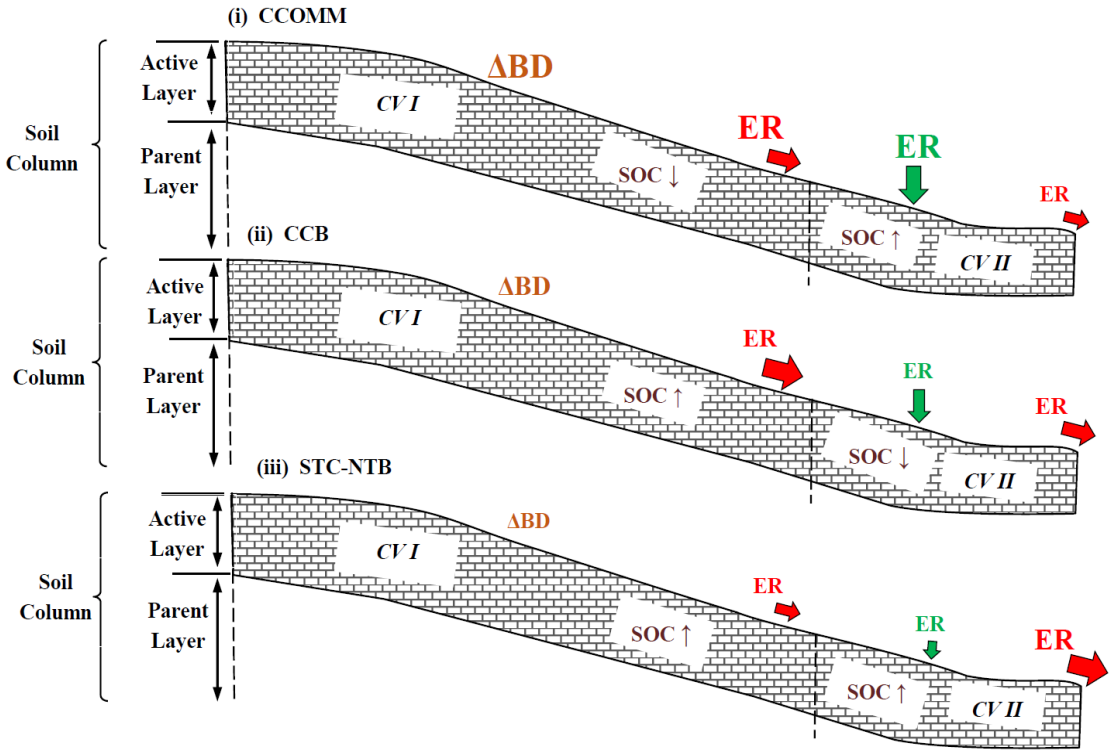

Figure 5.8 Summary of changes in Net Soil Fluxes, BD, ER, and SOC with Management Practice and Hillslope Location. Red arrows represent net erosional fluxes; green arrows represent net depositional fluxes, brown arrows represent changes in SOC stocks, and the ER and ΔBD symbols represent the enrichment ratios and changes in soil bulk densities respectively. Sizes of arrows/symbols reflect the relative magnitudes of the quantities. For changes in SOC stocks, up arrows indicate gains in SOC while down arrows indicate SOC loss

There was a clear distinction in simulated ER values between the upslope and the downslope. Net erosion fluxes exiting the upslope were consistently more enriched comparatively to net erosion fluxes from the downslope, suggesting that, under the same initial SOC stocks, SOC losses per unit eroded soil mass in the upslope would be greater than SOC losses per unit eroded soil mass in the downslope. The higher ER values in the

upslope were attributed to the relatively more important role of rainsplash (associated with greater selective transport of finer material) on the upper sections of the hillslope comparatively to the lower sections, where concentrated flow effects were more important. Enrichment of eroded material was largest during the CCOMM period due to rainfall/runoff events with low runoff coefficients that preferentially transported finer fractions.

The simulations also highlighted the importance of accounting for the enrichment of the soil active layer in the downslope through the preferential deposition of larger size fractions containing finer enriched material in their composition. On average, deposited material was 3-5% more enriched than the mobilized material from where it deposited. Furthermore, the ER values of material eroded from the downslope were generally close to 1 as the dominant erosion processes and updated soil textures were such that mobilized material was just as enriched as soil in the active layer. This finding has implications on the fraction of the enriched OC material that gets delivered into the stream under different management practices [Dalzell et al., 2007].

The fluctuations in BD were greatest during the first two years of the CCOMM rotation due to the use of the moldboard plow, which was the most intrusive tillage implement. The lowest BD fluctuations were observed during the STC-NTB due to the conservation practices adopted. Overall, the changes in BD during the simulation ranged between 20–40%, supporting the need to account for temporally updated values of BD in quantifying SOC fluxes.

The trends in SOC stocks differed between hillslope locations. In the upslope, SOC stocks declined during the CCOMM period due to intrusive tillage activities and

high erosion rates, but increased during the CCB and STC-NTB periods. The increase during the CCB period despite the highest erosion rates was due to enhanced crop production rates from increased fertilizer usage and genetic seed advancements. The continued increase during the STC-NTB period was also due to the lower erosion rates stemming from conservation tillage practices. In the downslope, SOC stocks increased during the CCOMM period due to net deposition and increased crop production. During the CCB period, however, the stocks decreased despite the high deposition rates due to reduced organic inputs from soybean and increased heterotrophic respiration from increased tillage frequency. SOC stocks increased during the STC-NTB period despite the greater erosion rates from the zone due to reduced heterotrophic respiration rates from conservation tillage and increased crop production rates.

Overall, the simulated SOC trends were in agreement with measured trends and values from a field site in Clear Creek that exhibited nearly identical properties with those of the representative hillslope used for the simulations (Figure 5.7). The field values of SOC in the upslope and downslope are both increasing over time, with the downslope values higher than the upslope values, which is consistent with the simulation results and literature reports [e.g., Liu et al., 2003; Wang et al., 2015].

As with any framework, there are some caveats associated to the approach considered herein. First, in our analysis we assumed that the soil composition of the active layer in 1930s is similar to the composition of the current active layer. This may not be the case in certain regions of the under investigation watershed where significant soil degradation may have occurred yielding the removal of the A horizon. A recent hydropedologic study by Papanicolaou et al. [2015] has shown that the steeper areas in

Clear Creek with gradients higher than 5% may experience significant degradation resulting in significant coarsening of the top soil.

Second, the framework considers fixed size fractions estimated from empirical relationships developed by Foster et al. [1985]. For our site, this produced size fractions with median diameters ranging from 0.002–0.48 mm. In reality, however, there may be larger size fractions or aggregates enriched in SOC [Di Stefano and Ferro, 2002; Zheng et al., 2012] whose mobilization and deposition could impact SOC dynamics on the hillslope as they offer further protection to the organic matter trapped within their structure [Berhe et al., 2012]. Furthermore, it is assumed that the median diameters of the size fractions do not change under either the impact of rainsplash or hydraulic shear, or as they travel downslope. This may not be the case, as mobilized fractions may break down or grow in size due to mechanical, chemical, or biological processes.

Third, it is assumed that a fixed fraction (20%) of the mobilized SOC is oxidized during transport. However, according to Lal [2006], the actual magnitude of oxidation may be dependent on the composition of the organic matter. Uncertainty in the estimate is reflected in the broad range of fractions proposed in the literature [e.g., Beyer et al., 1993; Lal, 1995; Schlesinger, 1990; Jacinthe and Lal, 2001; Smith et al., 2001].

The framework also adopts the concept of flow transport capacity which is embedded in WEPP as a means of determining whether or not net erosion or net deposition occurs. Under net erosion, the framework assumes that there is no deposition, whereas under net deposition it assumes that there is no erosion. However, in nature, erosional and depositional processes occur simultaneously and so the soil active layer continually loses and gains SOC during rainfall/runoff events in both erosional (upslope)

and depositional (downslope) zones [Cao et al., 2012]. This effect may be particularly important in the depositional zone, where material flux from the upslope could be deposited onto the active layer even when the transport capacity formula suggests that there should be net erosion.

Fifth, we assume that residue is uniformly distributed across the hillslope and does not simulate the mobilization and downslope transport of residue by runoff. The impact of residue redistribution on the landscape on SOC dynamics between the erosional and depositional zones is thus not accounted for [Thompson et al., 2008]. Lastly, the framework does not account for organo-mineral complexation phenomena, which appear to affect SOC storage differently in erosional and depositional zones [Berhe et al., 2012]. More research is however needed on this front to shed some light on the actual role that complexation plays in the persistence and storage of SOC in the two zones.

CHAPTER 6. CONCLUSIONS AND IMPLICATIONS FOR FUTURE RESEARCH

The primary objective of this research was to develop a landscape-oriented, process-based approach that can enhance understanding and prediction of SOC fluxes in IMLs by incorporating the key mechanisms impacting soil carbon dynamics when moving from the soilscape to the landscape. The mechanisms that are considered to be the focus of this study are redistribution of SOC due to erosion and deposition without neglecting the importance of litter incorporation into the soil column, decomposition due to microbial activity, and physical and chemical stabilization of carbon (see section 6.1). To accomplish this objective, several goals were considered.

- **Goal 1**: *Identify the dominant mechanisms impacting soil carbon dynamics in IMLs and how they vary in space and time*
- **Goal 2**: *Understand how management and hillslope position affect the selective entrainment of soil size fractions and their corresponding carbon content to provide enrichment ratios*
- **Goal 3:** *Understand the role of soil aggregates on carbon storage and how aggregate stability is related to both management and hillslope position*
- **Goal 4**: *Develop a landscape-oriented modeling framework that can capture SOC spatial heterogeneity in IMLs*
- **Goal 5**: *Use the developed modeling framework to determine the impacts that redistribution has on SOC dynamics*

This chapter provides a summary evaluation of the above goals (sections 6.1-6.4 below) with each section reflecting upon the limitations of the methods used in this study. The final section concludes this dissertation by providing suggestions concerning future research efforts and the implications arising from this work (section 6.5).

6.1 Dominant Mechanisms Impacting SOC in IMLs (Goal 1)

There are four dominant mechanisms impacting SOC stocks in IMLs:

- **(M1)** redistribution of SOC through tillage- and rainfall/runoff-induced erosion;
- **(M2)** litter incorporation into the soil active layer through tillage events;
- **(M3)** microbial decomposition and heterotrophic respiration; and
- **(M4)** stabilization into more recalcitrant forms of SOC, which includes both chemical and physical stabilization in aggregates.

Mechanisms M1 (SOC redistribution) and M2 (litter incorporation) are high amplitude, low-frequency processes comparatively to M3 and M4. Essentially they are episodic, resulting from higher intensity storm events and scheduled tillage events. M3 (respiration) is a continuous, or high frequency process that it can experience high amplitude, episodic fluctuations due to discrete tillage and fertilizer events, as well as pulse changes in the soil microclimatic, like with a rain event. The M3 term is null during dormant conditions. Mechanism M4 (stabilization) is a high-frequency but low amplitude process, resulting from biogeochemical cycling in the soil and it is a function of the carbon residence times.

The redistribution mechanism M1 is the centerpiece of this dissertation, as it has not been incorporated correctly in numerical modeling frameworks, and as a result these frameworks fail to capture the dynamicity occurring in IMLs. Redistribution includes the selective mobilization, transport and deposition of material along a downslope flow pathway. Furthermore, the landscape and biogeochemical characteristics change along the flow pathway leading to upslope interrill areas dominated by rainsplash which in turn deliver material to more concentrated flow networks, namely rills and gullies. To assess

accurately SOC fluxes within IMLs, information on the availability and selective entrainment of different soil size fractions (e.g., aggregates) and their corresponding carbon contents are needed.

6.2 Enrichment Ratio and the Role of Aggregates (Goal 2)

Field experiments were performed to address Goal 2 of this dissertation, which examines how selective entrainment of different soil size fractions, quantified through the enrichment ratio (ER), varies with management and hillslope position. The methodological design of the ER experiments consisted of a dual-level approach that assessed both static and dynamic size class availability. The static size classes are those that exist before a runoff event, while the dynamic size class pertains to those that are mobilized by the rainsplash and runoff. The ratio between these values comprises the enrichment ratio. The results of these ER experiments suggest a unique correspondence between the fractions, management, and hillslope position.

Differential modes in soil mobilization between rill and interrill areas were either elevated or dampened depending on the prevalent management practice, the gradient of the site and landscape position. Sites where sediment and runoff fluxes were highest were found to have lower ER values (around unity) due to the mobilization of all size classes making static and dynamic samples almost identical. This was best seen in areas under conventional tillage or in areas where the crop rows followed parallel to the main flow pathways. Lower runoff and sediment fluxes found in areas under conservation tillage where the crop rows ran perpendicular to the flow pathways fluxes or in restored grasslands, conversely had higher ER values due to selective size fraction mobilization by low flow conditions. The contour tillage provided large oriented roughness which

restricted the flow of material in the downslope, which behaved similar to the vegetative canopy found in the restored grassland.

The size fractions analyzed in these experiments were found to have varying levels of carbon associated with them, especially the larger aggregates, which encapsulate organic material. For this reason, we looked more closely at the role of aggregates in IMLs, specifically identifying how aggregate stability varies with respect to management and hillslope position, through controlled experiments.

6.3 The Role of Soil Aggregates and their Stability in Carbon Storage (Goal 3)

Size fractions analyzed in the ER experiments were found to have varying levels of carbon associated with them, especially the macroaggregates. Neglecting them in transport estimates could lead to large errors in predicted fluxes of SOC. In the next set of experiments, we looked at the composition and stability of the soil aggregates and how these characteristics are affected by the land management and the hillslope location where they are found. For these experiments we focused on the small macroaggregates (0.25 – 2.00 mm) as they were found to be most reflective to changes in management. A systematic methodology was developed to understand better the drivers of the aggregate stability. This methodology used both dry size distributions to reflect tillage disturbance and aggregate stability for rainsplash effects.

Aggregate stability was highest in grassland sites and these soils tended to have the larger sizes for this aggregate class, which was expected. However, comparable values were also observed in agricultural sites that practiced conservation sites and especially the contour ridge tillage. In both environments, enough time had passed between disturbances to allow the aggregates to grow and stabilize. The sites under

conventional tillage, due to a more constant frequency of disturbance, had less stable aggregates, which tended to be on the smaller end of the spectrum of the small macroaggregates.

Aggregate stability was also a function of hillslope position as the coarser size fractions were found at the top of the hillslopes, while the bottom positions were more prevalent in the smaller fractions. This could be attributed to the preferential removal of finer fractions from eroding portions of the hillslope and their deposition at the toe. The same pattern was observed with aggregate stability. The stability was higher in the eroding sections (crest, midslope) of the hillslope when compared to depositional toeslope. The coarser particles which remain behind have more time to stabilize.

6.4 Numerical Modeling Framework (Goals 4 & 5)

The remaining goals of this dissertation were to develop a landscape-oriented modeling framework that captures not only the SOC spatial heterogeneity in IMLs (Goal 4) but also determines the impacts that redistribution has on this heterogeneity and ultimately on SOC dynamics (Goal 5). The integrative modeling framework considers the collective effects of both rainsplash/rainfall- and tillage-induced erosion on SOC redistribution in IMLs. The ER-module was developed and woven within this framework to connect an upland erosion model with a soil biogeochemical model. It provides not only size fraction updates to the active layer and ER values, but also explicitly considers the effects of splash-driven interrill erosion on those ER estimates.

Clear distinctions were identified between the simulated upslope and downslope ER values. Net erosion fluxes from the upslope were consistently more enriched in an absolute sense (or equivalently depleted) comparatively to net erosion fluxes from the

downslope. This suggests that under the same initial SOC stocks, SOC losses per unit of eroded soil mass in the upslope would be greater than the corresponding SOC losses in the downslope. The higher ER values in the upslope were attributed to the relatively more prominent effects of rainsplash, which is associated with greater selective transport of finer material. The toeslopes are more affected by concentrated flow effects than the upper sections of the hillslope. ER values of material eroded from the downslope were generally close to unity (1.00) suggesting that the mobilized material had similar carbon contents as the soil in the active layer. This finding has implications on the fraction of the enriched material that gets delivered into the stream under different management practices [Dalzell et al., 2007].

It becomes apparent that management plays a significant role in SOC dynamics when looking at the historic time series of local practices and climatic conditions. Less intensive practices were shown to have lower runoff coefficients. The lower runoff volumes preferentially entrained and transported finer fractions, thereby leading to higher ER values. Overall, the simulated SOC stocks were found to agree well with measured values from a field site in Clear Creek that exhibited nearly identical properties with those of the representative hillslope used for the simulations. Both the simulated and measured field values of SOC in the upslope and downslope areas are both increasing in recent times. This is a positive reflection of the role that conservation plays in building SOC stocks, which has a positive effect on soil health and functionality. This is sorely needed in a time where we are facing food security issues under a series of market and climate variability.

6.5 Future Research

The enrichment ratio experiments are limited to an event-based scale, but they do provide dynamic (steady and unsteady) ER values that embody changes in microclimate and geomorphic evolution of the landscape surface. These experiments allow for controlled testing to isolate the key drivers impacting the selectivity of size fraction mobilization (e.g., rainfall intensity, gradient, tillage). Future experiments could be designed to identify how a sequence of rainfall events impacts the ER. In tandem with the simulations, runoff collector units could be placed in a variety of fields and hillslope locations to capture natural soil and SOC fluxes, thus providing time-aggregated estimates of ER.

Aggregate stability values were found to differ with respect to management and position. The rainfall simulators provided a controlled and reproducible forcing of the applied raindrops. More samples are needed that capture a diverse set of gradients and tillage intensities. In addition, relationships need to be identified between stability and levels of pH, texture, organic matter, and microbial biomass to simulate aggregate breakdown and assess aggregate dynamics (changes over time) for a variety of practices and gradients. More research is also needed to assess soil wetting-and-drying cycles and the impact of water table fluctuations.

Overall, this study, although limited at the hillslope scale, provides some insight on the impact that human perturbations (management) have on the degradation of SOC stocks. To assess the impact of management on SOC budgets at a larger scale where policy must be made (e.g., watershed), more detailed representation of the landscape and the inherent heterogeneous features is needed. High-resolution elevation data, like from

repeated LiDAR flights, could be incorporated into future modeling efforts to identify flow pathways more precisely, as well as track the geomorphic evolution of the landscape stemming from a sequence of erosion or deposition events [Young et al., 2014]. In this case, flow pathways and connectivity of the landscape with neighboring units must be considered. Future research should more explicitly account for the role of the drainage network on SOC storage as the eloquent work of Liu et al.[2011] has shown may play a significant role in SOC stocks as well as the role of exchanges between soil and atmosphere in IMLs.

APPENDIX A: SURFACE/SUBSURFACE FLOW FORMULATION

During a storm event, runoff is routed along the downslope of sequential control volumes (CVs) using the kinematic wave equation:

$$h_{i,j} + q_{i,i} = q_{li} \qquad \text{[Eq.A1a]}$$

where *i* denotes space; the CV element *i*; *j* denotes time; [,] denotes first order derivative; *h* is the flow depth (m) within CV *i*; q is volumetric flow discharge per unit width (m^2/s) in CV *i*; and q_l is a source term, a volumetric flow discharge, which incorporates the lateral (*l*) inflow rate of excess rainfall (m/s) to the CV, defined as:

$$q_{li} = r_i - f_i \qquad \text{[Eq. A1b]}$$

where *r* is the rainfall rate (m/s); and *f* is soil infiltration rate (m/s). In Eq. [A1a], the LHS term q, is estimated using a typical power law, depth-discharge relation:

$$q = \alpha h^{3/2} \qquad \text{[Eq. A2]}$$

where α is the kinematic depth-discharge coefficient determined as $\alpha = C\sqrt{S_o}$; *C* is the Chezy roughness coefficient; and S_o denotes the spatially average surface gradient of the CV. The infiltration rate of the active layer, *f*, in [Eq. A1b], is determined using the modified Green-Ampt equation to account for the effects of management and land use on flow partitioning through the inclusion of the effective hydraulic conductivity term:

$$f_i = F_{i,j} = \left(\frac{\Psi \vartheta_{di} + F_i}{F_i} \right) K_{ei} \qquad \text{[Eq. A3a]}$$

where Ψ is the average capillary potential (m); ϑ_d is the soil moisture deficit (m/m); K_e is the effective hydraulic conductivity (m/s) that accounts for the collective effects of

surface roughness and developed crust, tillage, raindrop impact, as well as canopy and residue cover within CV *i* [*Kidwell et al.*, 1997] ; and F is the cumulative infiltration depth (m), which is iteratively determined by applying the Newton-Raphson method to the equation:

$$F = K_e DT + \Psi \vartheta_d \ln\left(1 + \frac{F}{\Psi \vartheta_d}\right) \qquad \text{[Eq. A3b]}$$

where *DT* is a time period (s). All terms in Eqs. B1-B3 are written for the CV element *i*.

APPENDIX B: SOC DECOMPOSITION FORMULATION

In CENTURY, the mass of SOC that is decomposed per unit area during a period DT, $D_{soc_{ACT}}$, and within the active layer (g C/m^2), or rate of decay, is approximated by a multiparametric equation [*Parton et al.*, 2007] (assumption 3):

$$\left(D_{soc_{ACT}}\right)_i^j = \left(SOC_{ACT}\right)_i^{j-1}\left(K_{soc_{ACT}}\, ANERB_{ACT} CDI_{ACT} TEX_{ACT} TILL_{ACT}\right)_i^{j-1} DT \qquad \text{[Eq. B1]}$$

where $\left(SOC_{ACT}\right)_i^{j-1}$ is the stock of SOC (g C/m) present within the active layer of CV *i* at time *j*-1, $K_{SOC_{ACT}}$ is the maximum, equilibrated SOC decomposition rate (1/yr); $ANERB_{ACT}$ is a coefficient that adjusts $K_{SOC_{ACT}}$ due to anaerobic conditions and oxygen availability (-), which are dictated by the soil drainage, or downslope saturation; CDI_{ACT} the Climatic Decomposition Index, a correction coefficient that adjusts $K_{SOC_{ACT}}$ for seasonal changes in temperature moisture (-); TEX_{ACT} is a coefficient that accounts for soil texture effects on $K_{SOC_{ACT}}$ (-); and $TILL_{ACT}$ is a multiplier effect for enhanced $K_{SOC_{ACT}}$ following tillage under different management practices (-).

[94] In a similar manner, the decomposition of residue, $D_{Res_{ACT}}$, within the active layer (g C/m^2) is expressed as:

$$\left(D_{Res_{ACT}}\right)_i^j = \left(L_{ACT}\right)_i^{j-1}\left(K_{Res_{ACT}}\, ANERB_{ACT} CDI_{ACT} TILL_{ACT}\right)_i^{j-1} DT \qquad \text{[Eq. B2]}$$

where L_{ACT} is the stock of soil residue within the active layer (g C/m^2); and $K_{Res_{ACT}}$ is the maximum, equilibrated residue decomposition rate (1/yr).

A portion of the decayed stocks in Eqs.[B1-B2] can be stabilized into more decay-resistant forms of SOC within the soil active layer based on soil texture, prevalent C/N ratio, and residue lignin content [*Sorenson,* 1981; *Van Veen et al.,* 1984; *Holland and Coleman,* 1987]. The portion transferred to the more decay-resistant pools is what we define herein as "stabilized SOC" with the recognition though that this term has been presented in the literature in different ways somewhat inconsistent [B*erhe and Kleber, 2013*]. Taking into account these factors, the amount of SOC stabilized, $STAB_{SOC_{ACT}}$, in the active layer (g C/m^2) is expressed as (assumption 8):

$$\left(STAB_{SOC_{ACT}}\right)_i^j = STAB_{SOCD_{ACT}} + STAB_{ResD_{ACT}} = f_{SOC}\left(D_{SOC_{ACT}}\right)_i^j + f_{Res}\left(D_{Res_{ACT}}\right)_i^j \qquad \text{[Eq. B3]}$$

where f_{SOC} is the fraction of decomposed SOC that is stabilized (values found in *Parton* [1987]); and f_{Res} is the fraction of decomposed residue that is stabilized as SOC based on lignin availability [*Melillo et al.,* 1984]. Lastly, the portion of decayed stocks that is not stabilized within the soil is lost from the active layer in the form of CO_2, defined here as heterotrophic soil respiration (g C/m^2), $R_{Het_{ACT}}$, and expressed as:

$$\left(R_{Het_{ACT}}\right)_i^j = R_{HetSOC_{ACT}} + R_{HetRes_{ACT}} = (1 - f_{SOC})\left(D_{SOC_{ACT}}\right)_i^j + (1 - f_{Res})\left(D_{Res_{ACT}}\right)_i^j \qquad \text{[Eq. B4]}$$

APPENDIX C. KINTEC ENERGY OF RAINDROPS FOR SMAGG RUNS

The terminal velocity of an individual raindrop, v_{ti} (m/s) was approximated using the methods of Atlas et al. (1973) and Kathiravelu et al., (2016):

$$v_{ti} = 9.65 - 10.3\exp(-0.6D_i) \quad \text{(Eq.C1)}$$

where D_i is the diameter of a raindrop i (mm).

The kinetic energy (KE) corresponding to this distribution of raindrops was estimated using a collection of equations from Begueria et al. (2015):

$$KE_i = \frac{1}{2} m_i v_{t\,i}^2 \quad \text{(Eq.C2a)}$$

$$m_i = \rho_i V_i \quad \text{(Eq.C2b)}$$

$$V_i = \frac{4}{3}\pi\left(\frac{D_i}{2}\right)^3 \quad \text{(Eq.C2c)}$$

where m_i is the mass of raindrop i (kg), ρ_i is the density of raindrop i (kg/m^3), and V_i is the volume of the raindrop i (m^3) which assumes a spherical shape.

To determine the size distribution of the raindrops, , the methods identified in Elhakeem and Papanicolaou (2009) were used to determine the number of raindrops found per unit volume of rainfall, N_D, as a function of the raindrop diameter, D_i:

$$N_D = N_0\exp(-\Lambda D_i) \quad \text{(Eq.C3a)}$$

$$N_0 = 8000 \quad \text{(Eq.C3b)}$$

$$\Lambda = 4.1 * R^{-0.21} \quad \text{(Eq.C3c)}$$

where N_O is the value for N_D when $D_i = 0$; and R is rainfall intensity (mm/hr).

APPENDIX D. PRE-PROCESSING STEPS FOR SEDIGRAPH ANALYSIS

Below is a summary of the processing steps used for the sediGraph [Bettis, personal communication; Figure 3.6]:

- Grind the dry sample and sift through #10 (2mm) sieve
- Place approximately 5g of the sample into a 100-mL beaker, and record weight
- Add the following to the 100mL beaker:
    - Distilled water to the 50mL mark
    - 5mL hydrogen peroxide (30%)
    - 2.5mL acetic acid (1%)
- Cover the beaker with a watch glass and let the sample digest overnight (or until reaction is complete)
- Samples high in organics may require additional treatment with hydrogen peroxide (add in 5mL increments until all organics are removed)
- Bring the total volume of the beaker up to 75mL with distilled water
- Put the beaker on a hot plate at 500°F (260°C) and boil the sample until the total volume reaches 40mL (this will take about 2 hours). Beware the darker/organic rich samples as they may boil over.
- Wet sieve the remaining sample into a pre-weighed 250mL beaker with distilled water using a #230 (63um) sieve
- Wash the remaining sand fraction with distilled water into a pre-weighed 100mL beaker
- Dry the samples overnight in the oven
- Cool the sample and reweigh to determine the non-carbonate silt and clay fraction and the percent sand
- Add 80mL distilled water and 1mL dispersant to samples and allow to disperse. Be careful to maintain at least a 3% concentration or the SediGraph will not be able to analyze the sample; adjust the amount of water added accordingly)
- Allow to sit for two hours and check for flocculation
- Transfer the sample to a 6oz glass bottle and place on shaker table overnight- low setting DO NOT touch knob
- Remove the bottle from the shaker table
- Allow to cool
- Check for flocculation
- Run sample

REFERENCES

Abaci, O., & Papanicolaou, A. N. (2009). Long-term effects of management practices on water-driven soil erosion in an intense agricultural sub-watershed: Monitoring and modelling. *Hydrological Processes*, *23*(19), 2818-2837.

Abrahams, A. D., G. Li, C. Krishnan, and J. F. Atkinson, (2001), A sediment transport equation for interrill overland flow on rough surfaces, *Earth Surf. Proc. Land*., *26*(13), 1443-1459.

Alonso, C. V., W. H. Neibling, and G. R. Foster (1981), Estimating sediment transport capacity in watershed modeling, *Trans. ASAE*, *24*(5), 1211–1220.

Amezketa, E. (1999). Soil aggregate stability: A review. *Journal of Sustainable Agriculture*, *14*(2-3), 83-151.

Andreas, A. T. (1875), Illustrated historical atlas of the State of Iowa. *Andreas Atlas Company*.

Andrews, S. S., Mitchell, J. P., Mancinelli, R., Larlen, D. L., Hartz, T. K., Horwarth, W. R., Pettygrove, G. S., Scow, K. M., & Munk, D.S. (2002). On farm assessment of soil quality in California's Central Valley. *Agronomy Journal*, *94*, 12-23.

Arnold, J. G., and J. R. Williams (1989), Stochastic generation of internal storm structure, *Trans. ASAE*, *32*(1), 161-166.

Atlas, D., Srivastava, R. C., & Sekhon, R. S. (1973). Doppler radar characteristics of precipitation at vertical incidence. *Reviews of Geophysics*, *11*(1), 1-35.

Barnes, K. K., and D. A. Eash (1994), Flood of June 17, 1990, in the Clear Creek basin, east-central Iowa. *US Geological Survey*.

Beare, M. H., Hendrix, P. F., Cabrera, M. L., & Coleman, D. C. (1994a). Aggregate-protected and unprotected organic matter pools in conventional-and no-tillage soils. *Soil Science Society of America Journal*, *58*(3), 787-795.

Beare, M. H., Hendrix, P. F., & Coleman, D. C. (1994b). Water-stable aggregates and organic matter fractions in conventional-and no-tillage soils. *Soil Science Society of America Journal*, *58*(3), 777-786.

Beguería, S., Angulo-Martínez, M., Gaspar, L., & Navas, A. (2015). Detachment of soil organic carbon by rainfall splash: Experimental assessment on three agricultural soils of Spain. *Geoderma*, *245*, 21-30.

Berhe, A. A., & Kleber, M. (2013). Erosion, deposition, and the persistence of soil organic matter: mechanistic considerations and problems with terminology. *Earth Surface Processes and Landforms*, *38*(8), 908-912.

Berhe A, J. W. Harden, M. S. Torn, M. Kleber, S. D. Burton, and J. Harte (2012), Persistence of soil organic matter in eroding versus depositional landform positions. *J. Geophys. Res*., *117*(2), G02019.

Bettis, E. A., D. R. Muhs, H. M. Roberts, and A. G. Wintle (2003), Last glacial loess in the conterminous USA, *Quaternary Sci. Rev*., *22*(18), 1907-1946.

Beyer, L., R. Frund, U. Schleuss, and C. Wachendorf (1993), Colluvisols under cultivation in Schleswig-Holstein, 2. Carbon distribution and soil organic matter composition, *J. Plant Nutr. Soil Sci.*, *156*, 213–217.

Billings, S. A., Buddemeier, R. W., Richter, D., Van Oost, K., & Bohling, G. (2010). A simple method for estimating the influence of eroding soil profiles on atmospheric CO_2. *Global Biogeochemical Cycles*, *24*, GB2001, doi:10.1029/2009GB003560.

Blanco-Canqui, H., & Lal, R. (2004). Mechanisms of carbon sequestration in soil aggregates. *Critical Reviews in Plant Sciences*, *23*(6), 481-504.

Blanco-Canqui, H., & Lal, R. (2004). No-tillage and carbon sequestration: An on-farm assessment. *Soil Science Society of America Journal*, *72*, 693-701.

Blaschke, T., and G. J. Hay (2001), Object-oriented image analysis and scale-space: Theory and methods for modeling and evaluating multiscale landscape structure, *International Archives of Photogrammetry and Remote Sensing*. *34*(4):W5.

Blevins, R. L., Thomas, G. W., & Cornelius, P. L. (1977). Influence of no-tillage and nitrogen fertilization on certain soil properties after 5 years of continuous corn. *Agronomy Journal*, *69*(3), 383-386.

Blevins, R. L., Smith, M. S., Thomas, G. W., & Frye, W. W. (1983). Influence of conservation tillage on soil properties. *Journal of Soil and Water Conservation*, *38*(3), 301-305.

Bond, J. J., & Willis, W. O. (1969). Soil water evaporation: surface residue rate and placement effects. *Soil Science Society of America Journal*, *33*(3), 445-448.

Bortolon, E. S. O., J. Mielniczuk, C. G. Tornquist, F. Lopes, and H. Bergamaschi, (2011), Validation of the Century model to estimate the impact of agriculture on soil organic carbon in Southern Brazil, *Geoderma*, *167*, 156-166.

Bossuyt, Heleen, Johan Six, and Paul F. Hendrix. (2002) Aggregate-protected carbon in no-tillage and conventional tillage agroecosystems using carbon-14 labeled plant residue. *Soil Science Society of America Journal* 66(6), 1965-1973.

Bronick, C. J., & Lal, R. (2005). Manuring and rotation effects on soil organic carbon concentration for different aggregate size fractions on two soils in northeastern Ohio, USA. *Soil & Tillage Research*, *81*(2), 239-252.

Brown, D. J., E. R. Hunt, R.C. Izaurralde, K. H. Paustian, C. W. Rice, B. L. Schumaker, and T. O. West (2010), Soil organic carbon change monitored over large areas, *Eos, Transactions American Geophysical Union*, *91*(47), 441-442.

Bryan, R. B. (2000). Soil erodibility and processes of water erosion on hillslope. *Geomorphology*, *32*(3), 385-415.

Burkart M., D. James, M. Liebman, C. Herndl (2005), Impacts of integrated crop–livestock systems on nitrogen dynamics and soil erosion in western Iowa watersheds, J. *Geophys. Res.*, *110* (G1) (2005), p. G0100.

Burke, I. C., T. G. F. Kittel, W. K. Lauenroth, P. Snook, C. M. Yonker, and W. J. Parton (1991), Regional analysis of the central Great Plains, *BioScience*, 685-692.

Burras, C.L., J. M. McLaughlin, S. A. Wills, M. Barker, E.C. Brummer (2005), Soil carbon and quality in Seymour and Clarinda soil map units, Chariton Valley, Iowa. Final Report. Chariton Valley RC&D (*ISU Project 400-41-71-4216*).

Cambardella, C. A., Moorman, T. B., Andrews, S. S., and Karlen, D. L. (2004). Watershed-scale assessment of soil quality in the loess hills of southwest Iowa. *Soil & Tillage Research, 78*(2), 237-247.

C. A. Campbell, B. G. McConkey, R. Zentner, F. Selles, D. Curtin (1996), Long-term effects of tillage and crop rotations on soil organic C and total N in a clay soil in southwestern Saskatchewan, *Can. J. Soil Sci*., *76* (1996), pp. 395–401.

Cao, Z. X., Z. J. Li, G. Pender, P. Hu (2012), Non-capacity or capacity model for fluvial sediment transport, *Water Manage*., *165*, pp. 193–211

Castro-Filho, C., Lourenço, A., Guimarães, M. D. F., & Fonseca, I. C. B. (2002). Aggregate stability under different soil management systems in a red latosol in the state of Parana, Brazil. *Soil and Tillage Research*, *65*(1), 45-51.

Celik, I., M. M. Turgut, N. Acir (2012), Crop rotation and tillage effects on selected soil physical properties of a Typic Haploxerert in an irrigated semi-arid Mediterranean region, *Int. J. Plant Prod*., *6* (4), 457-480.

Chaney, K. and Swift, R. S. (1984), The influence of organic matter on aggregate stability in some British soils. *Journal of Soil Science*, 35: 223–230. doi: 10.1111/j.1365-2389.1984.tb00278.x

Chapin, F. S., III, P. A. Matson, and H. Mooney (2002), Principles of terrestrial ecosystem ecology, *Springer-Verlag*, New York, New York, USA.

Chatskikh, D., and J. E. Olesen (2007), Soil tillage enhanced CO_2 and N_2O emissions from loamy sand soil under spring barley, *Soil Till. Res*., *97*, 5–18.

Ciric, V., Manojlovic, M., Nesic, L., & Belic, M. (2012). Soil dry aggregate size distribution: effects of soil type and land use. *Journal of Soil Science and Plant Nutrition*, *12*(4), 689-703.

Coote, D. R., Malcolm-McGovern, C. A., Wall, G. J., Dickinson, W. T., & Rudra, R. P. (1988). Seasonal variation of erodibility indices based on shear strength and aggregate stability in some Ontario soils. *Canadian Journal of Soil Science*, *68*(2), 405-416.

Dal Ferro, N., Sartori, L., Simonetti, G., Berti, A., & Morari, F. (2014). Soil macro-and microstructure as affected by different tillage systems and their effects on maize root growth. *Soil and Tillage Research*, *140*, 55-65.

DeLucia, E. H., S. A. Heckathorn, and T. A. Day (1992), Effects of soil temperature on growth, biomass allocation and resource acquisition of Andropogon gerardii Vitman, *New Phytol*., *120*(4), 543-549.

Dermisis, D., Abaci, O., & Wilson, C. G. (2010). Evaluating grassed waterway efficiency in southeastern Iowa using WEPP. *Soil Use and Management*, *26*(2), 183-192.

Dlugoß, V., Fiener, P., & Schneider, K. (2010). Layer-specific analysis and spatial prediction of soil organic carbon using terrain attributes and erosion modeling. *Soil Science Society of America Journal*, *74*, 922–935.

Dlugoß, V., P. Fiener, K. Van Oost, and K. Schneider (2012), Model based analysis of lateral and vertical soil carbon fluxes induced by soil redistribution processes in a small agricultural catchment, Earth Surf. Proc. Land., 37(2), 193-208.

Di Stefano, C., and V. Ferro (2002), SW—Soil and Water: Linking Clay Enrichment and Sediment Delivery Processes. *Biosyst. Eng*., *81*(4), 465-479.

Dıaz-Zorita, M., Perfect, E., & Grove, J. H. (2002). Disruptive methods for assessing soil structure. *Soil & Tillage Research*, *64*(1), 3-22.

Du, P., and D. E. Walling (2011), Using 137 Cs measurements to investigate the influence of erosion and soil redistribution on soil properties, *Applied Radiation and Isotopes*, *69*(5), 717-726.

Elhakeem, M., and A. N. Papanicolaou (2009), Estimation of the runoff curve number via direct rainfall simulator measurements in the state of Iowa, USA. *Water Resour. Manag*., *23*(12), 2455-2473.

Elliott, E. T. (1986). Aggregate structure and carbon, nitrogen, and phosphorus in native and cultivated soils. *Soil Science Society of America Journal*, *50*(3), 627-633.

Elliott, E. T., & Cambardella, C.A. (1991). Physical separation of soil organic matter. *Agriculture, Ecosystem, and Environment*, *34*, 407–419

Eve, M. D., Sperow, M., Paustian, K., & Follett, R. F. (2002). National-scale estimation of changes in soil carbon stocks on agricultural lands. *Environmental Pollution*, *116*(3), 431-438.

Farmer, E. E. (1973). Relative detachability of soil particles by simulated rainfall. *Soil Science Society of America Journal*, *37*(4), 629-633.

Farres, P. J. (1980). Some observations on the stability of soil aggregates to raindrop impact. *Catena*, *7*(2), 223-231.

Favis-Mortlock, D. T., Boardman, J., Parsons, A. J., & Lascelles, B. (2000). Emergence and erosion: a model for rill initiation and development. *Hydrological Processes*, *14*(11-12), 2173-2205.

Finkner, S. C., M. A. Nearing, G. R. Foster, and J. E. Gilley (1989), A simplified equation for modeling sediment transport capacity, *Trans. ASAE*, *32*(5), 1545–1550.

Flanagan, D. C., and M. A. Nearing (2000), Sediment particle sorting on hillslope profiles in the WEPP model, Trans. ASAE, 43(3), 573-583.

Flanagan D. C., J. E. Gilley, T. G. Franti (2007), Water Erosion Prediction Project (WEPP): development history, model capabilities and future enhancements, *Trans. ASABE*, *50*(5), 1603–1612.

Foster, G. R., and L. D. Meyer (1972), Transport of soil particles by shallow flow, *Trans. ASAE*, *15*(1), 99–102.

Foster, G. R. (1982), Modeling the erosion process, in Hydrologic modeling of small watersheds, Monograph No. 5, edited by Haan et al., pp. 297-380, American Society of Agricultural Engineers, St. Joseph, MI.

Foster, G. R., R. A. Young, and W. H. Neibling (1985), Sediment composition for nonpoint source pollution analyses, *Trans. ASAE*, *28*(1), 133-139.

Foster, G. R., D. C. Flanagan, M. A. Nearing, L. J. Lane, L. M. Risse, and S. C. Finkner (1995), Hillslope erosion component, in USDA – Water Erosion Prediction Project: hillslope profile and watershed model documentation, 11.1–11.2., National Soil Erosion Research Laboratory, West Lafayette, IN

Fox, D. M., Darboux, F., & Carrega, P. (2007). Effects of fire-induced water repellency on soil aggregate stability, splash erosion, and saturated hydraulic conductivity for different size fractions. *Hydrological Processes*, *21*(17), 2377-2384.

Fox, J. F., and A. N. Papanicolaou (2007), The use of Carbon and Nitrogen isotopes to study watershed erosion processes, *J. Am. Water Resour. As*., 43(4),1047-1064.

Fox, J. F., and A. N. Papanicolaou (2008), Application of the spatial distribution of nitrogen stable isotopes for sediment tracing at the watershed scale, *J. Hydrol., 358*, 46–55.

Gabet, E. J., and T. Dunne (2003), Sediment detachment by rain power, *Water Resour. Re*s., *39*(1), 1002, doi:10.1029/2001WR000656.

Gete, Z., T. Winter, and D. Flanagan (1999), BPCDG: Breakpoint Climate Data Generator for WEPP using observed standard weather data sets.

Gilley, J. E., D. A. Woolheiser, and D. McWhorter (1985), Interril soil erosion, Part I. Development of model equations, *Trans ASAE*, *28*, 147-153.

Gregorich, E. G., K. J. Greer, D. W. Anderson, and B. C. Liang (1998), Carbon distribution and losses: erosion and deposition effects, Soil Till. Res., 47, 291-302.

Grieve, I. C., (1980) The magnitude and significance of soil structural stability declines under cereal cropping. *Catena*, *7*, 79-85.

Gugino, B. K., Abawi, G. S., Idowu, O. J., Schindelbeck, R. R., Smith, L. L., Thies, J. E., ... & Van Es, H. M. (2009). *Cornell soil health assessment training manual*. Cornell University College of Agriculture and Life Sciences.

Hajabbasi, M. A., and A. Hemmat. "Tillage impacts on aggregate stability and crop productivity in a clay-loam soil in central Iran." *Soil and tillage research* 56.3 (2000): 205-212.

Hancock, G. R. (2006), The impact of different gridding methods on catchment geomorphology and soil erosion over long timescales using a landscape evolution model, *Earth Surf. Proc. Land*., *31*(8), 1035-1050.

Handler, A. (1990), USA corn yields, the El Niñmo and agricultural drought: 1867–1988. *Int. J. Climatol*., *10*: 819–828. doi: 10.1002/joc.3370100804.

Harden, J. W., J. M. Sharpe, W. J. Parton (1999), Dynamic replacement and loss of soil carbon on eroding cropland, Global Biogeochem. Cycles, 13, 885–901. DOI: 0.1029/1999gb900061.

Hart, R. H. (2001), Plant biodiversity on shortgrass steppe after 55 years of zero, light, moderate, or heavy cattle grazing. *Plant Ecol*., *155*(1), 111-118.

Hassink, J. (1997). The capacity of soils to preserve organic C and N by their association with clay and silt particles. *Plant and Soil*, *191*(1), 77-87.

Hatfield, J. L., Allmaras, R. R., Rehm, G. W., & Lowery, B. (1998). Ridge tillage for corn and soybean production: environmental quality impacts. *Soil and Tillage Research*, *48*(3), 145-154.

Hatfield, J. L., and T. B. Parkin, 2012. Spatial variation of carbon dioxide fluxes in corn and soybean fields. Agricultural Sciences, 3(8), 986-995.

Haynes, R.J., (1993) Effect of sample pretreatment on aggregate stability measured by wet sieving or turbidimetry on soils of different cropping history. *Journal of Soil Science*, *44*, 261-270.

Heinitz, A.J. (1986), Floods in south-central Iowa: *U.S. Geological Survey Open-File Report 85-100*, 95 p.

Highland, J. D., and R. I. Dideriksen (1967), Soil survey of Iowa County, Iowa, U.S. Department of Agriculture, Soil Conservation Service, in cooperation with the Iowa Agricultural Experiment Station.

Holland, E. A., and D. C. Coleman (1987), Litter placement effects on microbial and organic matter dynamics in an agroecosystem, *Ecology*, 425-433.

Houghton, R.A. (2008), Carbon Flux to the Atmosphere from Land-Use Changes. in TRENDS: A Compendium of Data on Global Change, Carbon Dioxide Information Analysis Center, Oak Ridge National Laboratory, U.S. Department of Energy, Oak Ridge, Tenn., U.S.A.

Hoyos, N., & Comerford, N. B. (2005). Land use and landscape effects on aggregate stability and total carbon of Andisols from the Colombian Andes. *Geoderma*, *129*(3), 268-278.

Hu, Y., Fister, W., & Kuhn, N. J. (2013). Temporal variation of SOC enrichment from interrill erosion over prolonged rainfall simulations. *Agriculture*, *3*(4), 726-740.

Huang, C., C. Gascuel-Odoux, and S. Cros-Cayot (2002), Hillslope topographic and hydrologic effects on overland flow and erosion, *Catena*, *46*(2), 177-188.

Hubert, M., & Van der Veeken, S. (2008). Outlier detection for skewed data.*Journal of Chemometrics*, *22*(3-4), 235-246.

Huehn, M. (1993), Harvest index versus grain straw-ratio. Theoretical comments and experimental results on the comparison of variation, *Euphytica*, *68*, 27-32

Idowu, O. J., van Es, H. M., Abawi, G. S., Wolfe, D. W., Ball, J. I., Gugino, B. K., & Bilgili, A. V. (2008). Farmer-oriented assessment of soil quality using field, laboratory, and VNIR spectroscopy methods. *Plant and Soil*, *307*(1-2), 243-253.

Iowa Environmental Mesonet (2015), Climodat Reports, http://mesonet.agron.iastate.edu/climodat/Accessed: 2015.

Itami, K.; & Kyuma, K. (1995). Dispersion behavior of soil from reclaimed lands with poor physical properties and their characteristics, with special reference to clay mineralogy. *Soil Science and Plant Nutrition*, *41*, 45-54.

Jacinthe, P. and R. Lal (2001), A mass balance approach to assess carbon dioxide evolution during erosional events, *Land Degrad. Dev*., *12*, 329–339.

Jacinthe P.A., R. Lal, and L. B. Owens (2009), Application of stable isotope analysis to quantify the retention of eroded carbon in grass filters at the North Appalachian experimental watersheds, *Geoderma*, 148, 405–441.

Jarecki M. K., T. B. Parkin, A. S. K. Chan, J. L. Hatfield, and R. Jones (2008), Greenhouse gas emissions from two soils receiving nitrogen fertilizer and swine manure slurry, *J. Environ. Qual*. *37*, 1432–1438.

Jenkinson, D. S., S. P. S. Andrew, J. M. Lynch, M. J. Goss, and P. B. Tinker (1990), The turnover of organic carbon and nitrogen in soil [and discussion], *Philosophical Transactions of the Royal Society of London, Series B: Biological Sciences*, *329*(1255), 361-368.

Kaiser, J. (2011), Big Bluestem and Indiangrass for Biomass Production by Variety Selection and Establishment Methods for Missouri, Illinois, and Iowa, Agronomy Technical Note 39.

Kara, O., & Baykara, M. (2014). Changes in soil microbial biomass and aggregate stability under different land uses in the northeastern Turkey. *Environmental Monitoring and Assessment*, *186*(6), 3801-3808.

Karlen, D. L., J. L. Kovar, C. A. Cambardella, and T. S. Colvin (2013), Thirty-year tillage effects on crop yield and soil fertility indicators, Soil Till. Res., 130, 24–41.

Kathiravelu, G., T. Lucke, and P. Nichols. (2016) Rain drop measurement techniques: A Review. *Water*, *8*(1), doi:10.3390/w8010029.

Keeney, D. R., and J. L. Hatfield (2008), The nitrogen cycle historical perspective and current and potential future concerns, Nitrogen in the environment: sources problems and management, Academic Press, Elsevier Inc, 1-18.

Kemper, W. D., & Rosenau, R. C. (1986). Aggregate stability and size distribution. In. Klute, A. (ed). *Methods of Soil Analysis*. Part 1. Soil Science Society of America, Madison, WI.

Kidwell M. R., M. A. Weltz, D. P. Guertin (1997), Estimation of Green-Ampt effective hydraulic conductivity for rangelands, J. Range Manage, 50, 290–299.

Kravchenko, A. N. and G. P. Robertson (2011), Whole-profile soil carbon stocks: The danger of assuming too much from analyses of too little, Soil Sci. Soc. Am. J., 75, 235-240.

Kuhn, N. J., Hoffmann, T., Schwanghart, W., & Dotterweich, M. (2009). Agricultural soil erosion and global carbon cycle: controversy over?. *Earth Surface Processes and Landforms*, *34*(7), 1033-1038.

Lal, R. (1990). Ridge-tillage. *Soil and Tillage Research*, 18(2), 107-111.

Lal, R. (1995), Tillage systems in the tropics, Land and Water Div., 206 pp., FAO Soils Bulletin 71, Rome, Italy.

Lal, R. (2004), Soil carbon sequestration impacts on global climate change and food security, Science, 304(5677), 1623-1627.

Lal, R. (2005), Soil Erosion and Carbon Dynamics, Soil Till. Res., 81(2), 137-142, DOI:10.1016/j.still.2004.09.002.

Lal, R. (2006), Influence of soil erosion on carbon dynamics in the world, in Advances in soil science: soil erosion and carbon dynamics, edited by Roose et al., 23-36, Taylor and Francis, Boca Raton, FL.

Lal, R. (2011), Agronomic interactions with CO2 sequestration, in Encyclopedia of Sustainability Science and Technology, edited by R.A. Meyers, pp. 31-37, Springer, Berlin, Germany

Lagacherie, P., Robbez-Masson, J. M., Nguyen-The, N., & Barthès, J. P. (2001). Mapping of reference area representativity using a mathematical soilscape distance. *Geoderma*, *101*(3), 105-118.

Latshaw, W., and E. Miller (1924), Elemental Composition of the Corn Plant, Journal of Agric. Res., XXVII, 845–860.

Lauer, J. (2002), Methods for Calculating Corn Yield, Agronomy Advice, Univ. of Wisconsin-Madison, Online at http://corn.agronomy.wisc.edu/AA/pdfs/A033.pdf , Accessed May 2015.

Li, C., S. Frolking, G. J. Crocker, P. R. Grace, J. Klír, M. Körchens, and P. R. Poulton, (1997), Simulating trends in soil organic carbon in long-term experiments using the DNDC model, Geoderma, 81(1), 45-60.

Li, J., S. Ziegler, C. S. Lane, and S. A. Billings (2012), Warming-enhanced preferential microbial mineralization of humified boreal forest soil organic matter: Interpretation of soil profiles along a climate transect using laboratory incubations, J. Geophys. Res., 117, G02008, doi:10.1029/2011JG001769.

Lindley, M. R., B. J. Barfield, and B. N. Wilson (1995), Surface impoundment element model description, in USDA-Water Erosion Prediction Project: Hillslope Profile and Watershed Model Documentation, Rep. 10, edited by D. C. Flanagan and M. A. Nearing, chap. 14, pp. 1–28, Natl. Soil Erosion Res. Lab., Agric. Res. Serv., U.S. Dep. of Agric., West Lafayette, Indiana.

Liu, S., N. Bliss, E. Sundquist, and T. G. Huntington, (2003), Modeling carbon dynamics in vegetation and soil under the impact of soil erosion and deposition, Global Biogeochem. Cycles, 17(2), 1074, doi:10.1029/2002GB002010, 2003

Liu, S., Z. Tan, Z. Li, S. Zhao, W. Yuan (2011), Are soils of Iowa USA currently a carbon sink or source? Simulated changes in SOC stock from 1972 to 2007, *Agric Ecosyst Environ*, 140, 106–112, doi:10.1016/j.agee.2010.11.017

Loch, R. J., & Foley, J. L. (1994). Measurement of aggregate breakdown under rain-Comparison with tests of water stability and relationships with field measurements of infiltration. *Soil Research*, *32*(4), 701-720.

Logsdon, S. D., and D. L. Karlen, (2004), Bulk density as a soil quality indicator during conversion to no-tillage, Soil Tillage Res., 78(2), 143-149.

Macha, D., and L. Cihacek, (2009), Carbon Storage in Plant and Soil Components of Selected Grass Monocultures, SSSA AnMtgsAbsts 2009.53321, ASA, CSSA, and SSSA, Madison, WI.

Machinet, G. E., I. Bertrand, B. Chabbert, S. Recous, (2009), Decomposition in soil and chemical changes of maize roots with genetic variations affecting cell wall quality, Eur. J. Soil. Sci. 60, pp. 176-185.

Mangan, J. M., J. T. Overpeck, R. S. Webb, C. Wessman, and A. F. Goetz (2004), Response of Nebraska Sand Hills natural vegetation to drought, fire, grazing, and plant functional type shifts as simulated by the century model, Clim. Change, 63(1-2), 49-90.

Manies, K. L., J. W. Harden, L. Kramer, and W. J. Parton (2001), Carbon dynamics within agricultural and native sites in the loess region of western Iowa, Global Change Biol., 7, 545–555.

Mann L. K. (1986), Changes in soil carbon after cultivation, Soil Sci., 142, 279-288.

Markstrom, S. L., L. E. Hay, C. D. Ward-Garrison, J. C. Risley, W. A. Battaglin, D. M. Bjerklie, K. J. Chase, D. E. Christiansen, R.W. Dudley, R. J. Hunt, K. M. Koczot, M. C. Mastin, R. S. Regan, R. J. Viger, K. C. Vining, and J. F. Walker, 2012, Integrated watershed-scale response to climate change for selected basins across the United States: U.S. Geological Survey Scientific Investigations Report, 2011–5077, 143 p.

Marshall, J. S., & Palmer, W. M. K. (1948). The distribution of raindrops with size. *Journal of Meteorology*, *5*(4), 165-166.

Martinotti, W., M. Camusso, L. Guzzi, L. Patrolecco, M. Pettine (1997), C, N and their stable isotopes in suspended and sedimented matter from the Poestuary [Italy], Water, Air, Soil Poll., 99, 325–332.

Melillo, J. M., J. D. Aber, and J. F. Muratore (1982), Nitrogen and lignin control of hardwood leaf litter decomposition dynamics, Ecology, 63, 621–626.

Metherell, A. K., L. A. Harding, C.V. Cole, W.J. Parton, (1993), CENTURY soil organic matter model environment, technical documentation, Agroecosystem Version 4.0. Great Plains System Research Unit, Technical Report No. 4. USDA-ARS, Fort Collins, Colorado, p. 250

Metting, B., J. Smith and J. Amthor (1999), Science needs and new technology of soil carbon sequestration. in Carbon sequestration in soils: Science, monitoring, and beyond, edited by Rosenberg et al., Proceedings of the St. Michaels Workshop, December 1998, Coordinated by Pacific Northwest National Laboratory, Oak Ridge National Laboratory, and the Council for Agricultural Science Technology, Columbus, Ohio: Batelle Press.

Miller, R.O., and D.E. Kissel. 2010. Comparison of soil pH methods for soils in North America. *Soil Science Society of America Journal*. 74(1):2310-316.

Moebius, B. N., van Es, H. M., Schindelbeck, R. R., Idowu, O. J., Clune, D. J., & Thies, J. E. (2007). Evaluation of laboratory-measured soil properties as indicators of soil physical quality. *Soil Science*, *172*(11), 895-912.

Monreal C. M., R. P. Zentner, J. A. Robertson. (1997), An analysis of soil organic matter dynamics in relation to management, erosion and yield of wheat in long-term crop rotation plots, Can J Soil Sci, 77(4), 553 - 63.

Moore, I. D., and G. J. Burch (1986), Sediment transport capacity of sheet and rill flow: Application of unit stream power theory, Water Resour. Res., *22*(8), 1350-1360.

Mutel, C. F. (2010), A watershed Year: anatomy of the Iowa Floods of 2008, University of Iowa Press.

Nadeu, E., J. de Vente, M. Martínez-Mena, C. Boix-Fayos, (2011), Exploring particle size distribution and organic carbon pools mobilized by different erosion processes at the catchment scale, J. Soils Sediments, 11(4), 667-678, doi: 10.1007/s11368-011-0348-1.

NASS, (2012), National Agricultural Statistics Service, http://www.nass.usda.gov/, Accessed December, 2012.

Navas, A., L. Gaspar, L. Quijano, M. López-Vicente, and J. Machín (2012), Patterns of soil organic carbon and nitrogen in relation to soil movement under different land uses in mountain fields (South Central Pyrenees), Catena, 94, 43-52.

Nearing, M. A., and A. D. Nicks (1998), Evaluation of the Water Erosion Prediction Project (WEPP) model for hillslopes, in Modelling Soil Erosion, edited by W, J. Boardman and D. T. Favis-Mortlock, 55, 45–56, NATO ASI Ser., Ser. I.

Neitsch, S. L., J. G. Arnold, J. R. Kiniry, J. R. Williams, and K. W. King. (2002). Soil and Water Assessment Tool theoretical documentation. TWRI Report TR-191. Texas Water Resources Institute, College Station, Texas.

Norton, L. D. (2006) A linear variable intensity rainfall simulator for erosion studies. In: Wanielista, M., & Smoot, J. (eds.) Proc. of 2nd Biannual Stormwater Management Research Symp., May 4–5, 2006. Univ. of Central Florida, Orlando, pp 93–103.

Oades, J. M., & Waters, A. (1991). Aggregate hierarchy in soils. *Australian Journal Soil Research*, *29*, 815–828

Olchin, G. P., Ogle, S., Frey, S. D., Filley, T. R., Paustian, K., & Six, J. (2008). Residue carbon stabilization in soil aggregates of no-till and tillage management of dryland cropping systems. *Soil Science Society of America Journal*, *72*(2), 507-513.

O'neal. B. (2009), Quaternary stratigraphy and pedology of Clear Creek in Iowa County Iowa, Graduate Thesis Dissertations. Paper 10937.

Onstad, C.A., (1984), Depressional storage on tilled surfaces, Trans. ASAE, 27, 729–732.

Osunbitan, J. A., D. J. Oyedele, and K. O. Adekalu, (2005), Tillage effects on bulk density, hydraulic conductivity and strength of a loamy sand soil in southwestern Nigeria, Soil Till. Res., 82(1), 57-64.

Owens L. B., R. W. Malone, D. L. Hothem, G. C. Starr, and R. Lal (2002), Sediment carbon concentration and transport from small watersheds under various conservation tillage practices. Soil Tillage Res, 67(1), 65–73.

Palis, R. G., G. Okwach, C. W. Rose, and P. G. Saffigna (1990), Soil erosion processes and nutrient loss. 1. The interpretation of enrichment ratio and nitrogen loss in runoff sediment. Aust. J. Soil Res., 28(4), 623-639.

Palis, R. G., H. Ghandiri, C. W. Rose, and P. G. Saffigna (1997), Soil erosion and nutrient loss. III. Changes in the total enrichment ratio of total nitrogen and organic carbon under rainfall detachment and entrainment, Aust. J. Soil Res., 35, 891–905.

Pansu, M., J. Gautheyrou, and J. Y. Loyer (2001), Soil analysis, Balkema.

Papanicolaou, A. N., A. Bdour, and E. Wicklein, (2004), One-dimensional hydrodynamic/ sediment transport model applicable to steep mountain streams, J. Hydraul. Res., 42(4), 357-375.

Papanicolaou, A.N., and O. Abaci. (2008), Upland erosion modeling in a semi-humid environment via the Water Erosion Prediction Project, J. Irrig. Drain. Eng., 134(6), 796-806, doi.ireng-07-5256R1.

Papanicolaou, A.N., C.G. Wilson, O. Abaci, M. Elhakeem, and M. Skopec (2009), Soil quality in Clear Creek, IA: SOM loss and soil quality in the Clear Creek, IA Experimental Watershed, Journal of Iowa Academy of Science, 116(1-4), 14-26.

Papanicolaou, A. N., Sanford, J. T., Dermisis, D. C., & Mancilla, G. A. (2010). A 1-D morphodynamic model for rill erosion. *Water Resources Research*, *46*(9), W09541.

Papanicolaou, A. N., Wacha, K. M., Abban, B. K., Wilson, C. G., Hatfield, J. L., Stanier, C. O., & Filley, T. R. (2015). From soilscapes to landscapes: A landscape-oriented approach to simulate soil organic carbon dynamics in intensively managed landscapes. *Journal of Geophysical Research: Biogeosciences*, *120*(11), 2375-2401.

Papanicolaou, A. T. N., M. Elhakeem, C. G. Wilson, C. L. Burras, L. T. West, H. H. Lin, and B. E. Oneal (2015), Spatial variability of saturated hydraulic conductivity at the hillslope scale: Understanding the role of land management and erosional effect, Geoderma, 243, 58-68.

Parkin, T. B. (1993), Spatial variability of microbial processes in soil-a review, J. Environ. Qual., 22(3), 409-417.

Parton, W. J., Schimel, D. S., Cole, C. V., & Ojima, D. S. (1987). Analysis of factors controlling soil organic matter levels in Great Plains grasslands. *Soil Science Society of America Journal*, *51*(5), 1173-1179.

Parton, W., W. L. Silver, I. C. Burke, L. Grassens, M. E. Harmon, W. S. Currie, (2007), Global-scale similarities in nitrogen release patterns during long-term decomposition, Science, 315, 361–364.

Paustian, K., W. J. Parton, and J. Persson (1992), Modeling soil organic matter in organic-amended and nitrogen-fertilized long-term plots, Soil Sci. Soc. Am. J., 56, 476-488.

Paustian, K., N. H. Ravindranath, and A. van Amstel (2006), Agriculture, Forestry and other land use [AFOLU], in 2006 IPCC Guidelines for National Greenhouse Gas Inventories, edited by J. Penman et al., 4.

Perfect, E., Kay, B. D., van Loon, W. K. P., Sheard, R. W., & Pojasok, T., 1990b. Rates of change in soil structural stability under forage and corn. *Soil Science Society of America Journal*, 54, 179–186.

Pieri, L., M. Bittelli, J. Q. Wu, S. Dun, D. C. Flanagan, P. R. Pisa, and F. Salvatorelli (2007), Using the Water Erosion Prediction Project (WEPP) model to simulate field-observed runoff and erosion in the Apennines mountain range, Italy. J. Hydrol., 336(1), 84-97.

Pierson, F. B., & Mulla, D. J. (1990). Aggregate stability in the Palouse region of Washington: effect of landscape position. *Soil Science Society of America Journal*, *54*(5), 1407-1412.

Polyakov, V., & Lal, R. (2004). Modeling soil organic matter dynamics as affected by soil water erosion. *Environment International*, *30*(4), 547-556.

Post, W. M., and K. C. Kwon (2000), Soil carbon sequestration and land-use change: processes and potential. Glob. Chang. Biol., 6(3), 317-327.

Prince, S. D., J. Haskett, M. Steininger, H. Strand, and R. Wright (2001), Net primary production of U.S. Midwest croplands from agricultural harvest data, Ecol. Appl., 11, 1194-1205.

Prior, J.C. (1991), Landforms of Iowa University of Iowa Press, Iowa City, Iowa.

Pulido Moncada, M., Gabriels, D., Cornelis, W., & Lobo, D. (2013). Comparing aggregate stability tests for soil physical quality indicators. *Land Degradation & Development*, DOI: 10.1002/ldr.2225.

Quine, T. A., D. E. Walling, and X. Zhang (1999), Tillage erosion, water erosion and soil quality on cultivated terraces near Xifeng in the Loess Plateau, China, Land Degrad. Dev., 10(3), 251-274.

Reichstein, M., M. Bahn, P. Ciais, D. Frank, M. D. Mahecha, S. I. Seneviratne, and M. Wattenbach, (2013), Climate extremes and the carbon cycle, Nature, 500(7462), 287-295.

Reicosky, D. C., W. D. Kemper, G. W. Langdale, C. L. Douglas, Jr., and P. E. Rasmussen (1995), Soil organic matter changes resulting from tillage and biomass production. J. Soil Water Conserv., 50(1), 253-261.

Rhoton F.E., M.J. Shipitalo, and D.L. Lindbo (2002), Runoff and soil loss from midwestern and southeastern US silt loam soils as affected by tillage practice and soil organic matter content, Soil Tillage Res., 66, 1–11.

Richter, D. D., D. Markewitz, S. E. Trumbore, and C. G. Wells (1999), Rapid accumulation and turnover of soil carbon in a re-establishing forest, Nature, 400, 56–58, doi:10.1038/21867.

Rieke-Zapp, D. H., & Nearing, M. A. (2005). Slope shape effects on erosion. *Soil Science Society of America Journal*, *69*(5), 1463-1471.

Römkens, M. J. M., K. Helming, and S. N. Prasad (2002), Soil erosion under different rainfall intensities, surface roughness, and soil water regimes, Catena, 46(2–3), 103–123, doi:10.1016/s0341-8162(01)00161-8.

Rosenzweig, C., F. N. Tubiello, R. Goldberg, E. Mills, and J. Bloomfield (2002), Increased crop damage in the US from excess precipitation under climate change, Glob. Environ. Chang., 12(3), 197-202.

Rupnow, J., and C. W. Knox (1975), The growing of America: 200 years of U.S. agriculture, Fort Atkinson, Wis.: Johnson Hill Press, distributed by Nasco.

Salinas-García, J. R., J. J. Velázquez-García, M. Gallardo-Valdez, P. Díaz-Mederos, F. Caballero-Hernández, L. M. Tapia-Vargas, and E. Rosales-Robles, (2002), Tillage effects on microbial biomass and nutrient distribution in soils under rain-fed corn production in central western Mexico, Soil Tillage Res., 66, 143-152.

Santhi, C., Arnold, J. G., Williams, J. R., Dugas, W. A., Srinivasan, R., & Hauck, L. M. (2001). Validation of the SWAT model on a large river basin with point and nonpoint sources, J. Am. Water Resour. Assoc., 37(5), 1169-1188.

Schiettecatte, W., D. Gabriels, W. M. Cornelis, G. Hofman, (2008), Enrichment of organic carbon in sediment transport by interrill and rill erosion processes, Soil Sci. Soc. Am. J., 72, 50–55.

Schlesinger, W. H. (1990), Evidence from chronosequence studies for a low carbon-storage potential of soils, Nature, 348(6298), 232-234.

Schurgers, G., A. Arneth, and T. Hickler (2011), Effect of climate-driven changes in species composition on regional emission capacities of biogenic compounds, J. Geophys. Res., 116, D22304, doi:10.1029/2011JD016278.

Schwärzel, K., S. Carrick, A. Wahren, K. H. Feger, G. Bodner, and G. Buchan (2011), Soil hydraulic properties of recently tilled soil under cropping rotation compared with two-year pasture, Vadose Zone J., 10(1), 354-366.

Shouse, P. J., Gerik, T. J., Russell, W. B., & Cassel, D. K. (1990). Spatial distribution of soil particle size and aggregate stability index in a clay soil. *Soil Science*, *149*(6), 351-360.

Six, J., Paustian, K., Elliott, E. T., & Combrink, C. (2000). Soil structure and organic matter I. Distribution of aggregate-size classes and aggregate-associated carbon. *Soil Science Society of America Journal*, *64*(2), 681-689.

Six, J., R. Conant, E. Paul, and K. Paustian (2002), Stabilization mechanisms of soil organic matter: implications for C-saturation of soils, Plant Soil, 241, 155–176.

Smith, J. L. and E. A. Paul (1990), The significance of soil microbial biomass estimations, in Soil Biochemistry, edited by J. M. Bollag and G. Stotzky, 6, 357-396, Marcel Dekker, Inc, New York, USA.

Smith, P., Smith, J. U., Powlson, D. S., McGill, W. B., Arah, J. R. M., Chertov, O. G., Coleman, K., Frank, U., Frolking, S., Jenkinson, D. S., Jensen, L. S., Kelly, R. H., Klein-Gunnewiek, H., Komarov, A. S., Li, C., Moilna, J. A. E., Mueller, T., Parton, W. J., Thornley, J. H. M., & Whitmore, A. P. (1997). A comparison of the performance of nine soil organic matter models using datasets from seven long-term experiments. *Geoderma*, 81(1), 153-225.

Smith S. V., W. H. Renwick, R. W. Buddemeier, and C. J. Crossland (2001), Budgets of soil erosion and deposition for sediments and sedimentary organic carbon across the conterminous United States, Global Biogeochem. Cycles, 15, 697-707.

Sørensen, L. H. (1972). Stabilization of newly formed amino acid metabolites in soil by clay minerals. *Soil Science*, *114*(1), 5-11.

Sørensen, L. H. (1981), Carbon-nitrogen relationships during the humification of cellulose in soils containing different amounts of clay, Soil Biol. Biochem., 13(4), 313-321.

Sposito G. (1989), The Chemistry of Soils, 277 p., Oxford University Press, New York.

Sperow, M., M. Eve, and K. Paustian. 2003. Potential soil C sequestration on U.S. agricultural soils. *Climatic Change*, *57*, 319-339.

Stavi, I., & Lal, R. (2011). Variability of soil physical quality in uneroded, eroded, and depositional cropland sites. *Geomorphology*, *125*(1), 85-91.

Stewart C. E., K. Paustian, R. T. Conant, A. F. Plante, and J. Six (2007), Soil carbon saturation: concept, evidence and evaluation, Biogeochemistry, 86, 19-31

Stinner B. R., G. D. Hoyt, and R. L. Todd (1983), Changes in some chemical properties following a 12-year fallow: a 2-year comparison of conventional tillage and no-tillage agroecosystems, Soil Tillage Res., 3, 277-290

Teixeira P. C., and R. K. Misra (1997), Erosion and sediment characteristics of cultivated forest soils as affected by the mechanical stability of aggregates, Catena, 30, pp. 119-134.

Thevenot, M., M. F. Dignac, and C. Rumpel (2010), Fate of lignins in soils: a review. Soil Biol. Biochem., 42(8), 1200-1211.

Thompson, S., G. Katul, and S. M. McMahon (2008), Role of biomass spread in vegetation pattern formation within arid ecosystems, Water Resour. Res., 44, W10421, doi:10.1029/2008WR006916.

Tivy, J. (1990), Agricultural Ecology, 288pp, Longman Scientific and Technical, London.

Tisdall, J. M., & Oades, J. (1982). Organic matter and water-stable aggregates in soils. *Journal of Soil Science*, *33*(2), 141-163.

Tornquist, C. G., J. Mielniczuk, C. E. P. Cerri (2009), Modeling soil organic carbon dynamics in Oxisols of Ibirubá (Brazil) with the Century model, Soil Till. Res., 105, 33-43.

Trautmann, N. M., K. S. Porter, and R. J. Wagenet (1985), Modern agriculture: Its effects on the environment, Cornell University Cooperative Extension, Ithaca, NY.

Tucker, G. E., & Bras, R. L., 1998, Hillslope processes, drainage density, and landscape morphology. *Water Resources Research*, *34*, 2751-2764.

Vaccari, F. P., E. Lugato, B. Gioli, L. D'Acqui, L. Genesio, P. Toscano, and F. Miglietta (2012), Land use change and soil organic carbon dynamics in Mediterranean agro-ecosystems: The case study of Pianosa Island, Geoderma, 175, 29-36.

Van Es, H. M., Schindelbeck, R. R., Melkonian, A., Moebius, B. N., & Idowu, O. J. (2006). Assessment of soil aggregate stability using small rainfall simulators. *Department of Crop and Soil Sciences Research Series*, 06-01.

Van Groenigen K. J., A. Hastings, D. Forristal, B. Roth, M. Jones, and P. Smith (2011), Soil C storage as affected by tillage and straw management: an assessment using field measurements and model predictions, Agr. Ecosyst. Environ, 140, 218–222.

Van Oost, K., Govers, G., & Desmet, P. (2000). Evaluating the effects of changes in landscape structure on soil erosion by water and tillage. *Landscape Ecology*, 15(6), 577-589.

Van Oost, K., G. Govers, T. A. Quine, G. Heckrath, J. Olesen, and R. Merckx (2005), Landscape-scale modeling of carbon cycling under the impact of soil redistribution: the role of tillage erosion, Glob. Biogeochem. Cycles, 19:GB4014, doi:10.1029/2005GB002471.

Van Oost, K. V., G. Govers, T. A. Quine, and G. Heckrath (2006), Modeling soil erosion induced carbon fluxes between soil and atmosphere on agricultural land using SPEROS-C, in Soil erosion and carbon dynamics, edited by Eric. J. Roose et al., pp 37-51, CRC Press, Boca Raton, USA.

Van Oost, K., O. Cerdan, and T. A. Quine (2009), Accelerated sediment fluxes by water and tillage erosion on European agricultural land, Earth Surf. Process. Land., 34(12), 1625-1634.

Van Veen, J. A., J. N. Ladd, and M. J. Frissel (1984), Modelling C and N turnover through the microbial biomass in soil, Plant Soil, 76(1-3), 257-274.

Vázquez, E. V., J. V. Miranda, and A. P. Gónzalez (2005), Characterizing anisotropy and heterogeneity of soil surface microtopography using fractal models, Ecol. Model., 182(3), 337-353.

Wäldchen, J., I. Schöning, M. Mund, M. Schrumpf, S. Bock, N. Herold, and E. D. Schulze (2012), Estimation of clay content from easily measurable water content of air-dried soil, J. Plant Nutr. Soil Sci, 175(3), 367-376.

Wang, Z., G. Govers, K. V. Oost, W. Clymans, A. V. Putte, and R. Merckx (2013), Soil organic carbon mobilization by interrill erosion: Insights from size fractions, J. Geophys. Res., 118(2), 348–360.

Wang, Z., S. Doetterl, M. Vanclooster, B. van Wesemael, and K. Van Oost (2015),Constraining a coupled erosion and soil organic carbon model using hillslope-scale patterns of carbon stocks and pool composition. J. Geophys. Res. Biogeosci., 120, 452–465. doi: 10.1002/2014JG002768.

Warrington, D. N., et al. "Primary particle size distribution of eroded material affected by degree of aggregate slaking and seal development." *European Journal of Soil Science* 60.1 (2009): 84-93.

Weaver, J.E. (1968), Prairie plants and their environment, Univ. of Nebraska Press, Lincoln, NE.

Williams, J. R., C. A. Jones, and P. Dyke (1984), Modeling approach to determining the relationship between erosion and soil productivity, Trans. ASAE, 27(1), 129-144.

Wilson, C. G., A. N. T. Papanicolaou, and O. Abaci (2009), SOM dynamics and erosion in an agricultural test field of the Clear Creek, IA watershed, Hydrol. Earth Syst. Sci. Discuss., 6, 1581-1619.

Xiao, X. M., D. Hollinger, J. Aber, M. Goltz, E. A. Davidson, Q. Y. Zhang (2004), Satellite-based modeling of gross primary production in an evergreen needleleaf forest, Remote Sens. Environ., 89(4), 519-534.

Yadav, V., and G. P. Malanson (2009), Modeling impacts of erosion and deposition on soil organic carbon in the Big Creek Basin of southern Illinois, Geomorphology, 106(3), 304-314.

Yalin, M.S. (1963), An expression for bed-load transportation, J. Hydr. Eng. Div-ASCE, 89, 221-250.

Yalin, M. S. (1977), Mechanics of Sediment Transport, 2nd ed., 298 pp., Pergamon Press.

Yang, C.T. (1973), Incipient Motion and Sediment Transport, J. Hydr. Eng. Div-ASCE, 99(10), 1679-170.

Yang, X. M., & Wander, M. M. (1998). Temporal changes in dry aggregate size and stability: tillage and crop effects on a silty loam Mollisol in Illinois. *Soil and Tillage Research*, *49*(3), 173-183.

Yoder, R. E. (1936). A direct method of aggregate analysis of soils and a study of the physical nature of erosion losses. *Agronomy Journal*, *28*(5), 337-351.

Yoo, K., R. Amundson, A. M. Heimsath, and W. E. Dietrich (2005), Erosion of upland hillslope soil organic carbon: Coupling field measurements with a sediment transport model, Global Biogeochem. Cycles, 19, GB3003, doi:10.1029/2004GB002271.

Youker, R. E., & McGuinness, J. L. (1957). A short method of obtaining mean weight-diameter values of aggregate analyses of soils. *Soil Science*, *83*(4), 291-294.

Young, C.J., J.A. Schumacher, T.E. Schumacher, T. C. Kaspar, G.W. McCarty, S. Liu, and D. Napton (2014), Evaluation of a model framework to estimate soil and soil organic carbon redistribution by water and tillage using 137Cs in two U.S Midwest agricultural fields, Geoderma, 232,437-448.

Zhang G. H., B. Y. Liu, G. B. Liu, X. W. He, M. A. Nearing (2003), Detachment of undisturbed soil by shallow flow, Soil Sci. Soc. Am. J., 67, 713-719.

Zhang, X., Z. Li, Z. Tang, G. Zeng, J. Huang, W. Guo, and A. Hirsh (2013), Effects of water erosion on the redistribution of soil organic carbon in the hilly red soil region of southern China. Geomorphology, 197, 137-144.

Zhang, H., S. Liu, W. Yuan, W. Dong, A. Ye, X. Xie, Y. Chen, D. Liu, W. Cai, and Y. Mao (2014), Inclusion of soil carbon lateral movement alters terrestrial carbon budget in China, Sci. Rep., 4. doi: 10.1038/srep07247.

Zheng, Y., X. Luo, W. Zhang, B. Wu, F. Han, Z. Lin, and X. Wang (2012), Enrichment behavior and transport mechanism of soil-bound PAHs during rainfall-runoff events, Environ. Pollut., 171, 85-92.